Adsorption studies on $RuO_2(110)$ and $Ru(11\bar{2}1)$ surfaces

vorgelegt von
M.Sc. **Chaoyang Fan**
aus Jianou, Fujian (China)

Der Fakultät II - Mathematik- und Naturwissenschaften
der Technischen Universität Berlin
zur Erlangung des akademischen Grades
Doktor der Naturwissenschaften
genehmigte Dissertation

Berlin 2002
D 83

Promotionsausschuß:

Vorsitzender: Prof. Dr. E. Schöll
Berichter: Prof. Dr. K. Jacobi
Prof. Dr. W. Richter

Tag der mündlichen Prüfung: 28. Mai 2002

Acknowledgements

First of all, I would like to thank Prof. Dr. K. Jacobi, my supervisor. Without his guidance and help this work could not be successful. I have benefited a great deal from the discussions with him and many knowledge in surface science field which were introduced by him. His patience and support have given me the freedom to explore this field and to do the exciting research work.

I would like to thank Prof. Dr. G. Ertl, the director of the Department of Physical Chemistry at the Fritz-Haber-Institute of Max-Planck-Society. He give me the opportunity to work here.

I would like to thank Prof. Dr. W. Richter, my supervisor at the Technische Universität Berlin.

I am thankful to Dr. J. Wang for the fruitful cooperation in the research of the $RuO_2(110)$ surface. The discussions with him gave me great benefit.

I am grateful to P. Geng for technical support. His help was very important for the experiments in my thesis.

I am indebted to my colleagues in the group of Prof. Dr. K. Jacobi, to Y. Wang, Dr. J. Márquez, Dr. L. Geelhaar, Dr. K. Bedürftig, Y. Temko, Dr. T. Suzuki and M. Richard for their help and for the friendly and supportive atmosphere in the laboratory.

Special thanks have to be expressed to I. Reinhardt for her help in minimizing the mistakes of English grammar in my thesis.

Finally, I would like to thank my wife, Xiaoping Wu, for her support and encouragement.

Abstract

Adsorption and oxidation studies were performed on $RuO_2(110)$ and $Ru(11\bar{2}1)$ surfaces by using vibrational spectroscopy (HREELS) and thermal desorption spectroscopy (TDS). By using the latter method, information on the bonding strength of adsorbates can be derived.

Bare $RuO_2(110)$ surfaces were prepared by exposing 10^7 L O_2 to Ru(0001) at 700 K. The bare $RuO_2(110)$ surface is terminated by coordinatively unsaturated O (O-bridge) and Ru (Ru-cus) atoms. By exposure of oxygen, a weakly bonded atomic oxygen called O-cus can be adsorbed at Ru-cus, creating a more O-rich surface. At 85 K, CO adsorbs at Ru-cus and is called CO-cus. In contrast, at 300 K, CO reacts with O-bridge first, and is then attached to the Ru underneath O-bridge; it is therefore called CO-bridge.

CO is found to be able to react with the bare and the O-rich $RuO_2(110)$ surface. Two reaction channels are identified: CO may react with O-cus or with O-bridge. For the exposure values applied, only surface oxygen takes part in the CO oxidation. The oxygen depleted surface can be restored by O_2 exposure at RT. Thus $RuO_2(110)$ + O_2 + CO turned out to be a remarkable surface redox system operating at 300 K. This system is able to work under steady-state conditions. A remarkable agreement of the kinetic data was found between the $RuO_2(110)$ single crystal surface, typically operated at 10^{-7} mbar pressure, and small supported RuO_2 particles working at atmospheric pressure. It is demonstrated that the former "pressure gap" in CO oxidation on Ru actually is a "material gap" which could be bridged in the present thesis.

Hydrogen and CO adsorption on $Ru(11\bar{2}1)$ were studied. Three adsorption states of hydrogen, α-, β- and γ-H, were observed. At high coverage, three H atoms are suggested to be squeezed into one unit cell, in which α-H is adsorbed at fourfold symmetric sites, while β- and γ-H are adsorbed at pseudo-threefold sites.

For low coverage CO is adsorbed on $Ru(11\bar{2}1)$ at on-top sites. For high coverage CO forms a compression phase, in which some CO molecules are somewhat shifted away from the on-top sites but remain linearly bonded to the substrate, and additional CO adsorbs on bridge sites, similarly as on $Ru(10\bar{1}0)$. About 20 % CO can also be dissociated. The dissociation of CO is mainly determined by the CO occupation at the neighboring unit cells. This is explained here by the so-called "bonding competition" effect between CO in neighboring unit cells.

Kurzzusammenfassung

In dieser Arbeit wurden Studien zur Adsorption und zur Oxidation von CO auf $RuO_2(110)$- und $Ru(11\bar{2}1)$-Oberflächen durchgeführt. Verwendet wurden dabei Schwingungsspektroskopie (HREELS) und Thermodesorptions-Spektroskopie (TDS). Die letztere Methode erlaubt, Aussagen über die Bindungsstärke von Adsorbaten zu machen.

$RuO_2(110)$-Ausgangsoberflächen wurden präpariert, indem eine Ru(0001)-Oberfläche einer O_2-Dosis von 10^7 L bei 700 K ausgesetzt wurde. Diese Oberfläche wird von koordinativ ungesättigten O- (O-bridge) und Ru-Atomen (Ru-cus) terminiert. Mittels weiterer O-Zugabe kann eine O-reiche Oberfläche präpariert werden, bei der die zusätzlichen O-Atome (O-cus) auf Ru-cus adsorbieren. Bei 85 K adsorbiert CO auf Ru-cus (CO-cus). Im Gegensatz dazu reagiert CO bei 300 K mit O-bridge zu CO_2. Weiter hinzukommende CO-Moleküle adsorbieren auf den durch Abreaktion von O-bridge freigewordenen Ru-bridge-Atomen (CO-bridge).

CO kann mit der Ausgangs- und der O-reichen RuO_2-Oberfläche reagieren. Zwei Reaktionskanäle werden identifiziert: Reaktion von CO mit O-cus und mit O-bridge. Dabei wird CO zu CO_2 oxidiert und verlässt die Oberfläche. An diesen Reaktionen nimmt nur der Oberflächensauerstoff teil. Die abreagierte (reduzierte) Oberfläche kann durch O_2-Zugabe bei 300 K regeneriert werden. $RuO_2(110) + O_2 + CO$ stellt daher ein bemerkenswertes Redoxsystem dar, das sogar bei 300 K und unter Gleichgewichtsbedingungen arbeitet. Weiterhin wird eine auffällige Ähnlichkeit zwischen kinetischen Daten gefunden, die an $RuO_2(110)$ bei 10^{-7} mbar und an RuO_2-Partikeln auf SiO_2-Trägerkatalysatoren gewonnen wurden. Damit kann gezeigt werden, dass eine ursprünglich als "Drucklücke" bezeichnete Diskrepanz bei der CO-Oxidation an Ru tatsächlich eine "Materiallücke" ist. Diese Lücke kann in dieser Arbeit überbrückt werden.

Ausserdem wurden die H- und CO-Adsorptionen an $Ru(11\bar{2}1)$ untersucht. Drei H-Zustände, α-, β- und γ-H, wurden gefunden. Bei Sättigung wird auf eine Belegung der Einheitszelle mit drei H-Atomen geschlossen. Es wird vorgeschlagen, dass β-H und γ-H auf Dreifachplätzen und α-H auf einem Vierfachplatz adsorbiert sind.

Bei kleiner Bedeckung adsorbiert CO an $Ru(11\bar{2}1)$ auf Ontop-Plätzen. Bei hoher Bedeckung wird CO teilweise zur Seite gedrängt; dabei bleibt es zum Teil linear gebunden, sitzt aber zum Teil auch auf Brückenplätzen. Etwa 20 % CO können auch dissoziieren. Diese Menge an dissoziiertem CO wird durch den "bonding competition"-Effekt zwischen benachbarten CO-Molekülen erklärt.

Table of Contents

List of Figures

List of Tables

Acronyms

cus	coordinatively unsaturated site
DFT	density functional theory
ER	Eley-Rideal
HREELS	high-resolution electron loss spectroscopy
IR	infrared
LEED	low-energy electron diffraction
LT	low temperature
LH	Langmuir-Hinshelwood
ML	monolayer
RT	room temperature
SCLS	surface core-level shift
STM	scanning tunneling microscopy
TDS	thermal desorption spectroscopy
UHV	ultra-high vacuum
UP	Ultraviolet photoemission
XPS	X-ray photoelectron spectroscopy

1 Introduction

Heterogeneous catalysis is an important part of the technology that supports industrially developed societies. Many chemical reactions can be efficiently catalyzed by transition metals, as well as by transition-metal oxides. Studies on well-defined single-crystal surfaces under ultra-high vacuum (UHV) conditions enable to elucidate the microscopic reaction mechanisms underlying heterogeneous catalysis. Real catalysis is often performed under pressure of over hundred bar. On the other hand, the methods of surface science are limited to a very small pressure range (UHV range). If the reactivity is different within the two pressure regimes, it is called "pressure gap". However, the transfer of results derived along the so-called "surface science" approach to the high pressure conditions of "real" catalysis could be successfully achieved in a few cases, including, for example, ammonia synthesis on Fe [1, 2] and Ru [3, 4], or CO oxidation on Rh [5].

CO oxidation on metal surfaces is one of the most important catalytic reactions in both technological and scientific fields. Apart from its enormous practical importance, such as for automotive exhaust control, the catalytic oxidation of CO is one of the simplest catalytic reactions and is thus widely used as a model system to understand heterogeneous catalysis [6–9].

The CO oxidation can be efficiently catalyzed by the platinum group metals. Among them Ru is special. Under UHV conditions Ru is an extraordinarily poor catalyst for CO oxidation [10], while the activity of supported Ru as well as of Ru(0001) under high pressure and oxidizing conditions turns out to be superior to the other platinum group metals [11, 12]. Recently, it was found that an "O-rich Ru(0001)" surface, which contains an oxygen amount equivalent to at least three oxygen monolayers (ML), shows a pronounced enhancement of the CO conversion

rate by more than two orders of magnitude with respect to a surface covered with a complete Ru(0001)-(1 × 1)O monolayer [13]. The studies related to CO oxidation on the surface were performed in both experimental and theoretical methods by Böttcher et al. [13–18], Over et al. [19–26] and other groups [27–31]. The pronounced enhancement was suggested by Böttcher et al. to be due to the presence of oxygen in the subsurface region [17]. By combining scanning tunnelling microscopy (STM) images, low-energy electron diffraction (LEED) intensity analysis and density functional theory (DFT) calculations, Over et al. [19] demonstrated later that the surface consists in fact of patches of Ru(0001)-(1 × 1)O and RuO_2(110), and suggested that the active phase of oxygen is on the RuO_2(110) domains. The debates about the active part of the "O-rich Ru(0001)" surface will be presented in Chapter 3. It is becoming clearer that the active part is RuO_2(110). RuO_2 powder (presumably with some content of water) prepared from aqueous solution was recently reported to catalyze CO oxidation even at 295 K [32]. However, the elementary steps of the CO oxidation on RuO_2 are still not clear. In this thesis, the studies of adsorption and reaction of CO and oxygen on the RuO_2(110) surface will be presented.

Besides the CO oxidation, the ammonia synthesis was found to be efficiently catalyzed by Ru-based catalysts [33, 34]. The advantage for using Ru-based instead of the Fe-based catalysts is that the Ru-based catalysts can be operated at lower pressures and temperatures [35]. In order to better understand the details of the reaction involved, a number of experiments on Ru single-crystal surfaces were performed [36, 37]. Since hydrogen adsorption is an important step in ammonia synthesis, the investigation of hydrogen adsorption on the Ru surfaces is necessary.

Ru can also efficiently catalyze many reactions such as methanation and the Fischer-Tropsch synthesis. The adsorption and dissociation of CO are the elementary steps for these reactions [38, 39]. In addition, the chemisorption of CO on transition-metal surfaces is a prototype system for the interaction between diatomic molecules and transition-metal surfaces. Therefore, the investigations of the CO adsorption and dissociation on the Ru surfaces are very important.

For the CO and H adsorption on the Ru surface, one parameter to be changed is the crystallographic orientation of the Ru surface. CO and H adsorption on the close-packed surface of Ru, Ru(0001), were extensively studied [40–53] because of its simple structure. However, the real catalysts are composed of both the close-packed

and the open surfaces, and in some cases the active sites for the catalysis are on the open surfaces. One obvious example is the dissociated adsorption of N_2 on the Fe surfaces. It was shown that the coefficient of N_2 dissociation on the more open Fe(111) surface is about two orders of magnitude larger than that on the closed-packed Fe(110) surface [54, 55]. Similarly, it was reported that the open Ru(11$\bar{2}$1) surface, shows a very high activity for the dissociation of ammonia [56, 57]. In this thesis, the investigations of the CO and hydrogen adsorption on the Ru(11$\bar{2}$1) surface are presented.

The high-resolution electron loss spectroscopy (HREELS) and thermal desorption spectroscopy (TDS) are powerful methods in the surface-science field. HREELS can be used to identify the adsorbate species, and TDS to study occupation and bonding strength of the adsorption states. In this thesis, the CO oxidation on RuO_2(110) and the hydrogen and CO adsorption on Ru(11$\bar{2}$1) will be investigated by using HREELS and TDS. In addition, the CO oxidation is also investigated under steady-state conditions by using a special setup in our UHV chamber.

In chapter **2** the experimental methods and the setup of the apparatus are introduced.

In chapter **3** the CO oxidation on the RuO_2 surface as well as on the Ru surfaces are reviewed. The structure of RuO_2(110) is introduced.

In chapter **4** the oxygen adsorption on RuO_2(110) is discussed, and the different oxygen species on the RuO_2(110) surface are identified in the HREEL spectra.

In chapter **5** the HREEL and TD spectra of CO adsorption on RuO_2(110) are presented and the adsorption site of CO is determined.

In chapter **6** the CO oxidation on RuO_2(110) is investigated with titration-type experiments by using HREELS. Different reaction channels are found. The CO and oxygen coadsorbate is also investigated.

In chapter **7** the steady-state results of CO oxidation on RuO_2(110) are presented and the reaction steps are discussed. It is demonstrated that the former "pressure gap" in CO oxidation on Ru actually is a "material gap".

In chapter **8** the investigation of hydrogen adsorption on Ru(11$\bar{2}$1) is presented. The adsorption sites of hydrogen on Ru(11$\bar{2}$1) are proposed.

In chapter **9** the CO adsorption and dissociation on Ru(11$\bar{2}$1) are presented. The structure of adsorbed CO and the factors which affect the CO dissociation are discussed.

In chapter **10** the conclusion is given.

2 Experiment

2.1 Experimental methods on surfaces

2.1.1 Low-Energy Electron Diffraction (LEED)

In most surface physics laboratories, LEED is used as the standard technique to check the crystallographic quality of a surface and to observe the reconstruction of a clean surface or an ordered adsorbate overlayer. In these experiments a beam of electrons with a primary energy between 50 and 300 eV is incident on the surface, and the elastically backscattered electrons give rise to diffraction spots that are imaged on a phosphorous screen, giving rise to the LEED pattern. Since the escape depth of electrons in this energy range is smaller than 10 Å, the information from the elastically backscattered electrons is mainly coming from the surface, so that it can be used to study the surface structure. The LEED pattern reflects the 2D surface reciprocal lattice, and the surface structure information can be derived from it.

At the beginning of an experiment on a crystalline sample, LEED can be used to check the crystallographic quality of the surface. If there is no disorder on the surface, the LEED pattern must exhibit sharp spots with high contrast and low background intensity. The symmetry of the LEED pattern for a sample without reconstruction is consistent with that derived from a bulk-truncated structure, giving a (1×1) LEED pattern. More complex LEED patterns with non-integer diffracted spots are obtained when a reconstruction is found. The LEED pattern can also be modified by adsorbed atoms or molecules when they form an ordered superstructure. Thus, the periodic information in real space of the bare or adsorbate covered surface can be derived from the LEED pattern. In addition, the intensity of the diffracted spots also includes the

surface-structure information. The electron energy (voltage) dependence of LEED beam intensities, the so-called I–V curves, can be used in an iterative procedure to determine the geometrical arrangement of surface atoms. First, an arrangement of atoms is postulated that is consistent with the symmetry of the LEED pattern. Second, the intensity of a number of diffracted beams is calculated as a function of incident electron energy by explicit solution of the Schrödinger equation for electron wave functions in the first few atomic layers. Third, the resulting I–V curves are compared to that from experiment, and the process is continued with a refined geometry until satisfactory agreement is obtained. It must be emphasized that this "trial and error" method involves significant computational efforts. In this thesis, the LEED patterns were used to control the crystallographic quality of a clean surface as well as the epitaxial growth of thin layers.

2.1.2 High resolution electron energy loss spectroscopy (HREELS)

So far, the most prevalent technique used in surface vibrational spectroscopy is HREELS. A monochromatic electron beam (primary energy < 20 eV, usually about 1–10 eV) is directed onto a surface, and the energy distribution of the scattered beam is measured, perhaps varying the primary energy, angle of incidence or scattering. The electron in this energy range can effectively excite the vibrations of surface atoms or adsorbates and therefore, the widest application of HREELS is concerned with the study of vibrations of adsorbed atoms or molecules. It is usually used to identify adsorbates and to get information about adsorption sites and bonding geometry.

Fig. 2.1 is a schematic drawing of the HREEL spectrometer which was used in our experiment. This spectrometer was mount in the laboratory of H. Ibach at Jülich and is the penultimate type. It was set into operation by M-Gruyters in his thesis work [59, 60].The electrons are emitted from the filament and then focused into the first monochromator by the electrode lenses A_1, A_2 and A_3. After being monochromatized by the first and the second monochromator and focused by electrode lenses B_1 and B_2, the highly monochromatic electrons are directed onto the sample. The electrons, which are elastically and inelastically scattered by the sample, are focused into the first analyzer by electrode lenses B_3 and B_4. Through the

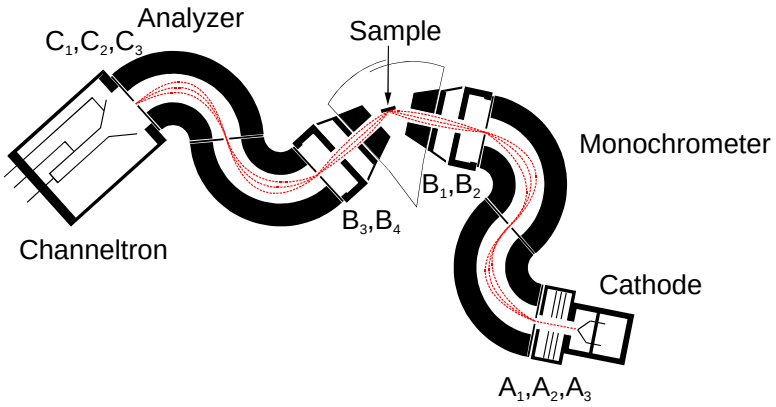

Figure 2.1: Schematic drawing of HREELS.

first and second analyzer the electrons are focused into the channeltron by electrode lenses C_1, C_2 and C_3. The intensity of the detected electrons as a function of their energy loss (related to the elastic peak) can be recorded by the spectrometer.

The identification of an adsorbed species relies on the knowledge of its vibrational spectrum from the infrared (IR) absorption in the gas phase. Compared to the IR spectroscopy which can also investigate the vibrations of adsorbed species, the sensitivity of HREELS, especially in the vibrational low-energy range, is very high. Therefore, the accessible spectral range of HREELS is significantly wider than that of the IR spectroscopy. A loss peak as low as 6 meV was observed for Ru(0001)-(1×1)O by HREELS [58]. The energy resolution of HREELS is also very high. An energy resolution as high as 0.75 meV was reported [61].

Different from the IR spectroscopy, in which only dipole excitation (see below) is available, the excitation mechanisms in HREELS comprise dipole, "impact" and resonance scattering. Each of these modes permits access to different information since different selection rules and potential energy surfaces control the outcome of the spectroscopic process.

Dipole scattering

The dipole scattering is the most important excitation mechanism of adsorbates in HREELS. It results from the long-range interaction between the electric field of the incoming electron with the dynamic dipole of the adsorbate or surface. The

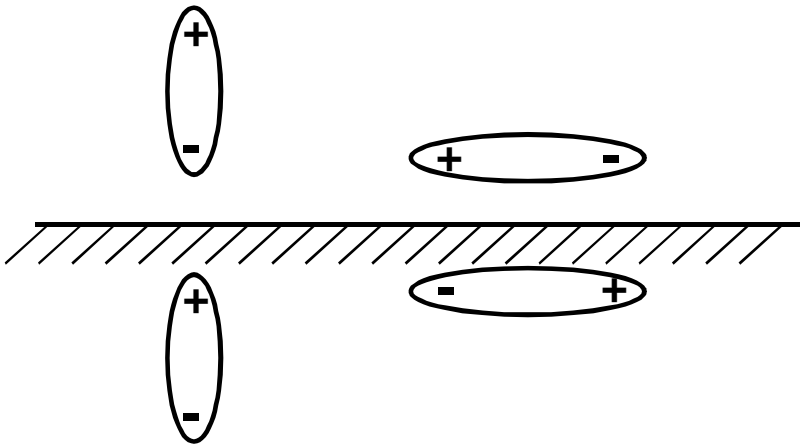

Figure 2.2: The dipoles and their induced image dipoles.

inelastic dipole scattering involves little momentum transfer and thus, the angular distribution of inelastically scattered electrons is close to the specular direction.

Due to the screening of a dipole on a metal surface, there is a selection rule in the dipole excitation. A dipole on a metal surface can induce an image dipole within the substrate, as shown in Fig. 2.2. It is noticed that the perpendicular component is doubled, whereas the parallel component is cancelled by its instantaneous image. Therefore, only the modes with a component of dynamic dipole moment perpendicular to the surface can be observed in loss spectra. The selection rule can help to identify the geometrical structure of an adsorbate-surface complex.

The principal features of dipole scattering are as follows: It is of long-range interaction, sensitive, close to the specular direction and only sensitive to the perpendicular component of an adsorbate dipole.

Impact scattering

The impact scattering is a short-range direct Coulomb interaction between the incident electron and the "higher poles" or the ion cores of the adsorbate. The details of the impact scattering are complicated. The momentum transfer via this mechanism is strong. In contrast to dipole scattering, the impact scattering is not concentrated in the specular direction. The cross section of impact scattering is about 2 or 3 orders of magnitude lower than that of dipole scattering. Thus, it is usually observed

only when measured in an off-specular direction.

The principal features concerning impact scattering are summarized as follow: It is of short-range interaction, low intensity, wide angular distribution, and usually observed in an off-specular direction.

Negative ion resonance

The other important type of vibration excitation mechanisms involves the temporary negative ion creation due to electron capture in a shape resonance during an EELS event. It is usually observed for physisorbed systems and the overtones of the excitation are relatively strong and can hence be observed in the loss spectra. It is useful in investigating potential energy surfaces.

2.1.3 Thermal Desorption Spectroscopy (TDS)

The desorption of adsorbates can be induced by heating the substrate. The information on surface adsorption and desorption states and the thermodynamical properties can be obtained by measuring the variation of the flux of desorbed molecules with increasing temperature. The main experimental method is called TDS, in which the partial pressure of desorbing species during linearly increasing the sample temperature is recorded by a mass spectrometer. When the pump speed is high enough, the desorption rate is proportional to the partial pressure of the desorbing species.

The desorption process can be described by the Wigner-Polanyi equation:

$$r(\theta) = -\frac{\partial\theta}{\partial t} = \nu(\theta)\theta^n \exp(-\frac{E(\theta)}{RT}) \quad , \tag{2.1}$$

here r, θ, E, ν and n denote the desorption rate, coverage, desorption energy, frequency factor and desorption order of the adsorbate, respectively. T and t denote temperature and time. If the temperature increases linearly by heating, i.e., if $\beta = \frac{\partial T}{\partial t} = \text{const}$, the equation can be written as:

$$r(\theta) = -\frac{\partial\theta}{\partial T}\beta = \nu(\theta)\theta^n \exp(-\frac{E(\theta)}{RT}) \quad . \tag{2.2}$$

At very high pump speed the desorption rate is proportional to the partial pressure of the desorbing species which is measured in a mass spectrometer. Supposing that

the frequency factor ν and desorption energy E are independent of the coverage θ, we have:

$$\begin{aligned}\frac{\partial r}{\partial T} &= \nu\theta^n \exp\left(-\frac{E}{RT}\right)\cdot\frac{E}{RT^2} + \nu\exp\left(-\frac{E}{RT}\right)\cdot n\theta^{n-1}\cdot\frac{\partial\theta}{\partial T} \\ &= r(\theta)\cdot\frac{E}{RT^2} + \nu n\theta^{n-1}\exp\left(-\frac{E}{RT}\right)\cdot\left(-\frac{r(\theta)}{\beta}\right) \\ &= r(\theta)\cdot\left[\frac{E}{RT^2} - \frac{\nu n\theta^{n-1}}{\beta}\exp\left(-\frac{E}{RT}\right)\right] \quad . \end{aligned} \tag{2.3}$$

At the temperature of maximum desorption rate (T_{max} in TDS), we have:

$$\frac{\partial r}{\partial T}|_{T=T_{max}} = 0 \quad . \tag{2.4}$$

Therefore,

$$\frac{E}{RT_{max}^2} = \frac{\nu n\theta_{T_{max}}^{n-1}}{\beta}\exp(-\frac{E}{RT_{max}}) \quad . \tag{2.5}$$

For the first-order desorption (i.e., n = 1), we get:

$$\frac{E}{RT_{max}^2} = \frac{\nu}{\beta}\exp(-\frac{E}{RT_{max}}) \quad . \tag{2.6}$$

When measuring TD spectra with different β values, different T_{max} can be obtained. Then the desorption energy and frequency factors can be calculated by solving the equation.

There is another method to estimate the desorption energy by simply assuming a frequency factor of 10^{13} s^{-1} when measuring TD spectra with only one β (heating rate). The desorption energy can easily be calculated in this case by solving the Eq. (2.6). For the second-order desorption (i.e., n = 2), we get:

$$\frac{E}{RT_{max}^2} = \frac{\nu 2\theta_{T_{max}}}{\beta}\exp(-\frac{E}{RT_{max}}) \quad . \tag{2.7}$$

From Eq. (2.7), the desorption energy can also be roughly estimated by using the frequency factor of 10^{13} s^{-1}.

Furthermore, for different initial coverages of the adsorbate, the desorption temperature at the maximum desorption rate changes also. When writing the equation in the form:

$$\theta_{T_{max}} = \frac{E\beta}{\nu RT_{max}^2}\exp(\frac{E}{RT_{max}}) \quad , \tag{2.8}$$

and fitting the function of $\theta_{T_{max}}(T_{max})$, the desorption energy E and the frequency factor ν can be obtained as fitting parameters.

Besides using the desorption temperature at maximum desorption rate, T_{max}, the desorption energy and frequency factor can be obtained by analyzing the shape of the TD spectra. The detailed discussion is given in the references [62–65].

2.2 Experimental equipment

The experiments presented in this thesis were performed in an UHV apparatus. As shown in Fig. 2.3, the apparatus consists of two separable chambers which are connected through a valve to allow preparation of the sample in a chamber separated from the HREEL spectrometer(see Pages 22, 23). The upper chamber with a base pressure of 4×10^{-9} Pa contains facilities for LEED, TDS, gas dosing, and surface cleaning by Ar^+ ion sputtering. The lower chamber with a base pressure of 2×10^{-9} Pa contains a HREEL spectrometer. The ionization gauge used in this work was not calibrated. The actual exposure amount could be 5 times the value shown in this work. The HREEL spectra were taken at 60° of incidence and emission (both with respect to the surface normal) and with a primary energy of 3.0 eV for the measurement on $RuO_2(110)$ and of 4.0 eV for that on the $Ru(11\bar{2}1)$ surface. An energy resolution of 2.5 meV was reached at the counting rate of 1×10^5 electrons/s for both surfaces studied. The energy resolution was usually set to 3.0–4.0 meV in order to get a counting rate as high as 3×10^5 electrons/s.

The upper chamber is used for sample preparation and TDS measurements. In order to avoid errors during the TDS measurements, that the measuring gases are not from the sample surface, e.g., but from the sample holder, a special setup was used in TDS experiments, which is shown in Fig. 2.4. The sample was positioned in front of a short tantalum tube with a diameter somewhat smaller than the size of the sample surface, so that the ionizer of the mass spectrometer mainly accepts molecules desorbing from the sample surface. As shown in Fig. 2.4, the tube can be withdrawn when the TDS measurement is finished, so that it does not hinder the other experiments and the movement of the sample. The mass spectrometer is connected with an ion-getter pump by a separate valve to get a high pumping speed

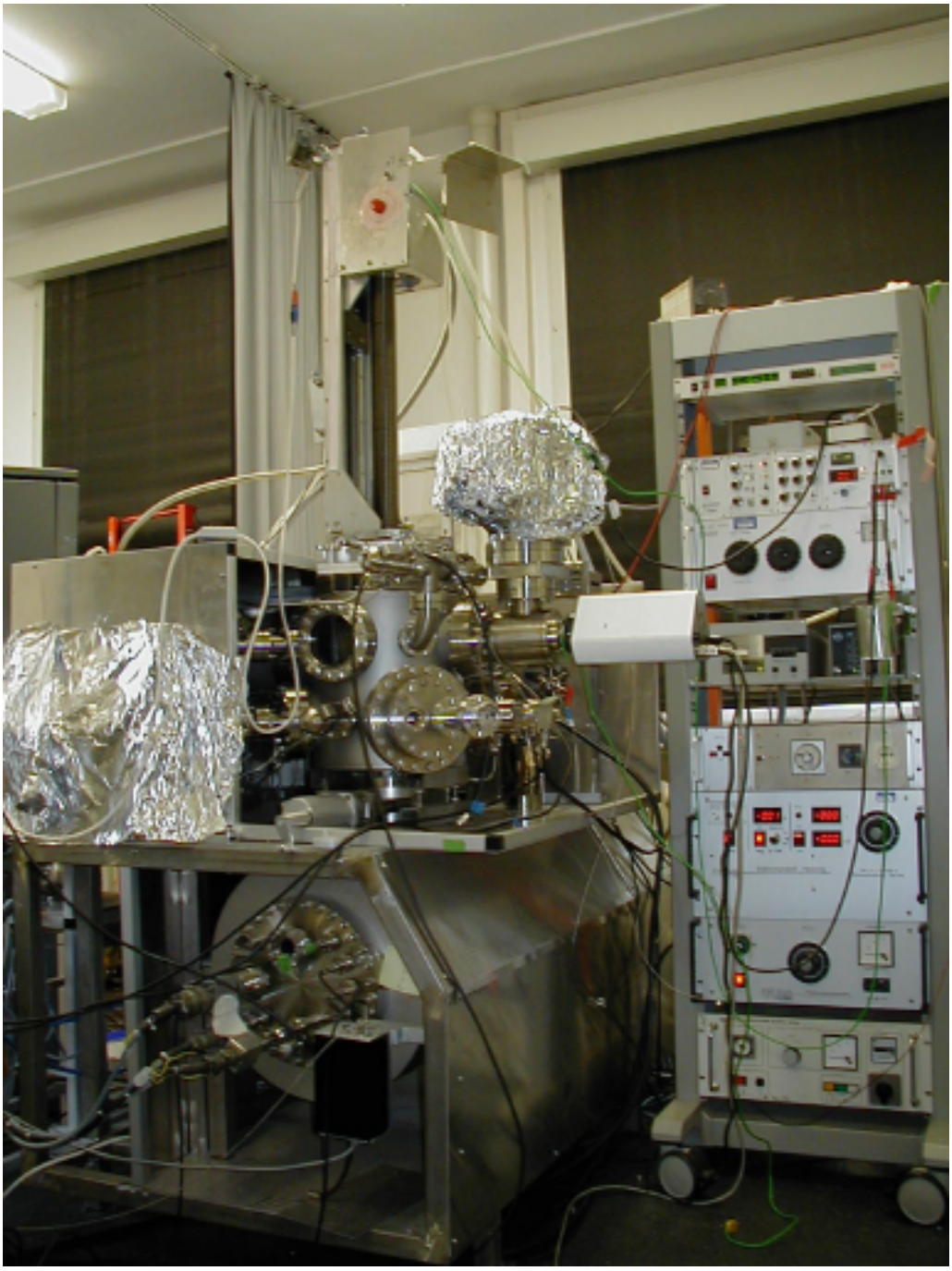

Figure 2.3: Apparatus used in the experiments.

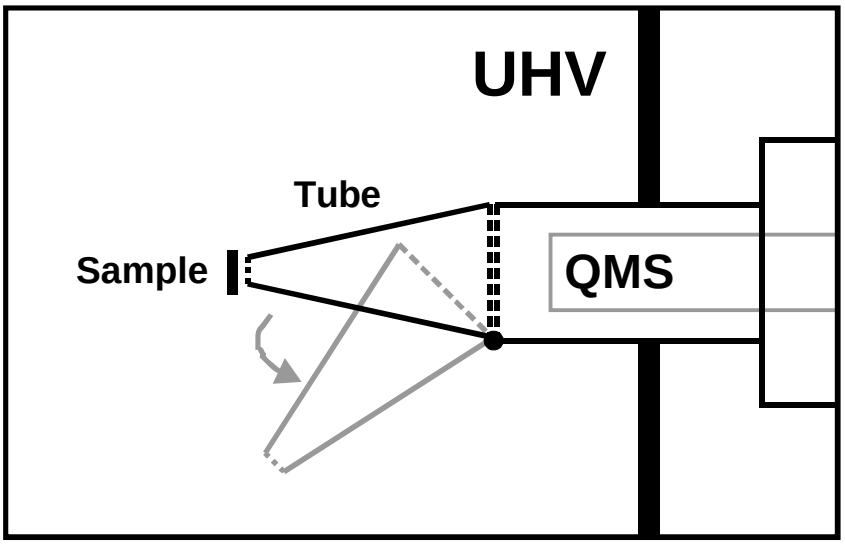

Figure 2.4: Setup for TDS measurement.

during TDS measurement, in order to acquire high quality TD spectra.

The setup of TDS can also be used to measure the reaction rate under steady-state conditions, as shown in Fig. 2.5. In our CO oxidation steady-state measurements, the angle between the plane of the sample and the hole of the tube was set to 45°. In this configuration the CO and oxygen molecules from the gas phase can reach the sample and the mass spectrometer, and the product (CO_2) can also be collected and recorded.

2.3 Sample preparation

Ruthenium is a transition metal with a hcp crystal lattice. Its close-packed surface is the (0001) surface. Its preparation is well known from the foregoing studies in the laboratory. The $RuO_2(110)$ surface was epitaxially grown on Ru(0001) following recent recipes [15, 19]. In addition, experiments on $Ru(11\bar{2}1)$ surfaces were also performed. The preparation of the $RuO_2(110)$ and $Ru(11\bar{2}1)$ surfaces is described below in more detail.

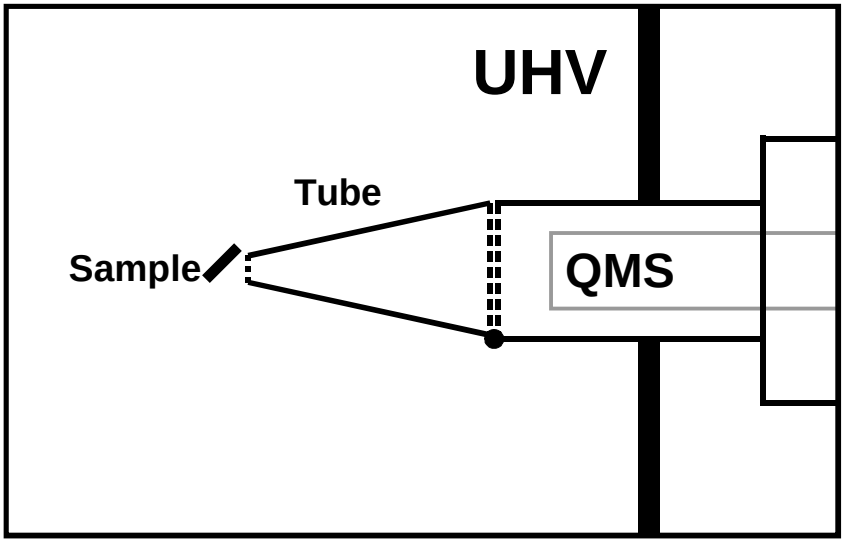

Figure 2.5: Setup for steady-state measurements.

2.3.1 RuO_2(110) surface

The RuO_2(110) surface was epitaxially grown on Ru(0001). The Ru(0001) sample was mounted using W wires in narrow slits at the edges of the sample and could be heated by electron bombardment from the backside. The NiCr/Ni thermocouple was spot-welded to the upper edge of the sample. Cleaning of the sample is achieved by repeated cycles of Ar^+ ion sputtering and annealing. The cleanliness of the sample is checked by LEED and HREELS. The RuO_2(110) surface was produced by exposing a well-prepared single-crystal Ru(0001) to 1×10^7 L of O_2 at a sample temperature of 700 K. To reduce the background pressure in the UHV chamber after oxygen exposure, a glass capillary array doser was used at a close distance of 15 mm from the sample, yielding an enhancement of the pressure at the sample surface by a factor of about 30 with respect to the background. After the background pressure in the UHV chamber had dropped to the order of 10^{-8} Pa, the sample was briefly annealed to 770 K, in order to remove away contamination by residual gas adsorption. This procedure results in a surface which is covered by a thin single-crystalline layer of RuO_2(110) (ordered in patches of three different domains, rotated laterally by 120°), as checked by LEED in accordance with Ref. [19, 21]. As it has already been shown, for a smaller exposure of about 1×10^6 L at 600–800 K, the surface is composed of patches of the (1×1)O phase and of 2 nm thick RuO_2(110) platelets [19]. In

our case, we used larger doses (typically 10^7 L), so that the surface is completely covered by $RuO_2(110)$. We believe that also in our case the thickness of the RuO_2 layer is of the order of 2 nm. During the experiments on the $RuO_2(110)$ surface, the sample was occasionally annealed to 770 K to get a clean and well-ordered surface back. The preparation can be repeated after the cleaning of the Ru(0001) substrate by sputtering and annealing cycles.

2.3.2 Ru(11$\bar{2}$1) surface

The Ru(11$\bar{2}$1) sample has an oval shape with a diameter of about 10 mm and a thickness of about 3.5 mm. It was clamped between two Ta wires and could be heated by electron bombardment from the backside. The NiCr/Ni thermocouple was spot-welded to the upper edge of the sample. The cleaning of the sample was achieved by repeated cycles of sputtering and annealing up to 1560 K. The cleanliness of the sample was checked by LEED and HREELS. The well-prepared Ru(11$\bar{2}$1) surface showed a LEED pattern with very sharp diffraction spots. The LEED pattern is 1×1, which indicates that there is eventually relaxation but no reconstruction on the clean Ru(11$\bar{2}$1) surface.

3 Aspects of CO oxidation on the Ru(0001) and the RuO_2(110) surface

3.1 The CO oxidation on Ru(0001)

Ruthenium was found to be peculiar for CO oxidation among the platinum-group metals: very active under high pressure and oxidizing conditions and very poor under UHV condition [10, 11]. By using the coupling of a microcatalytic reactor for the measurement of reaction kinetics at realistic pressures with a traditional UHV apparatus for surface analysis, Peden et al. found that the Ru(0001) surface is as active as a supported Ru catalyst under high pressure and oxidizing conditions [12]. The original suggestion about this enhanced activity was attributed to the presence of a complete monolayer (ML) of oxygen atoms chemisorbed on the Ru(0001) surface, because the reaction rate depends distinctly on the coverage of oxygen and increases drastically with oxygen coverage, and the surface concentration of oxygen present after the reaction at optimum rates is approximately the level of 1.0 ML [12, 66].

As an important elementary step of CO oxidation, the oxygen adsorption on the Ru(0001) surface has been extensively studied in experiments as well as in the density-functional theory (DFT) calculations. For some time there was general agreement that the oxygen exposure leads only to the formation of adlayers with 2×2 or 2×1 symmetry at room temperature (RT), corresponding to coverages of 0.25 and 0.5 ML, respectively [67–69]. The oxygen atoms are bonded in the hcp threefold-

hollow sites in both cases [67–69].

However, experiments by using a high pressure cell suggested that a higher coverage is in fact achievable upon heavy dosages [70]. According to the DFT calculations, an oxygen adlayer with 1×1 periodicity and a coverage of 1.0 ML was also predicted [71]. This indicates that the lack of a high-coverage phase may be due to kinetic hindrance of dissociation. An alternative approach to prepare higher oxygen coverages is to use oxidizing molecules like NO_2. When keeping the sample temperature above the desorption temperature of NO and dosing NO_2, the NO_2 molecule dissociates into NO and oxygen. The NO molecule subsequently desorbs, leaving the oxygen atom on the surface. Actually, the approach has been successfully employed on Pt(111) [72, 73], and a Ru(0001) surface with $\theta_O > 1$ ML was also prepared in this way [74, 75]. By first exposing the Ru(0001) surface to O_2 at RT until the saturation was reached, and subsequently exposing to NO_2 at a sample temperature of 600 K, a (1×1)O overlayer on Ru(0001) with a sharp 1×1 LEED pattern could be prepared. This surface was examined by quantitative LEED [76] and vibrational spectroscopy [58]. The oxygen coverage near to 1 ML can also be achieved by exposing high doses of molecular oxygen at elevated temperatures such as 600 K. In this way, an other ordered structure, (2×2)3O with 0.75 ML coverage, was also observed as well as the (1×1)O structure [77, 78]. All of the four ordered superstructures were studied by DFT and LEED I-V calculations. It was demonstrated that the atoms are adsorbed at the hcp 3-fold-hollow sites. The oxygen binding energy in the four ordered structures on Ru(0001) was also calculated by using the DFT method. The corresponding results are shown in Table 3.1.

Table 3.1: Calculated DFT binding energies for the O/Ru(0001) system [23]

O species	(2×2)O	(2×1)O	(2×2)3O	(1×1)O
binding energy (eV)	5.87	5.52	5.29	5.07

From Table 3.1, one recognizes that the binding energy of oxygen decreases with increasing coverage. The more weak oxygen is bonded to the Ru surface, the more easy it may be activated to take part in CO oxidation. The oxygen species in the (1×1)O phase is most favorable due to its relatively low binding energy. However, it will be shown in this thesis that it is still too strongly bonded, instead only the more weakly bonded oxygen of the RuO_2 surface is able to efficiently oxidize CO.

The oxygen and CO coadsorption have been studied with many surface science methods [70, 79]. For the lower-coverage phases of oxygen ($\theta_O \leq 0.5$ ML) on Ru(0001), CO can adsorb on the surface. The bond between CO and Ru is significantly weakened by the coadsorption with oxygen, as indicated by the obvious decrease of the CO desorption temperature [70, 79]. For the oxygen coverage close to 1.0 ML, in which the CO oxidation is at the optimum rate, the adsorption of CO is nearly prohibited at T $\geq$ 85 K [70, 80, 81]. Thus, the reaction at the optimum rate ($\theta_O = 1.0$ ML) was suggested to proceed via the Eley-Rideal (ER) mechanism [80], in which CO interacts directly from the gas phase with adsorbed oxygen species, which is different from the Langmuir-Hinshelwood (LH) mechanism, in which both reactants have to be adsorbed on the catalyst's surface before the actual recombination step takes place.

The reaction was also studied by using DFT calculations. For the low oxygen coverage surface (Ru(0001)-(2×2)O), the minimum energy pathway for CO oxidation was calculated. It was found [82] that the CO oxidation mechanism of CO with Ru(0001)-(2×2)O is very similar to that on the close-packed surface of other platinum metals [83] but with a substantially higher reaction barrier. Thus, Ru is one of the least active catalysts for CO oxidation under UHV conditions in the platinum group metals [84]. The oxygen position in the transition state was found to be in a bridge site [82–84]. For the high oxygen coverage, $\theta_O = 1$ ML, the reaction barrier, which is determined by using the DFT calculation, is too high to account for the high reaction rate [85, 86, 88] in an ER mechanism, which was proposed in experiments [80]. Stampfl et al. suggested: The CO can be adsorbed on an imperfect Ru(0001)-(1×1)O surface. By this way the reaction barrier is lower than that for the ER mechanism, i.e., the CO oxidation proceeds via the LH mechanism [85, 86, 88].

3.2 The "O-rich Ru(0001)" surface and RuO_2(110)

In the following it could not be confirmed that the origin of the enhanced reactivity of Ru in CO oxidation is due to the presence of a complete monolayer of oxygen chemisorbed on Ru(0001). Recently, the "O-rich Ru(0001)" surface was found to show a CO conversion rate enhanced by more than two orders of magnitude with respect to the (1×1)O surface. This happens when the total O coverage is larger than

3.0 ML. Such an O-rich suface was prepared by exposing large O_2 doses ($> 10^6$ L) to Ru(0001) at elevated temperatures (600–800 K) [13]. The obvious enhancement of reactivity for CO oxidation was attributed to the presence of oxygen in the subsurface region. Böttcher et al. [17] proposed that oxygen atoms located between the first two Ru layers may induce a redistribution of the electron density also at the topmost surface layer. In consequence, the activation barrier for the reaction of CO with the topmost oxygen atoms may be significantly lowered.

Several experiments about the CO oxidation on the "O-rich Ru(0001)" surface were performed by Böttcher et al. [14] using molecular beam methods. The CO oxidation was shown to react via the LH mechanism. Since the structure of the "O-rich Ru(0001)" surface was not determined, they interpreted the results only qualitatively. They argued: At sample temperatures below 350 K, the CO oxidation proceeds through an active on-surface oxygen species. At temperatures above 500 K, the reactions are dominated by a second channel, which is governed by oxygen diffusion from the near-surface region toward the surface [14]. In addition, weakly bonded oxygen species were found by post-exposing oxygen to the active "O-rich Ru(0001)" surface, and the desorption temperature of the oxygen species was about 400 K. This oxygen species was found to be also very active for CO oxidation and was suggested to be probably bonded to some sites offered by oxide domains in the topmost layer of the surface [15].

By combining STM images, LEED intensity analysis and DFT calculations it was demonstrated that the "O-rich Ru(0001)" surface actually consists of patches of Ru(0001)-(1×1)O and $RuO_2(110)$, and it was suggested that the active part for CO oxidation is on the $RuO_2(110)$ domains, whereas the (1×1)O regions are inactive for CO oxidation [19–21].

The activity of the "O-rich Ru(0001)" surface towards CO oxidation depends also on the preparation condition even if the surface contains more than 3 ML or even a few tens ML. When the surface is prepared by exposing several 10^6 L O_2 at a temperature between 600–800 K, the surface is active for CO oxidation. The LEED pattern consists of a superposition of the hexagonal arrangements of spots with 1×1 periodicity and additional spots, which were shown to arise from three incommensurate, epitaxially grown $RuO_2(110)$ domains of a rectangular mesh [20]. When dosing O_2 at a temperature higher than 1100 K, the surface is inactive for CO

oxidation even if the surface contains very high oxygen coverage in the subsurface region (e.g. a few tens ML). The structure of this surface exhibits a 2×2 LEED pattern [17, 18, 21].

There are significant discrepancies between the explanations of the two kinds of surfaces of Böttcher et al. [17] and Kim et al. [20, 21]. The active surface with a 1×1 LEED pattern and some weak additional spots was explained by Böttcher et al. as due to the formation of a subsurface-oxygen phase without a significant admixture of RuO_x complexes. The inactive surface, which was prepared T > 1100 K and showed a sharp 2×2 LEED pattern, was suggested to be due to the formation of RuO_2 [17]. The inactive surface was marked by intense emission of RuO_x molecular fragments, appearing in TD spectra in the temperature range of 1000–1300 K. Furthermore, Böttcher et al. found that the Ultraviolet photoemission (UP) spectra of the O-rich 2×2 surface, which was inactive in CO oxidation, was different from those of O overlayers on Ru(0001). Together with some theoretical considerations adopted from [89] and the experimental UP spectrum of bulk-RuO_2 [90], the inactive O-rich phase was assigned to RuO_2 [17].

The LEED intensity analysis performed by Kim et al. [21] showed that, opposite to the opinions of Böttcher et al., the additional spots on the active "O-rich Ru(0001)" surface belong to RuO_2(110). When exposing CO to the active "O-rich Ru(0001)" surface at 200 K, the LEED intensity of the 1×1 spots is not affected, but the intensity of the additional spots, which corresponds to RuO_2(110), is markedly varied, indicating that CO adsorbs only on the RuO_2(110) domains [20]. As discussed in the last section, the CO molecules are held on the Ru(0001)-(1×1)O surface only at temperatures below 80 K. Since the CO oxidation on this surface was suggested [14] to proceed via the LH mechanism, i.e., CO has to be adsorbed on the surface before reaction, that CO adsorbs on the RuO_2(110) domains instead of the (1×1)O domain indicates that the CO oxidation should proceed in the RuO_2(110) domains [21].

In addition, when the surface is exposed to high doses of NO_2 instead of molecular oxygen at 600 K, the surface consists of a (1×1)O overlayer with subsurface oxygen, but there is no indication for the formation of RuO_2 patches, as indicated by the LEED pattern [21]. The surface is also inactive for CO oxidation, although the surface may contain more than 3.0 ML oxygen.

The inactive O-rich surface with a 2×2 LEED pattern was also analyzed by using the LEED intensity analysis. The LEED I–V data of the O-rich 2×2 surface is found to be identical to that of pure $(2 \times 2)3O$ surface with $\theta_O = 0.75$ [21]. Hence, the inactive O-rich 2×2 surface is covered by the $(2 \times 2)3O$ overlayer. The $(2 \times 2)3O$ surface overlayer is distinctly different from a surface Ru-oxide, and any assignment of the 2×2 LEED pattern to an oxide is questionable [21]. The observation of RuO_x in the TD spectra [17] for sample temperatures higher than 1050 K can also be rationalized without introducing a surface oxide for the "O-rich Ru(0001)" surface prepared at 1050 K. At such high temperatures, the dissolved oxygen atoms may migrate towards the surfaces, and therefore desorb partly as RuO_x. In addition, the surface of bulk RuO_2 transforms into a metallic Ru layer upon annealing to 1000 K or higher temperature under UHV conditions [91]. This indicates that the surface was not an oxide surface when it was prepared at T > 1000 K. These results disagree with the opinion that the inactive 2×2 O-rich surface is a surface oxide. In addition, the (110) surface of bulk RuO_2 was found to be able to also react with CO, and the CO/CO_2 conversion rate of impinging CO is also similar to that in the titration experiments with "O-rich Ru(0001)" [21]. This supports the idea that the RuO_2 surface is active in CO oxidation.

Recently, more and more evidence supports the opinion that the active parts of the "O-rich Ru(0001)" surface are the $RuO_2(110)$ patches. RuO_2 powder prepared from aqueous solution (and therefore presumably with some content of water) was recently reported to catalyze CO oxidation even at 295 K [32]. The calculated reaction barrier on $RuO_2(110)$ is considerably lower than that on Ru(0001) [27], indicating a high reactivity of $RuO_2(110)$ for CO oxidation. In the mean time the formation of $RuO_2(110)$ from the O-rich $(1 \times 1)O$ surface had been investigated by DFT calculations [29, 30]. After the on-surface chemisorption is completed, incorporated O agglomerates in sub-surface islands between the first and the second substrate layer, locally destabilizing the metal surface through the separation of an O–Ru–O film from the underlying substrate. Inside these islands the continued oxidation results in the successive formation of such trilayers, which finally unfold into the rutile-bulk-oxide structure after a critical thickness is exceeded [29, 30]. The DFT calculations of Ru 3d and O 1s surface core-level shifts (SCLSs) (including final-state effects) at the Ru(0001)-$(1 \times 1)O$ and the $RuO_2(110)$ surface were performed [24, 28] and the

results are consistent with that in experiments [24].

In this thesis, we have measured the vibrational spectra of differently prepared RuO_2(110) surface. We could differentiate between different oxygen surface species. Furthermore titration experiments show that these oxygen species are active for CO oxidation. This will be discussed in Chapter 6. Our results strongly support that RuO_2(110) patches are the active part of the "O-rich Ru(0001)" surface.

3.3 RuO_2(110) and its structure

As mentioned before, it becomes more and more clear that RuO_2 is responsible for the catalytic activity of the Ru-based catalyst. In order to better understand the following results of adsorption and reaction of CO and oxygen on RuO_2, the structure of RuO_2 should be introduced as follows: The RuO_2 crystal exhibits the rutile structure. The Ru atoms are sixfold coordinated to oxygen atoms, while the O atoms are coordinated to three Ru atoms in a planar sp^2 hybridization. Along the [110] direction this structure can be viewed as a stacking of one RuO and two O layers. A bulk-truncated surface can exhibit three different terminations of (1×1) periodicity, which are shown in Fig. 3.1.

After briefly annealing to 700 K under UHV condition, the RuO_2(110) surface epitaxially grown on Ru(0001), exhibits a termination shown in Fig. 3.1 a, which was determined by using the combination of LEED intensity analysis, DFT calculations and STM measurements [19]. Different from the Ru atom in the bulk, which is six-fold coordinated, the Ru atom at the surface is coordinated to only five oxygen atoms. Thus, it is coordinatively unsaturated. We call it Ru-cus. The other kind of surface atom on the RuO_2(110) surface is oxygen, which sits on a bridge site between Ru atoms, i.e., is coordinated only to two Ru atoms underneath. We call it O-bridge. The Ru atom under the O-bridge is called Ru-bridge. The other type of oxygen atom at the surface, whose coordination is the same as that in the bulk, is called O-layer. Since the Ru-cus site at the RuO_2(110) surface is empty, hereafter we call it the bare RuO_2(110) surface.

When all Ru-cus atoms on the bare RuO_2(110) surface are covered by oxygen atoms, the surface exhibits another termination structure, as shown in Fig. 3.1 b.

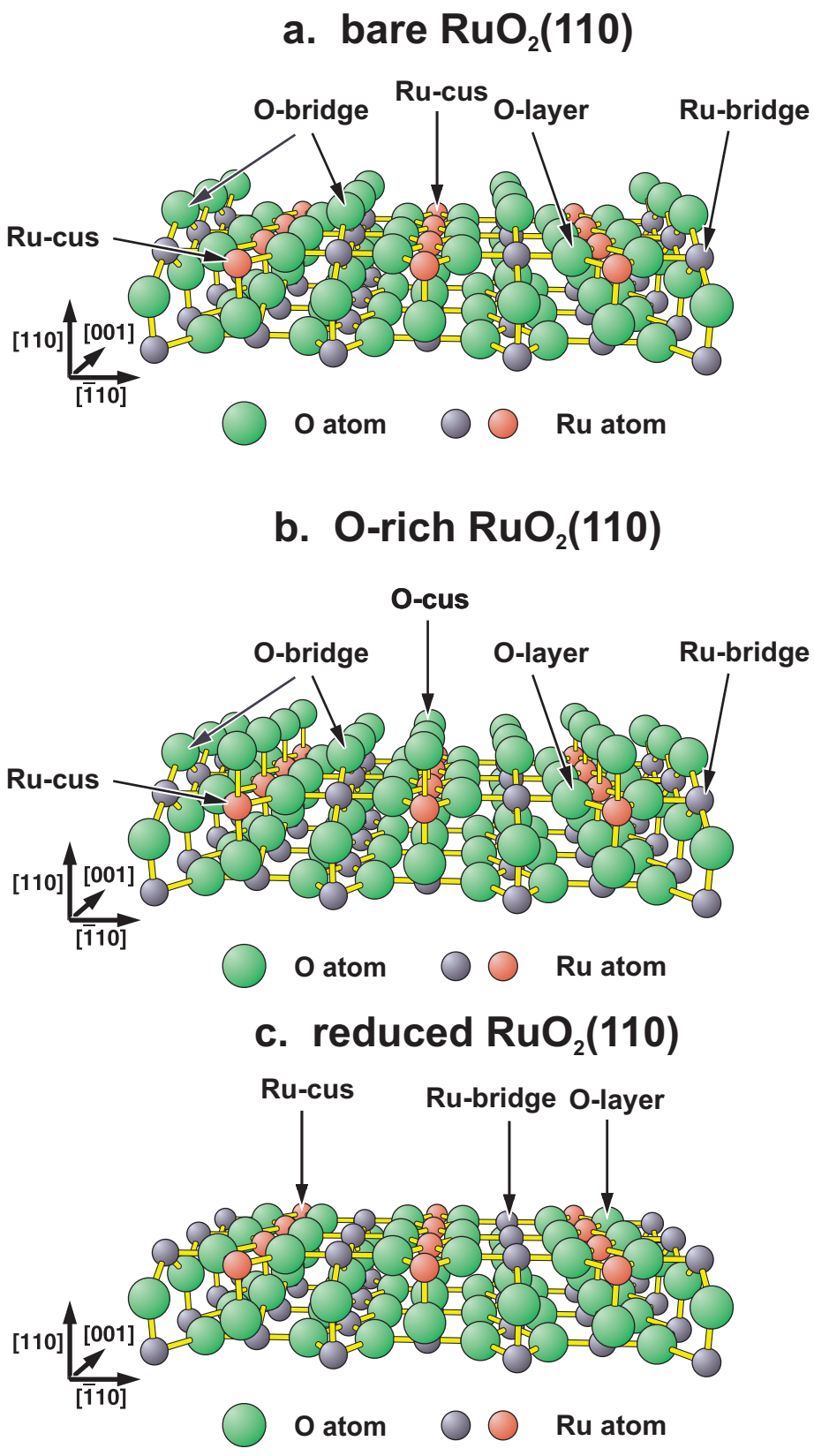

Figure 3.1: Stick and ball model of the $RuO_2(110)$ surface.

We call this surface the O-rich RuO_2(110) surface. The oxygen atom, which sits on a Ru-cus site, is called O-cus.

When all O-bridge atoms are removed, the RuO_2(110) surface is terminated by the RuO layer, as shown in Fig. 3.1 c. We call it the reduced RuO_2(110) surface. Two kinds of Ru atoms, Ru-bridge and Ru-cus, are exposed. The surface is not stable according to the DFT calculations [19, 21, 31].

The hybridization of the O-bridge and Ru-cus atoms on the bare RuO_2(110) surface are very similar to that of the related bulk atoms. Thus, these surface atoms expose a kind of dangling bonds [19]. This feature is responsible for their high chemical reactivity. The Ru-cus atom was thought to be a good candidate for oxygen and CO adsorption. LEED intensity analysis and DFT calculations show that the CO, N_2 and atomic oxygen can be adsorbed at on-top site of Ru-cus [22, 23].

Table 3.2: Comparison of binding energy of O-cus and O-bridge on RuO_2(110) and (1×1)O on Ru(0001) [23]

O species	Ru(0001)–(1×1)O	RuO_2(110)–O-bridge	RuO_2(110)–O-cus
binding energy (eV)	5.07	4.60	3.20

The binding energies of O-bridge and O-cus with the Ru atom underneath have been calculated by using DFT methods [23], and are shown in Table 3.2, together with that of oxygen species on Ru(0001). Obviously, the binding energies of O-cus and O-bridge of RuO_2(110) are significantly smaller than that of oxygen species adsorbed on Ru(0001) (see Table 3.1 on Page 33). Therefore, O-cus and O-bridge are expected to be more active for CO oxidation.

4 Oxygen adsorption on $RuO_2(110)$

4.1 Introduction

As discussed in the last chapter, the surface oxygen-species on $RuO_2(110)$, O-bridge and O-cus, are expected to be very active in CO oxidation. It will be shown in this chapter that the O-cus species correlates with the adsorption properties of oxygen on bare $RuO_2(110)$. Thus, in order to understand the catalytic oxidation of CO on this surface, investigations of its preparation and of the adsorption of oxygen are essential. In this chapter, therefore, the bare $RuO_2(110)$ surface will be studied by using HREELS and the stretching mode of O-bridge against the Ru atom underneath will be identified. The adsorption of oxygen on bare $RuO_2(110)$ at RT as well as at LT was also investigated. The results of HREELS and TDS show that a weakly bonded oxygen species and a molecular oxygen species are created by exposing O_2 to bare $RuO_2(110)$ at LT. The weakly bonded atomic oxygen species will be confirmed to belong to O-cus.

4.2 The bare $RuO_2(110)$

The $RuO_2(110)$ thin layer used in our experiment was prepared by exposing 10^7 L oxygen to Ru(0001) at 700 K. By exposing 6×10^6 L oxygen to Ru(0001) at 600 K, Over et al. prepared an "O-rich Ru(0001)" surface which coexists of both Ru(0001)-(1×1)O and $RuO_2(110)$ patches [20]. It will be shown that the surface under our preparation conditions is completely covered by $RuO_2(110)$ patches. To check the quality of the epitaxially grown $RuO_2(110)$ film, the LEED pattern was studied.

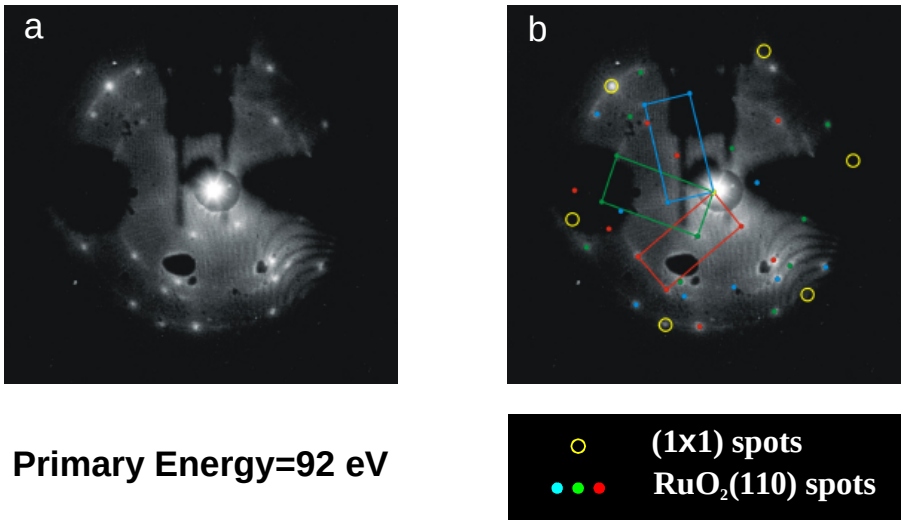

Figure 4.1: The LEED pattern of $RuO_2(110)$ grown on Ru(0001). It was taken after the surface was briefly annealed to 700 K.

Fig. 4.1 shows the LEED pattern of the "O-rich Ru(0001)" surface under our preparation condition. Similarly as in earlier work [19, 20], the LEED pattern is composed of a weak (1×1) hexagonal pattern (marked by open circles in Fig. 4.1b) and of additional spots, which can be attributed to the presence of three rotational domains with a rectangular symmetry as indicated in Fig. 4.1b. These additional spots are due to $RuO_2(110)$, which was derived from LEED intensity analysis and DFT calculations [19, 20]. The diffraction spots of $RuO_2(110)$ are clearer in Fig. 4.1 than those in earlier works [19, 20], while the spots of (1×1) are weaker in Fig. 4.1.

There are two possibilities to explain the existence of (1×1) spots in the LEED pattern. First, there may be coexistence of Ru(0001)-(1×1)O and $RuO_2(110)$ patches, and second, the Ru(0001) surface may be uniformly coated by a very thin $RuO_2(110)$ film and the incident wave field of low-energy electrons diffracted by the underlying substrate is still visible. The stronger spots from $RuO_2(110)$ and weaker spots from (1×1) domains in Fig. 4.1 seem to indicate the latter case.

If the surface prepared under our conditions would be composed of both $RuO_2(110)$ and Ru(0001)-(1×1)O domains, the characteristic loss peak of Ru(0001)-(1×1)O should be detectable by HREELS. The HREEL spectra were taken for the "O-rich Ru(0001)" surface at RT. Curve a in Fig. 4.2 is dominated by a vibrational loss at 69 meV. As shown in curve b of Fig. 4.2, the stretching mode of the chemisorbed

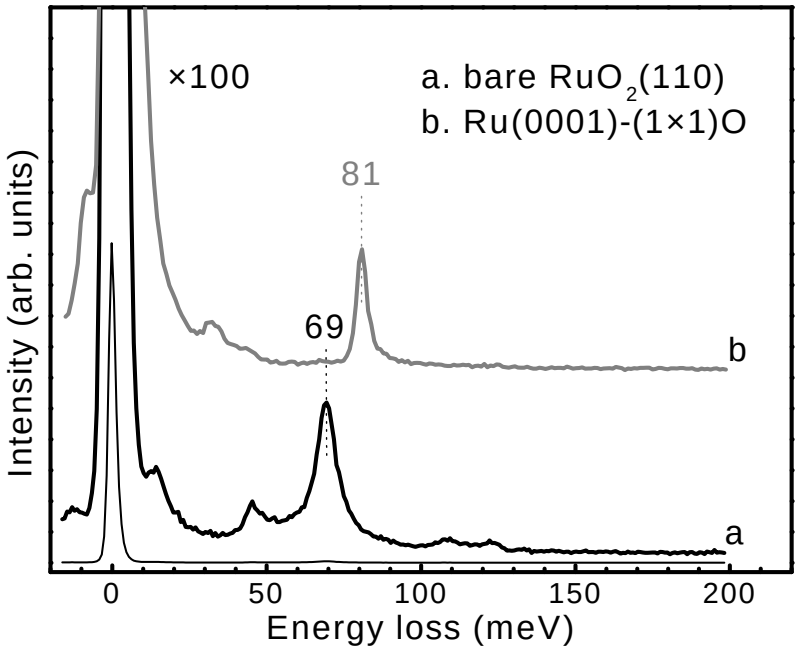

Figure 4.2: HREEL spectra of: (a) bare $RuO_2(110)$ and (b) Ru(0001)-(1×1)O.

(1×1)O on Ru(0001) is at 81 meV [58]. No loss peak around 81 meV can be observed in the curve a. Therefore, it is confirmed that the surface is completely covered by $RuO_2(110)$.

The dominating peak at 69 meV is attributed to the stretching mode of O-bridge against the Ru atom underneath. Since the O-bridge is the major species on the bare $RuO_2(110)$ surface, its dipole moment should be the strongest due to its position on the surface. Furthermore, the value of this peak is consistent with the results of DFT calculations, which have given 63 meV [23]. This supports our assignment that the peak at 69 meV is due to O-bridge.

Normally, for surfaces of polar materials, the HREEL spectra are dominated by strong Fuchs-Kliewer phonons. It should be noted that the spectra of RuO_2 are not disturbed by them. In this case, the Fuchs-Klewer phonons are obviously screened out by the electric conductivity of RuO_2 [92].

The nature of the two weak peaks at 108 and 123 meV is not clear. They may belong to modes of oxygen in the domain boundaries according to the result of a matrix-isolation experiment, in which two vibrational bands for symmetric and asymmetric stretching of the RuO_2 molecule were observed at 112 and 115 meV [93].

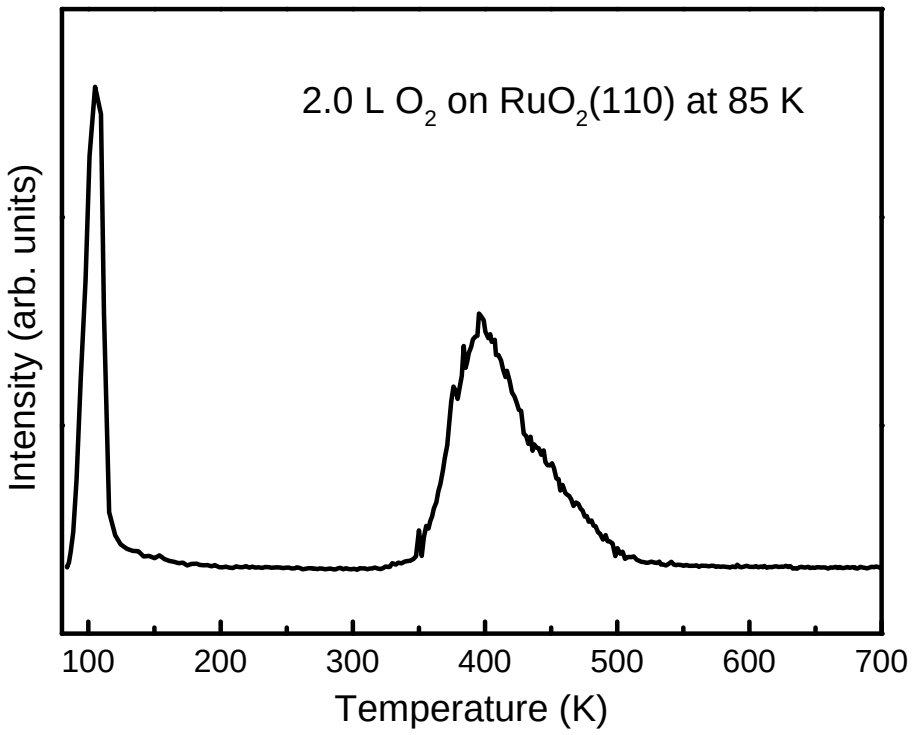

Figure 4.3: TD spectrum after 1.0 L oxygen was exposed to the bare $RuO_2(110)$.

The configuration of the hanging oxygen in that case is similar to the configuration of oxygen in the domain boundary of the bare $RuO_2(110)$ surface. The peak of 45 meV may be the vibrational mode of the O-layer species. Since no isotope shift for the peak was observed, as shown in Fig. 6.3 of Chapter 6 which shows the HREEL spectrum after the O-bridge was replaced by ^{18}O species, the peak is not due to O-bridge. The peak around 15 meV is suggested to be due to the surface phonon.

4.3 Oxygen adsorption on $RuO_2(110)$

In order to study the adsorption of oxygen species on $RuO_2(110)$, the TDS measurement was performed after 1.0 L oxygen was exposed to the bare $RuO_2(110)$ surface at 85 K. The corresponding spectrum is shown in Fig. 4.3. Two desorption peaks, whose desorption maxima are at 105 and 400 K, respectively, appear in the spectrum.

The oxygen species which desorbs around 400 K was attributed to the O-cus

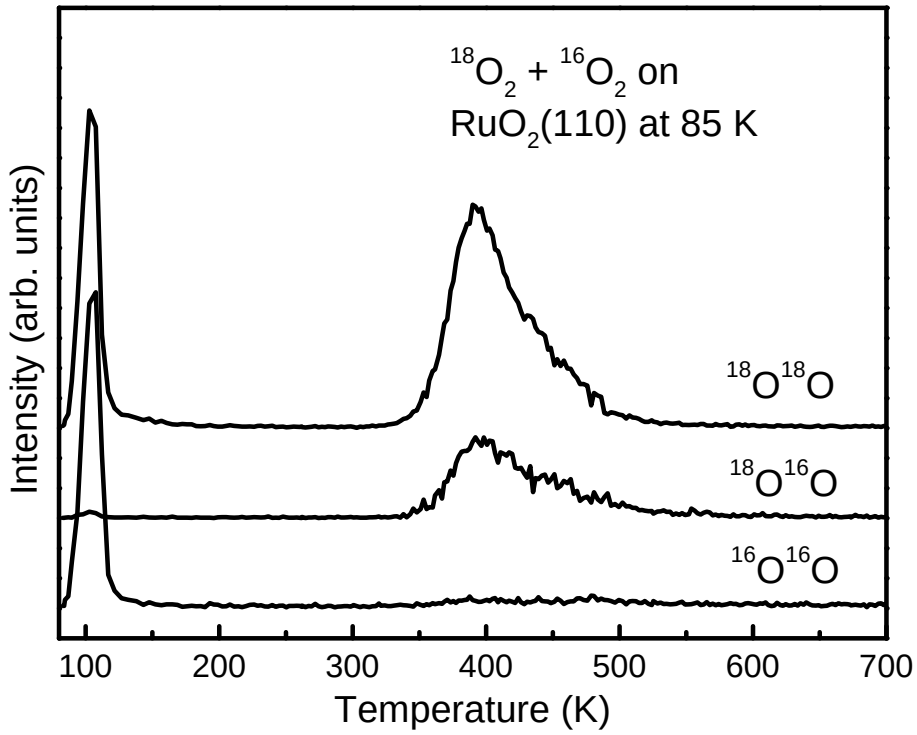

Figure 4.4: TD spectra after dosing 0.5 L $^{18}O_2$ then 0.5 L $^{16}O_2$ at 85 K.

species by using LEED intensity and DFT analysis [21, 31]. In a recent work of Böttcher et al. [15], it was shown that a weakly held oxygen can be created by oxygen postexposure to an "O-rich Ru(0001)" surface which in fact consists of patches of Ru(0001)-(1×1)-O and $RuO_2(110)$. This oxygen species is in fact the O-cus on $RuO_2(110)$. The saturation coverage of O-cus is about 0.8 ML [20, 21]. The reasons are as follows: The dissociation of oxygen needs two neighboring sites. On the other hand, STM images taken at RT indicated that the O-cus species appear almost exclusively as pairs (or multiples of pairs) and exhibit rather limited mobility [25]. For a model which describes the adsorption of dimers on a line of sites, and each dimer taking up two sites, Masel [94] found that the maximum coverage is 0.864.

The other oxygen species which desorbs around 105 K is assigned to a molecular species, because the TD spectra reveal first-order desorption, and the desorption temperature is very low. To confirm this assignment, ^{18}O was used in the TDS measurements. Fig. 4.4 shows the TD spectra taken after dosing 0.5 L $^{18}O_2$ first and then 0.5 L $^{16}O_2$ at 85 K. For the desorption state at 105 K, the desorbed oxygen molecules are only $^{18}O_2$ with mass 36 and $^{16}O_2$ with mass 32, indicating that the

oxygen species is molecularly adsorbed. For the desorption state around 400 K, $^{18}O^{16}O$ molecules with a mass 34, which can only result from the recombination of ^{18}O and ^{16}O atoms, are observed at the same desorption temperature as $^{18}O_2$ and $^{16}O_2$ species, confirming that this oxygen species is atomically adsorbed on the surface.

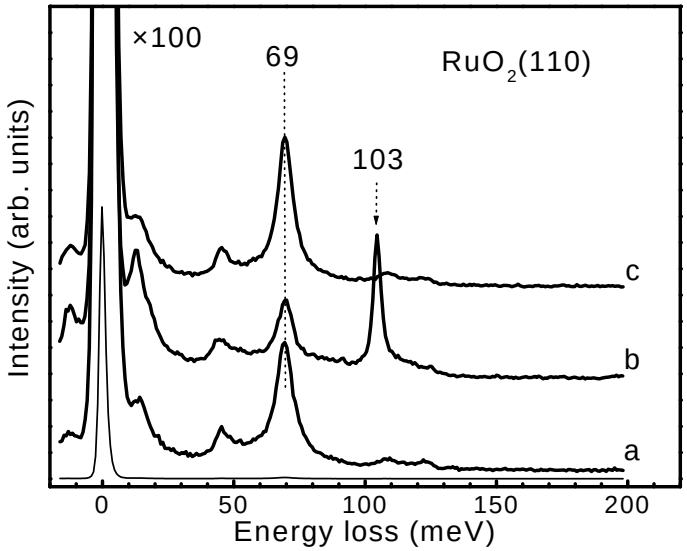

Figure 4.5: HREEL spectra recorded at RT: (a) bare $RuO_2(110)$, (b) after exposing 1.0 L O_2 to bare $RuO_2(110)$ at RT, (c) after heating the surface in (b) to 550 K.

The vibrational properties of the adsorbed oxygen on the bare $RuO_2(110)$ surface were studied by HREELS. First, the HREEL spectrum of the bare $RuO_2(110)$ surface is reproduced in curve a of Fig. 4.5, in which the dominating loss peak is at 69 meV. In order to avoid the influence of the molecular oxygen species, the oxygen was exposed to the $RuO_2(110)$ surface at RT. The spectrum for 1.0 L oxygen exposure is shown as curve b of Fig. 4.5. An additional strong loss peak at 103 meV is observed, which is the dominating peak. Obviously, it is due to O-cus. The intensity of O-bridge is reduced by the new adsorption species. This effect can be attributed to dynamical screening of the O-bridge dipole moment by the presence of the neighboring O-cus with a higher position above the surface. According to the DFT calculations [23], the vibrational energy of the stretching mode of O-cus against the substrate is 99 meV. This again compares favorably with the experimental value of 103 meV. After heating the O-rich $RuO_2(110)$ surface to 550 K (the corresponding spectrum is shown

in curve c), the loss peak at 103 meV disappears, while O-cus desorbs during heating. This further confirms the assignment that the loss peak at 103 meV is the stretching mode of O-cus against the surface.

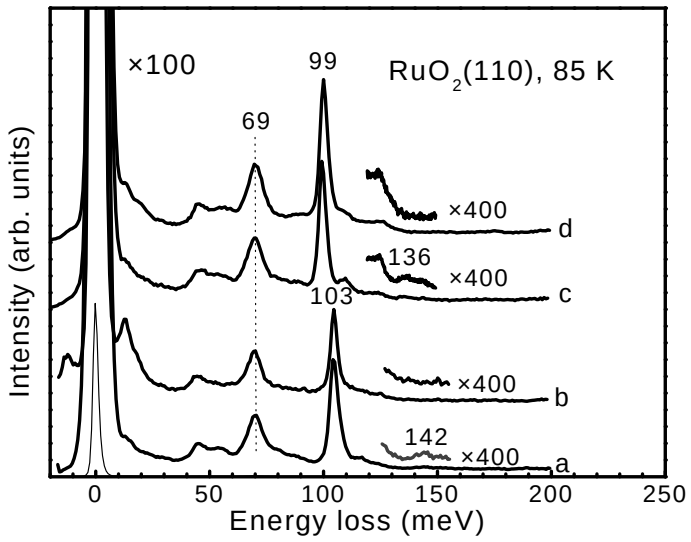

Figure 4.6: The HREEL spectra recorded at 85 K, (a) after exposing 1.0 L $^{16}O_2$ to bare $RuO_2(110)$ at 85 K, (b) after heating the surface in (a) to 150 K, (c) after exposing 1.0 L $^{18}O_2$ to bare $RuO_2(110)$ at 85 K, (d) after heating the surface in (c) to 130 K.

To investigate the vibrational mode of the molecular oxygen species on $RuO_2(110)$, the HREEL spectra were taken after 1.0 L oxygen was exposed at 85 K. Except for the loss peak at 103 meV, which corresponds to the stretching mode of O-cus, an additional weak peak at 142 meV was found in the curve a of Fig. 4.6. After heating the sample to 150 K, the loss peak at 142 meV disappears, as shown in the curve b of Fig. 4.6. According to the TDS, the molecularly adsorbed oxygen desorbs during heating. Thus, the loss peak at 142 meV results from molecularly adsorbed oxygen. In addition, the calculated value of the O–O stretching mode was found to be 134 meV [23], supporting the assignment of the loss peak at 142 meV. According to the results of DFT calculations, this O_2 species is adsorbed with two neighbor Ru-cus sites [23]. The value of 142 meV is in the range of the O–O stretching mode of superoxo-like O_2^- species. Thus, the molecular adsorbed oxygen may be a superoxo-like O_2^- species.

In order to further confirm the assignment that the loss peak at 142 meV results

from the molecularly adsorbed oxygen, 1.0 L $^{18}O_2$ was exposed to the bare $RuO_2(110)$ surface at 85 K. The corresponding spectrum is shown in the curve c of Fig. 4.6. Instead of 142 meV, a loss peak at 136 meV is observed. The loss-energy ratio of this peak between $^{16}O_2$ and $^{18}O_2$ is 1.045 (142/136). Since the vibrational energy is proportional to $1/\sqrt{M}$ (M denotes the mass of an adsorbate), the ratio of the vibrational energies is given by $\sqrt{M_2/M_1}$ for two isotopes with mass M_1 and M_2. The value of 1.045 is near to $\sqrt{M_{^{18}O}/M_{^{16}O}}$ of 1.06 ($M_{^{18}O}$ and $M_{^{16}O}$ denote the mass of the ^{18}O and ^{16}O atom, respectively). Thus, the loss peak at 142 meV results from the molecular oxygen species. As seen in Fig. 4.6, the energy of the O-cus stretching mode shifts from 103 meV for ^{16}O to 99 meV for ^{18}O. This is also due to the isotope effect. In addition, the loss peak at 136 meV for $^{18}O_2$ also disappears after the sample was heated to 130 K. This again supports the assignment to molecular oxygen.

4.4 Summary

In this chapter the oxygen adsorption and the vibrational properties of the bare and the O-rich $RuO_2(110)$ surfaces were studied by TDS and HREELS. The Ru–O stretching energy of O-bridge is 69 meV. By oxygen exposure at RT, oxygen atomically adsorbs on the Ru-cus atoms. This O-cus is weakly bonded to Ru. The Ru–O stretching energy of O-cus is 103 meV. Adsorption of oxygen at 85 K results in two oxygen species. Besides atomic oxygen, O-cus, molecular oxygen is adsorbed at Ru-cus. The O–O stretching mode of the molecular oxygen species is at 142 meV. From this energy we conclude that is a superoxo-like species (O_2^-).

5 Adsorption of CO on $RuO_2(110)$

5.1 Introduction

Genreally, the CO oxidation reaction is believed to follow the LH mechanism [6], i.e., to occur between oxygen and CO accommodated on the surface. To gain a deeper insight into the activity of $RuO_2(110)$, a detailed knowledge of the adsorption of CO and oxygen on this surface is mandatory. The adsorption of oxygen on $RuO_2(110)$ was discussed in the last chapter, and two kinds of atomic oxygen species, O-cus and O-bridge, were identified in HREELS. Similarly, the CO adsorption is also an important step in CO oxidation. The adsorption of CO is complicated at RT because O-bridge of bare $RuO_2(110)$ can react with the impinging CO, which will be shown in this chapter. When the O-bridge is removed, two kinds of Ru sites with different coordination are exposed. Although it was claimed by Over et al. [19] that CO is adsorbed at Ru-cus sites at RT, it will be shown here that this is not the case. In this chapter, the CO adsorption on bare $RuO_2(110)$ was studied using HREELS and TDS. It will be shown that the adsorption of CO on $RuO_2(110)$ at RT is totally different from that at LT due to the high activity of the O-bridge species.

5.2 CO adsorption at LT

The HREEL spectrum of the bare surface is reproduced in curve a of Fig. 5.1. It is dominated by a peak at 69 meV (= 560 cm^{-1}), caused by the stretching vibration normal to the surface of the O-bridge, which was shown in the last chapter.

Due to the high activity of $RuO_2(110)$ for CO oxidation the sample is cooled

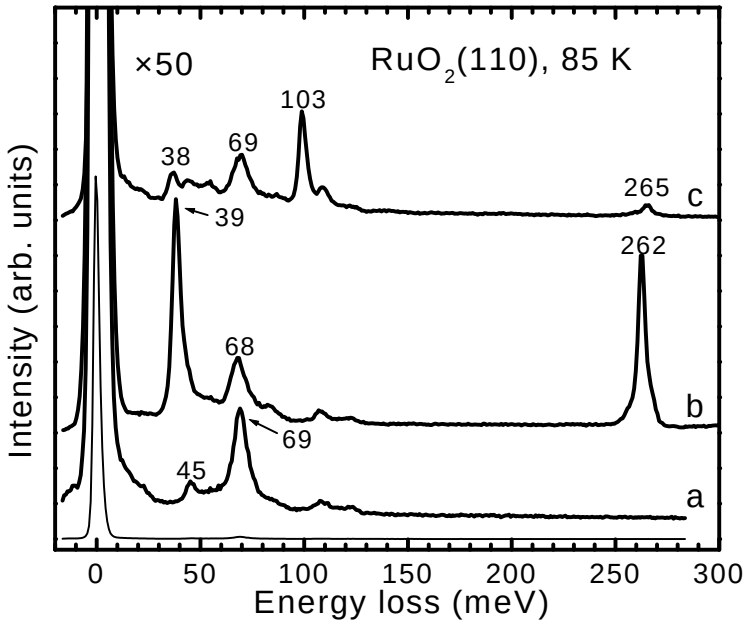

Figure 5.1: HREEL spectra recorded at 85 K: (a) clean surface after preparation at 700 K and cooling down in UHV, (b) after exposure to 1 L CO at 85 K, (c) after exposing the surface first to 0.2 L O_2 and then to 0.2 L CO.

down to 85 K before CO exposure in order to avoid the reaction of CO and oxygen species on the $RuO_2(110)$ surface. After the exposure of 1.0 L CO at 85 K, two new pronounced peaks at 39 and 262 meV (315 and 2115 cm^{-1}, respectively) are observed, as shown in curve b of Fig. 5.1. In general, two strong dipole active stretching modes can be observed in HREEL spectra, when CO is adsorbed on transition-metal surfaces. They are attributed to the S–CO stretching mode of the CO molecule against the surface, ν_{S-CO}, and to the internal C–O stretching mode, ν_{C-O}, respectively. Obviously, the two peaks observed in curve b of Fig. 5.1 belong to the S–CO and C–O stretching modes, according to their vibrational energy.

The bonding mechanism of CO adsorption on transition-metal surfaces is usually described in the Blyholder model [95]. During CO chemisorption on metal surfaces, electrons are donated from the 5σ orbital of the CO molecule into the metal d orbital, strengthening the S–CO (metal–carbon) bond. At the same time, electrons are back-donated from the metal d orbital into the CO $2\pi^*$ orbital, strengthening the S–CO bond again and weakening the C–O bond. When CO adsorbs on a metal surface, the C–O bond is weakened due to the back-donation. The C–O stretching

energy also depends on the coordination of CO on metal surfaces. In general, the relation between the C–O stretching energy and the adsorption site fits the so-called "frequency rule": $\nu_{C-O} > 248$ meV for an on-top site; 248 meV $> \nu_{C-O} > 233$ meV for a twofold bridge site; $\nu_{C-O} < 233$ meV for a higher coordinated site. The ν_{C-O} of CO-cus is around 262 meV, which is near to that of CO in the gas phase, indicating that the CO is an on-top CO species, and the bond between the CO-cus and $RuO_2(110)$ is very weak. The fact that there exists only a single narrow peak in the C-O stretch region excludes the possibility of the existence of any other adsorbed CO species. In particular, substantial adsorption on the O-bridge sites can be ruled out. Therefore, we conclude that CO is adsorbed at the on-top site of Ru-cus on the $RuO_2(110)$ surface at LT.

To further support this conclusion, the next experiment was done, in which the Ru-cus atoms were first capped by O-cus atoms through preexposure to 0.2 L O_2 and subsequently exposed to CO. The corresponding spectrum is shown in curve c of Fig. 5.1. The spectrum exhibits the pronounced peak at 103 meV due to O-cus, while the two peaks of adsorbed CO are very weak in intensity. This indicates that the O-cus atoms inhibit the adsorption of CO. Therefore, it is concluded that CO is adsorbed at a Ru-cus site of the $RuO_2(110)$ surface, which is well in agreement with a recent structure determination (using LEED intensity analysis and DFT calculations) for a CO layer saturated at 100 K [21]. ν_{C-O} is quite large and near to the value of CO in the gas phase (265 meV), indicating a very weak back-donation for this CO species. Since the charge distribution of Ru-cus is perpendicular to the surface like a dangling bond, the overlap between the d orbital of Ru-cus and the $2\pi^*$ orbital of CO is not so strong. This induces the very weak back-donation from the Ru orbital into the CO $2\pi^*$ orbital, according to the Blyholder-model. Therefore, the vibrational energy of the C–O stretching mode is near to the value of CO in the gas phase, and the bond of the CO is very weak.

Comparing the curves a and b in Fig. 5.1, one recognizes that the intensity of the O-bridge peak at 69 meV is reduced by CO adsorption. This effect is attributed to the dynamical screening of the O-bridge dipole moment due to the presence of the neighboring CO-cus species. Removal of the latter by thermal desorption is hence expected to restore the initial intensity of the O-bridge peak. This effect is not observed from the inspection of spectra a and b in Fig. 5.2: The data recorded after

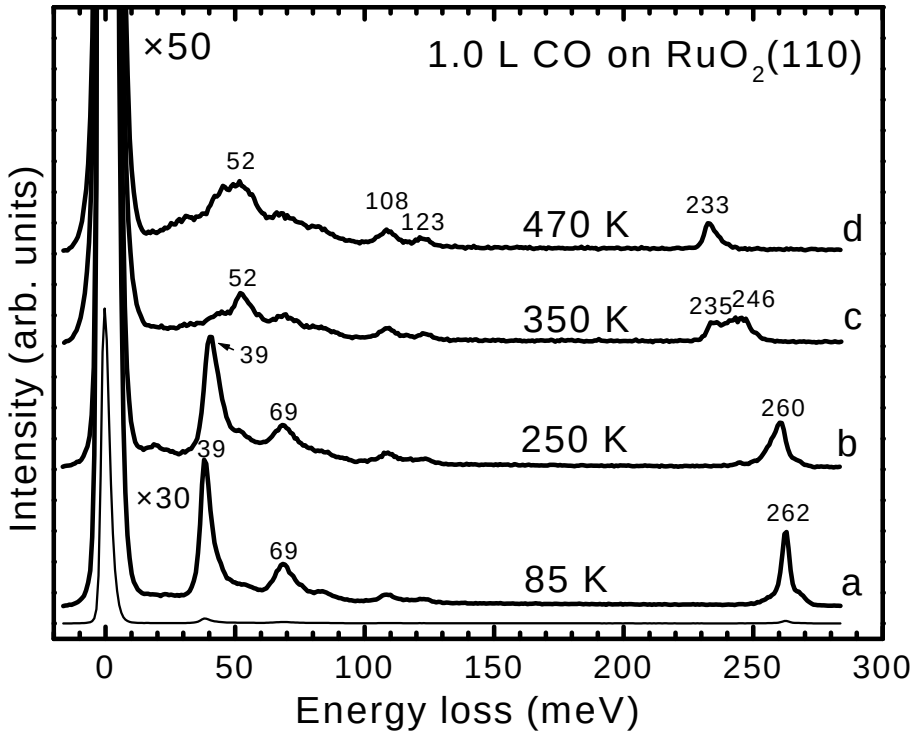

Figure 5.2: HREEL spectra (a) after exposure to 1 L CO at 85 K and (b-d) after subsequent short heating to the temperatures indicated.

exposing the $RuO_2(110)$ surface to 1.0 L CO at 85 K are analogous to those of the curve b in Fig. 5.1. After briefly annealing to 250 K (curve b in Fig. 5.2), not only the intensity of the CO features at 39 and 262 meV has decreased, but also that of O-bridge at 69 meV. This suggests that this type of thermal treatment already consumes part of the O-bridge atoms. For completeness we note that the weak peaks at 108 and 123 meV are intrinsic features of $RuO_2(110)$ [23] which are not influenced by adsorbates. After annealing to 350 K, the two loss peaks around 39 and 262 meV vanish and the new peaks at 50, 220 and 245 meV appear. These loss peaks are still from CO species. The broad peak at 50 meV is due to the stretching mode (or modes) of CO against the surface. Thus, this CO is more strongly bonded to the surface than CO-cus observed after adsorption of CO at 85 K. Its bonding site will be identified in the following.

First, we performed TDS experiments which are reproduced in Fig. 5.3. The fill points mark the evolution of CO (squares) and CO_2 (circles) during heating the surface with a rate of 3 K/s after 1.0 L CO exposure at 85 K. Apart from the desorption

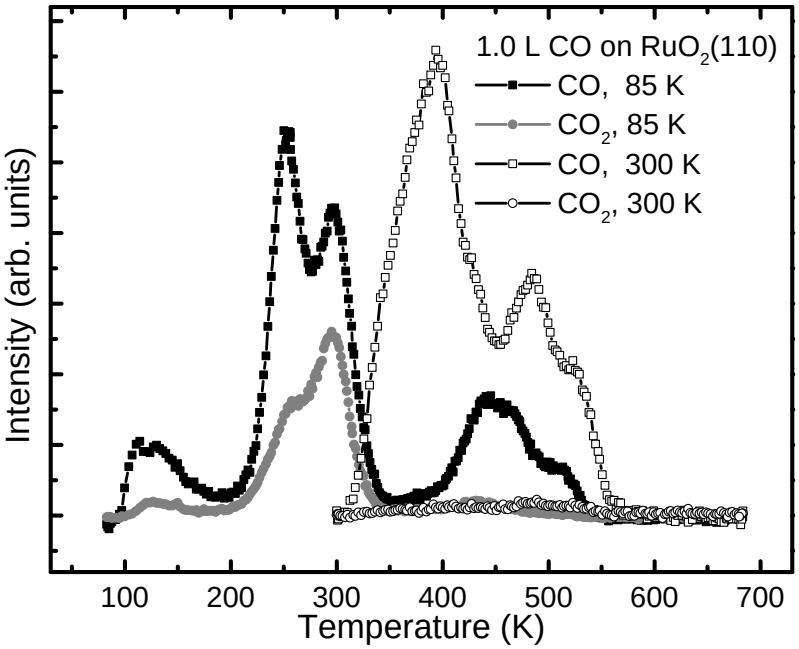

Figure 5.3: Thermal desorption spectra for CO and CO_2 after exposing the surface to 1 L CO at 85 K and at 300 K. The heating rate is 3K/s.

of CO with peaks around 250 and 300 K, there is also a pronounced formation of CO_2 with a maximum rate at 300 K. (The additional CO desorption maximum around 450 K will be discussed later.) It is still not clear why CO desorbs in two states since the HREELS data at 85 K exhibit only one single species. Presumably the repulsive interactions between adsorbed CO molecules will be reduced by lowering the coverage during desorption which will cause an increase of the desorption temperature. The observation of a red shift by 3 meV (24 cm^{-1}) of ν_{C-O} by raising the temperature from 85 to 250 K may be attributed to the reduction of dipole coupling by increasing the mutual CO distances. It might, however, be of the similar origin as that in the CO/Ru(0001) system where this effect was explained by increasing inharmonic coupling between different vibrational modes [96]. A desorption temperature around 300 K for the CO-cus species is consistent with the theoretical value of 1.2 eV for the adsorption energy from DFT calculations [19, 22]. The evolution of CO_2 in the same temperature range indicates that thermal activation of the adsorbed CO leads, apart from desorption, also to a reaction with neighboring O-bridge species, and hence to the decrease of the intensity of the vibrational band at 69 meV in the curve b of Fig. 5.2. That the CO oxidation reaction occurs at the same temperatures

as the desorption may be explained with the, compared to metal surfaces, unusually high diffusion barrier of CO of 1.0 eV across the Ru-cus atoms [22]. The observation of CO_2 and the weakening of the O-bridge peak indicate that O-bridge is removed from the surface. The removing of O-bridge creates coordinatively unsaturated Ru-bridge sites which may serve as adsorption sites for CO. In order to elucidate this idea further, we performed CO adsorption at RT as described in the following.

5.3 CO adsorption at RT

Fig. 5.2 and Fig. 5.3 show that CO can react with O-bridge at RT. Therefore, the adsorption of CO at RT will be totally different from that at LT. This is confirmed by the TDS measurement after 1.0 L CO exposure to the $RuO_2(110)$ surface at RT. The open circles in Fig. 5.3 demonstrate that, following CO exposure at 300 K, no CO_2 formation takes place any more. Thus, thee O-bridge atoms have already been consumed during the CO exposure at RT. Over et al. [19] claimed that CO bonds stationarily to the Ru-cus atom and the O-bridge remains on the surface, which is similar to that at LT. Obviously, this is wrong according to the TDS results since the O-bridge has been consumed by the CO exposure at RT.

Fig 5.4 shows the HREEL spectra taken after increasing the CO exposure at RT. No band at 262 meV as characteristic for CO adsorbed on Ru-cus is discernible. Instead, the O-bridge band at 69 meV first decreases in intensity, and then disappears. These spectra prove that CO consumes O-bridge immediately, leading to the creation of new CO adsorption sites above the Ru-bridge atoms. Two bands at 235 and 245 meV (1895 and 1975 cm^{-1}, respectively) in the C–O stretching vibration region grow after most of O-bridge is consumed. The associated peak for the S–CO vibration is located at 52 meV. The fact that the shape and the splitting of these bands vary with increasing coverage (cf. curves b to d in Fig. 5.4) suggests the operation of effects of partial structural transformation and/or lateral interactions between the adsorbates. Anyway, the energies of these bands are substantially lower than that of the CO/Ru-cus species, suggesting a more pronounced "back-donation" in bond formation and a stronger adsorption bond. This is indeed confirmed by the TDS data shown in Fig. 5.3 (open squares): There are two desorption maxima around 400 and 500 K. These temperatures are similar to the value of CO on typical

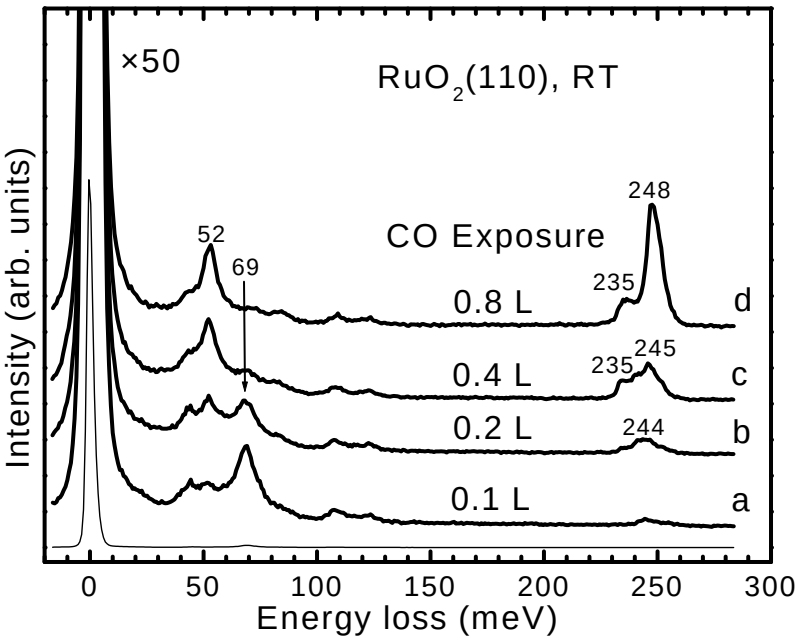

Figure 5.4: HREEL spectra after different CO exposures at 300 K.

transition metal surfaces. In fact, the desorption of CO from a Ru(0001) surface takes place around 450 K [44], and hence the high-temperature desorption peak in Fig. 5.3 indeed reflects similar bonding properties as that with bulk-Ru.

When the O-bridge is removed, the Ru-bridge site is liberated. Therefore, two kinds of Ru sites, Ru-cus and Ru-bridge, are available for CO adsorption. Due to the totally different properties between the CO species exposed at RT and LT, which were shown in the HREEL and TD spectra, the CO species exposed at RT does not occupy Ru-cus. Thus, the CO species is adsorbed at the Ru-bridge site (we call it CO-bridge). After removing the O-bridge atoms, the Ru-bridge atom is more "electron-rich" than Ru-cus, so that the back-donation from Ru-bridge into CO $2\pi^*$ orbital is stronger than that from Ru-cus. This fits well to the observation that the C–O stretching energy is obviously lower for CO exposure at RT than at LT. In addition, the Ru-bridge site offers two dangling bonds for CO to bond with. Therefore, it is expected for CO to preferentially adsorb above the Ru-bridge site.

In order to confirm this conclusion, whereupon CO adsorbs at a Ru-bridge site as soon as the O-bridge species is removed, the following experiment shown in Fig. 5.5 was performed: After an 1.0 L CO exposure at 300 K (curve a in Fig. 5.5), the sample was cooled down to 85 K, and then exposed to 0.5 L O_2 (curve b in Fig. 5.5). The

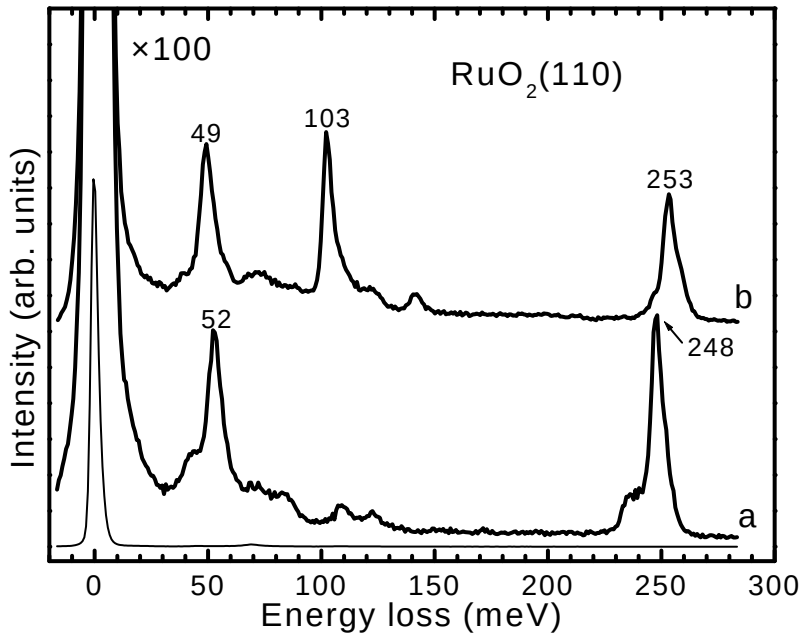

Figure 5.5: HREEL spectra (a) after exposure of 1 L CO at 300 K and (b) same as (a) with an additional exposure of 0.5 L O_2 at 85 K.

appearances of losses at 103 and 142 meV correspond to the weakly bound atomic and the molecular oxygen species, respectively. Both oxygen species are adsorbed at Ru-cus sites. This clearly demonstrates that CO does not occupy these Ru-cus sites. Thus, CO should adsorb at the Ru-bridge site.

Now, also the remaining features in Fig. 5.3 for the experiment at 85 K, namely the additional release of CO around 450 K can be readily explained. During increasing temperature, some of the Ru-bridge atoms on the surface are liberated from their O-bridge atoms by the reaction with CO, and part of the CO molecules, initially weakly adsorbed at Ru-cus sites, move over to these Ru-bridge sites, from which they desorb only at the higher temperature. The HREEL spectra c and d in Fig. 5.2 reflect this effect of site exchange.

Two kinds of CO-bridge species appear in the HREEL spectra with C–O stretching energies of 235 and 245 meV, respectively. Obviously, the loss peak at 235 meV corresponds to CO adsorbed at a bridge site of Ru-bridge. Since the 245 meV is between the typical energy of an on-top and a bridge CO, the adsorption site of the CO is expected to be a near on-top site, i.e., bonded mainly with one atom but not on a standard on-top site. Interestingly, our proposed model was fully confirmed

by a more recent LEED intensity and DFT analysis [26]. Indeed, at low coverage the CO was found to bond to two Ru-bridge sites at a bridge site. For higher CO coverage CO is bonded only to one Ru-bridge atom in a bent configuration. The latter agrees with our on-top orientation. The interesting result is the finding that CO takes an inclined configuration.

From the result presented for CO adsorption at RT, it is completely clear that CO reacts with O-bridge first, then adsorbs on Ru-bridge. This is in contradiction to the conclusion of Over et al. [19], in which the CO molecule was suggested to adsorb at a Ru-cus site at RT by using LEED intensity analysis, DFT calculations and STM images. What might be responsible for these discrepancies? First, the DFT calculations do not include the fact that CO can react with O-bridge by exposure at RT. Second, they got the similar conclusion according to the LEED measurements performed at LT, as shown in their other paper [20], but the surface by CO exposure at RT is actually different from that at LT. Thus, something should be wrong in their experiments. Third, their interpretation for their STM images is questionable. The bright rows in their STM images were assigned to O-bridge. The authors acknowledged [19] that this assignment is unusual since it differs from the clean TiO_2(110) surface and the imaging of O-bridge is sensitively affected by the state of the STM tip [97]. Under similar tunneling conditions the oxygen atoms in the Ru(0001)-(2×2)O phase were imaged as dark spots [98].

5.4 Summary

At LT the CO molecule adsorbs at Ru-cus, but as soon as the temperature reaches values around 250 K, CO either desorbs or reacts with neighboring O-bridge atoms, decapping the underlying Ru-bridge atoms. The bare Ru-bridge forms stronger adsorption bonds with CO than Ru-cus. Thus, contrary to the previous suggestion [19], Ru-cus is not able to stabilize CO at RT. It is concluded that for the temperature above 250 K, Ru-cus acts only as transient adsorption site from which CO and presumably other adsorbate species may be supplied, thus enabling the rather remarkable catalytic activity of this system.

6 CO oxidation on $RuO_2(110)$

6.1 Introduction

The "O-rich Ru(0001)" surface, which contains more than 3 ML oxygen, was found by Böttcher et al. [13] to be very active for CO oxidation. They interpreted their results based on the assumption that the high reactivity of the surface is due to the presence of subsurface oxygen. Unfortunately, their discussions were not on the atomic scale because the structure of the "O-rich Ru(0001)" surface was unknown. They found that the reaction proceeded through an active on-surface oxygen species at T $<$ 450 K and was determined by oxygen diffusion from the near-surface region toward the surface at T $>$ 500 K [14]. In addition, by post-exposing oxygen to the "O-rich Ru(0001)" surface, a weakly held oxygen species was created, which was very active for CO oxidation [15]. This oxygen species is actually O-cus, as shown in Chapter 4.

More recently, it was shown that the active part of "O-rich Ru(0001)" is $RuO_2(110)$ [19, 20]. The CO oxidation on the $RuO_2(110)$ surface was suggested by Over et al. [19] to proceed between CO-cus and O-bridge, according to DFT calculations and STM measurements. The reaction barrier and the reaction pathway between CO-cus and O-bridge were studied by Liu and Hu using DFT calculations [27]. It was suggested that the high reactivity of O-bridge is due to the electronic charge and potential energy surface around O-bridge. As shown in Fig. 5.4 of the last chapter, CO reacts with the O-bridge of the bare $RuO_2(110)$ surface during CO exposures at RT.

In fact, the reaction proceeds not only between O-bridge and CO-cus. This will

be shown in this chapter. In the last two chapters, the adsorption of oxygen and CO on the $RuO_2(110)$ surface was studied, and the different oxygen and CO species, O-bridge, O-cus, CO-bridge and CO-cus, were identified in HREELS. This gives us the opportunity to do titration-type experiments. On the O-rich $RuO_2(110)$ surface we can discriminate between different oxygen species, which interact with CO. In this chapter it will be shown that the reaction proceeds via two reaction channels by reaction of CO with O-cus or O-bridge. Furthermore, it will be shown that the oxygen, consumed in the CO oxidation reaction, can be fully restored at room temperature.

6.2 CO oxidation on bare and O-rich $RuO_2(110)$

When CO is exposed to the bare $RuO_2(110)$ surface, CO can react with O-bridge immediately, as shown in the Fig. 5.4 of the last chapter. When O-bridge is removed, CO adsorbs on the Ru-bridge site. Since the binding energy of O-cus on Ru-cus is smaller than that of O-bridge on Ru-bridge, O-cus is expected to be very reactive in CO oxidation. To investigate the reaction channels of CO oxidation on an O-rich $RuO_2(110)$ surface, the following experiments were performed: First, 1.0 L O_2 was exposed to the bare $RuO_2(110)$ surface, inducing a nearly saturated surface. Second, CO was sequentially exposed to the surface, and the HREEL spectra were recorded accordingly.

Fig. 6.1 shows the respective HREEL spectra. Two loss peaks at 69 and 103 meV, which correspond to the O-bridge and O-cus species, respectively, are shown in the bottom curve. With increasing CO exposure, the loss peak at 103 meV decreases continuously. No CO-induced feature is observed for CO exposures less than about 1.0 L, suggesting that the intermediately adsorbed molecules react rapidly with the O-cus species. The presumably formed CO_2 is not stable at 300 K and desorbs immediately. The decrease of the loss peak at 103 meV is accompanied by a recovery of the loss peak at 69 meV due to a reduced screening. In order to see the change of loss peaks corresponding to the different surface species, the intensity (Gaussian peak areas) of the oxygen loss peaks at 69 and 103 meV and of the C–O stretching mode at 235 and 245 meV was derived and is shown in Fig. 6.2 as a function of CO exposure.

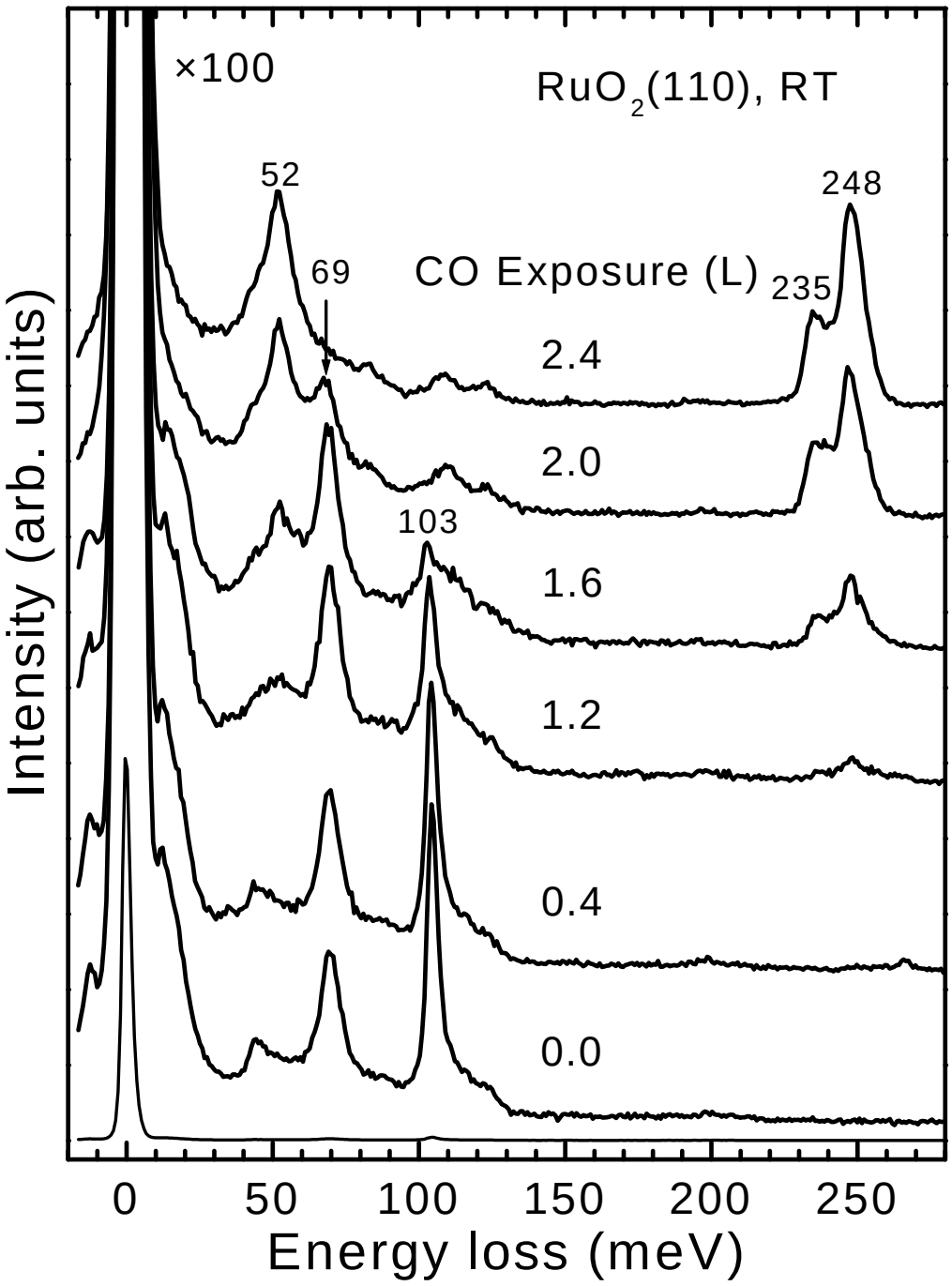

Figure 6.1: HREEL spectra for $RuO_2(110)$ saturated with O-cus (exposure 1.0 L O_2) and different exposures of CO at 300 K.

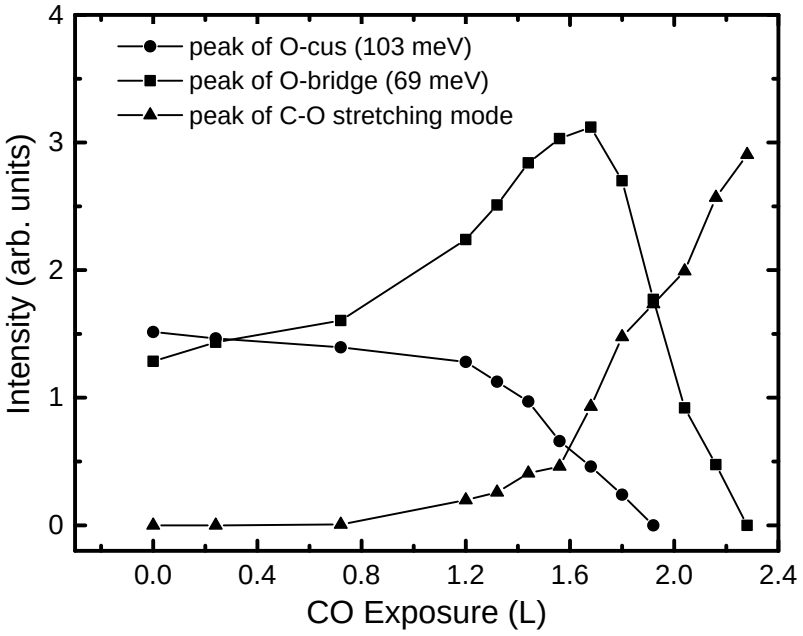

Figure 6.2: Variation of the HREELS intensities with CO exposure for the loss peaks of O-bridge at 69 meV, of O-cus at 103 meV, and of the C–O stretching modes. The data were collected from a sequence of spectra similar to those in Fig. 6.1.

Fig. 6.2 clearly shows that the O-cus intensity decreases continuously, slowly first and more quickly later, up to an exposure of about 1.9 L. At about 1.2 L, the first losses of chemisorbed CO are observed. Interestingly, after about 70 % of O-cus are reacted off, the intensity of the O-bridge loss peak starts decreasing, and that of the C–O loss peak starts increasing. This means that the reaction channel of CO with O-bridge is open only at low concentration of O-cus. After an exposure of 2.4 L, both oxygen species, O-cus and O-bridge, are almost completely removed. During the removal of O-bridge, an increasing amount of CO is chemisorbed at the surface, which is similar to the case of CO exposure to the bare $RuO_2(110)$ surface. Clearly, the reactions of CO with O-cus and O-bridge are independent of each other, because CO can also react with O-bridge by CO exposure to the bare $RuO_2(110)$ surface, i.e., the reaction with O-bridge is not affected by an eventually preceding reaction with O-cus.

From these findings we can derive the following model: There are two independent reaction channels for the CO oxidation: (1) If there is O-cus on the surface, CO reacts

according to

$$\mathrm{CO-cus + O-cus \longrightarrow CO_2 \uparrow} \quad . \tag{6.1}$$

This is the main oxidation channel as long as O-cus is present. To react with O-cus, CO has to be adsorbed at a Ru-cus site. This is concluded from our data because the reaction rate is slow at the beginning when most Ru-cus sites are occupied by O-cus. As the number of O-cus atoms decreases, more Ru-cus sites become available and the reaction rate increases. Probably, this reaction was recently observed on the O-rich surface [15].

If most of O-cus is reacted off, the second oxidation channel opens up:

$$\mathrm{CO-cus + O-bridge \longrightarrow CO_2 \uparrow} \quad , \tag{6.2}$$

i.e., on the bare $RuO_2(110)$ surface the bridge oxygen can also react with CO. At a high concentration of O-cus, this reaction channel is inhibited. According to their DFT calculations, Liu and Hu suggested [27] that the high activity results from the nature of O-bridge on the oxide surface. Thus, it is possible that the existence of O-cus affects the electronic charge and potential energy surface around O-bridge, so that the reactivity of O-bridge is reduced. The other point is that the reaction barrier between O-cus and CO is lower than that between O-bridge and CO, so that more CO reacts primarily with O-cus until most of O-cus is removed. When most of O-cus is removed, the concentration of O-bridge is obviously higher than that of O-cus. Therefore, the reaction between O-bridge and CO becomes the main reaction channel (6.2). Also in this reaction, CO has to adsorb at a Ru-cus site first. The speed of O-bridge consumption is appreciably higher than that of O-cus consumption, nevertheless, CO reacts with the O-cus first. It is reasonable to suggest that this is because there are more empty cus-sites on the bare $RuO_2(110)$ surface, and CO has to adsorb at a Ru-cus site first before any reaction with O-bridge can occur.

6.3 Restoration of the $RuO_2(110)$ surface

The O-bridge species can be completely removed during CO oxidation. Thus, the question arises whether the surface state after previous CO oxidation can be restored.

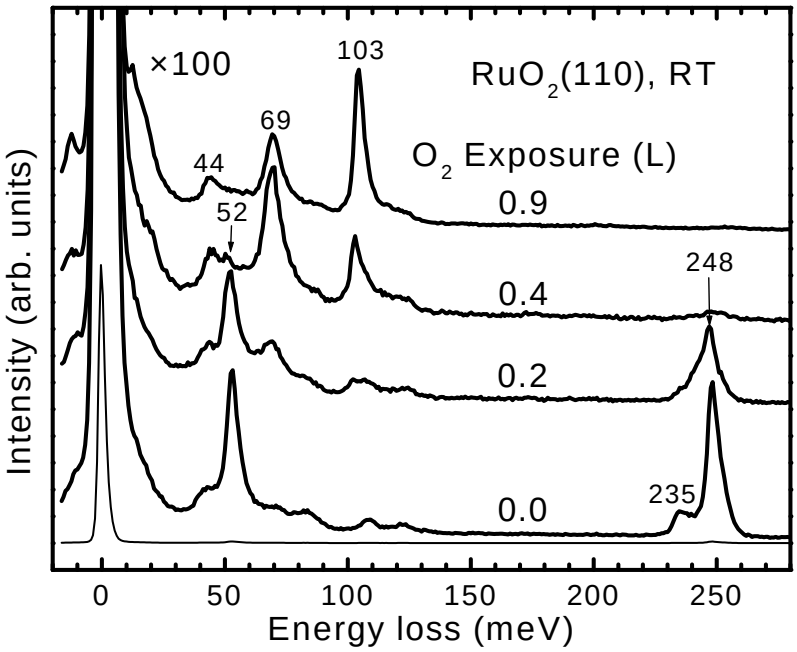

Figure 6.3: HREEL spectra of a $RuO_2(110)$ surface after the reaction with 1.0 L CO at 300 K and for additional exposure of O_2 at 300 K.

We performed HREELS measurements, after a series of O_2 exposures were applied to the CO-covered $RuO_2(110)$ surface.

Figure 6.3 shows the result. First, O_2 reacts with adsorbed CO on the $RuO_2(110)$ surface. Second, after CO is removed, oxygen can restore O-bridge and then O-cus. When we compare the uppermost curve of Fig. 6.3 with curve b of Fig. 4.5 in Chapter 4 and the bottom curve of Fig. 6.1, it can be recognized that the $RuO_2(110)$ surface is almost completely restored by dosing 0.9 L O_2. It is known that, after the CO-covered $RuO_2(110)$ surface is briefly heated to 600 K, the subsequently recorded STM image exhibits the formation of holes in the originally perfect $RuO_2(110)$ surface [19]. The RuO_2 surface with many holes can only be restored when the surface is exposed to O_2 at elevated temperatures or is simply heated to 700 K [19]. Remarkably, in our experiments, dosing O_2 at RT can remove all CO and restore the formerly CO-covered surface afterwards. It shows that the surface is not partially damaged during CO oxidation at RT. This means that only surface oxygen, either weakly adsorbed as O-cus or from the lattice as O-bridge, takes part in the CO oxidation reaction. Interestingly, the surface state is readily shifted between an oxidized and a reduced one by varying the relative oxygen exposure, establishing a remark-

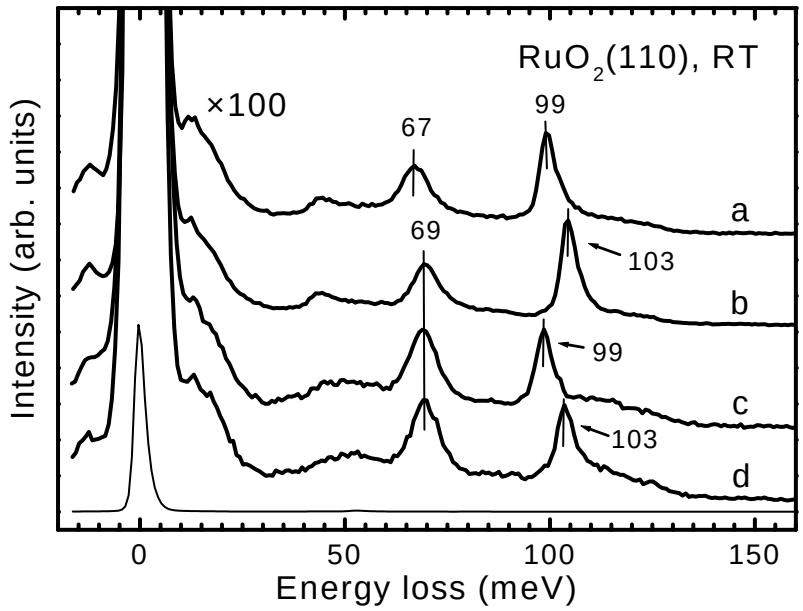

Figure 6.4: HREEL spectra for differently prepared and reacted $RuO_2(110)$ surfaces as indicated. The following gas exposures were applied to the bare $RuO_2(110)$ surface: curve a: first 1.0 L CO and then 1.0 L $^{18}O_2$; curve b: first 1.0 L CO and then 0.9 L $^{16}O_2$; curve c: first 1.0 L $^{18}O_2$ and then 1.2 L CO; curve d: first 1.0 L $^{16}O_2$ and then 1.2 L CO.

able surface redox system. Also, we expect that under steady-state flow conditions an oxygen-deficient surface will exist whose stoichiometry will be determined by the ratio of partial pressures.

So far, we have interpreted the results shown in Figs. 6.1, assuming that CO reacts first with O-cus, when O-cus and O-bridge are both on the surface, and then with O-bridge, when O-cus is mostly removed. Interestingly, another reaction sequence is conceivable in which CO would always react with O-bridge which would then be rapidly replaced by an O-cus. In order to exclude this reaction sequence, we performed a number of isotope-substitution experiments, as shown in Fig. 6.4. In these experiments we always started with the bare $RuO_2(110)$ surface, i.e., with all O-bridge sites filled but without any O-cus on the surface. For curves a and b of Fig. 6.4, an exposure of 1.0 L CO has removed O-bridge completely. A following exposure of O_2 has restored O-bridge and O-cus. That this is the case is recognized from the isotope shift of 2.5 meV for O-bridge and 4.0 meV for O-cus if we expose

$^{18}O_2$ instead of $^{16}O_2$.

For curve a in Fig. 6.4, both O-bridge and O-cus are occupied by ^{18}O, and both stretching frequencies have experienced an isotope shift to lower energy. Curve b in Fig. 6.4 shows the same restoration performed with ^{16}O. For curves c (^{18}O) and d (^{16}O), we have first filled the O-cus state with 1.0 L O_2. An exposure of 1.2 L of CO will empty the O-cus state by about 50 %. If CO would always react with O-bridge, the O-bridge loss peak in curve c would be isotope shifted to smaller energy, as it would be filled up with ^{18}O from the Ru-cus site after reaction with CO. This is not the case, so that our interpretation of the CO reaction sequence, first with O-cus and then with O-bridge, is verified.

Finally, there is a further question to be answered by the isotope experiment. We have seen in Fig. 6.1 that the loss peak of O-bridge (69 meV) disappeared after exposing CO. Instead of removing O-bridge through reaction with CO to CO_2, one may wonder whether the energy loss due to O-bridge is shielded by CO. This possibility is excluded by the experiment of curve a in Fig. 6.4. If O-bridge would not have been removed, it would not have been restored by ^{18}O.

6.4 Coadsorption of CO and oxygen on $RuO_2(110)$

The CO oxidation in real catalysis does not proceed by exposing CO to a bare or O-rich $RuO_2(110)$ surface, or by exposing oxygen to a CO-covered $RuO_2(110)$ surface, but CO and oxygen are simultaneously exposed to the surface. Hence, in real catalysis, the surface exhibits a mixture of CO and oxygen on the surface. In contrast to metal surfaces, the $RuO_2(110)$ surface is composed of two types of Ru atoms with different coordinations, Ru-cus and Ru-bridge. Under different conditions, the two kinds of Ru sites can be occupied by either CO or O, which results in CO-cus, CO-bridge, O-cus or O-bridge, respectively. The CO_2 formation might take place between these CO and oxygen species. When heating a mixture of CO and oxygen and then measuring the dependence of the desorption and reaction products on the temperature, i.e., measuring the TDS of the coadsorption phase, the kinetic properties of CO_2 formation can be obtained. The coadsorption phase of O-bridge and CO-bridge can be prepared at RT, as shown in Fig. 5.4 of the last chapter. After

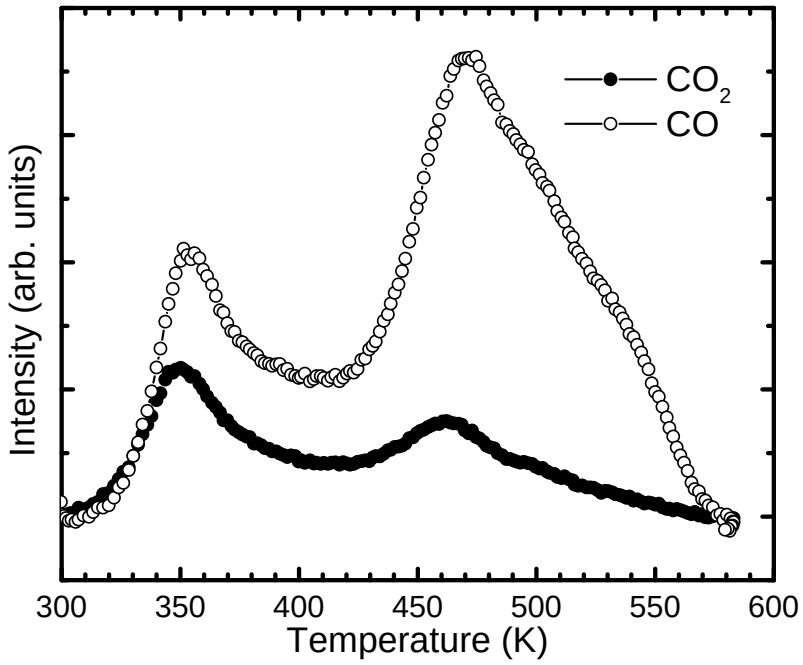

Figure 6.5: TD spectra after 0.2 L CO exposure to the bare $RuO_2(110)$ surface at RT.

0.2 L CO exposure to the bare $RuO_2(110)$ surface at RT, both loss peaks of CO-bridge and O-bridge were observed. As discussed in the last two sections, O-cus and O-bridge react immediately with CO at RT, and CO-bridge also reacts immediately with oxygen at RT. Obviously, CO-cus with O-cus and O-bridge or CO-bridge with O-cus species cannot coexist on the $RuO_2(110)$ surface at RT. Hence, $RuO_2(110)$ should be cooled to LT in order to prepare these coadsorption phases.

When exposing CO to the bare $RuO_2(110)$ surface at LT, O-bridge and CO-cus are coadsorbed, as shown in Fig. 5.3 of the last chapter. CO_2 (filled circles) desorbs with peaks around 250 and 300 K, which is in the same temperature range as the CO desorption. This indicates that thermal activation of the adsorbed CO leads to desorption and reaction at the same time.

A $RuO_2(110)$ surface, on which CO-bridge and O-bridge are coadsorbed, can be created by 0.2 L CO exposure to the bare $RuO_2(110)$ surface at RT, as shown in Fig. 5.4. The TD spectra of this surface are presented in Fig 6.5. Interestingly, the CO_2 formation occurs at the same temperatures as the desorption of CO, which is around 350 K. In addition, another kind of CO desorption species around 500 K is

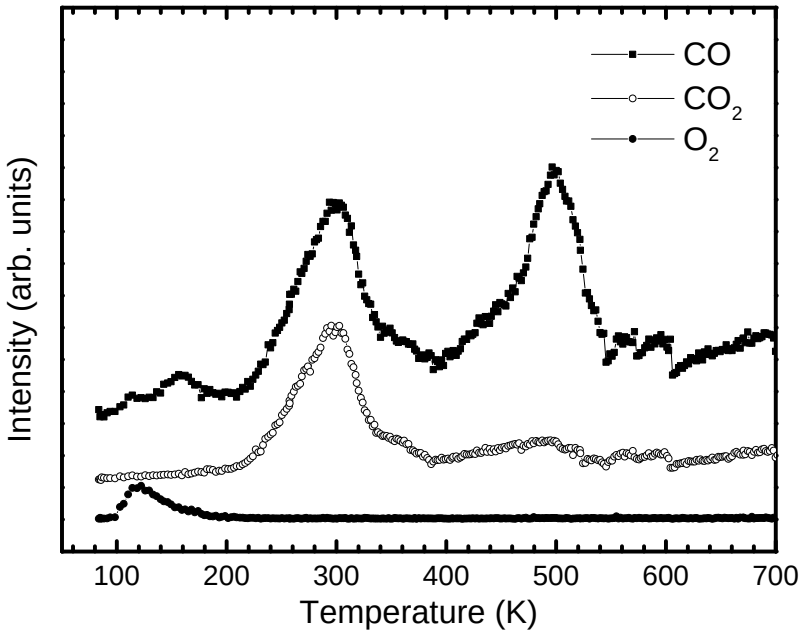

Figure 6.6: TD spectra after exposure of 1.0 L CO at RT, then with an additional exposure of 0.5 L O_2 at 85 K.

observed, which is similar to that in Fig. 5.3. An accompanying peak of CO_2 around 450 K is also observed. The origin of this kind of CO_2 is not clear. Presumably, it originates from a reaction of the CO-bridge with the oxygen which is in the boundary of $RuO_2(110)$ domains or diffuses from the bulk.

As shown in Fig. 6.3, both loss peaks of O-cus and CO-bridge can be observed by exposing 0.5 L oxygen to the CO-covered $RuO_2(110)$ surface at LT, indicating coadsorption of CO-bridge and O-cus. The corresponding TD spectra of this surface are shown in Fig. 6.6. The CO_2 formation is around 300 K. Similarly, CO desorbs at the same temperature range. The other CO desorption peak appears around 500 K. No oxygen desorption was observed, indicating that O-cus in the surface was mostly consumed by reacting with CO-bridge. Thus, the CO desorption around 500 K results from the residual CO-bridge.

Since the binding energy of either oxygen or CO with Ru-bridge is higher than that with Ru-cus, the Ru-bridge sites should be occupied by either oxygen or CO in the coadsorbed surface of O-cus with CO-cus. Two kinds of coadsorbed surfaces of O-cus with CO-cus, i.e., together with O-bridge or CO-bridge, respectively, were also prepared at low temperature. The TD and HREEL spectra of the two kinds of

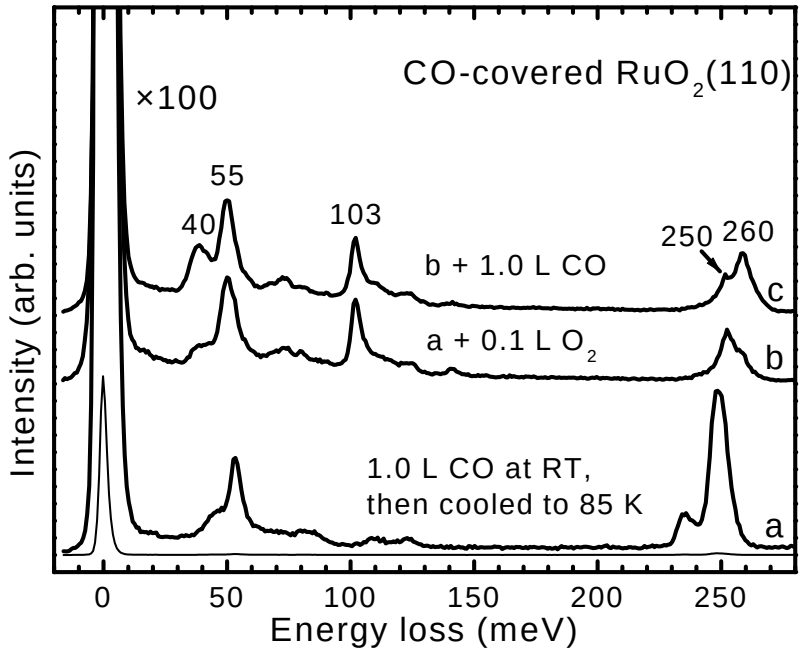

Figure 6.7: HREEL spectra (a) after first exposing 1.0 L CO at RT, then cooling to 85 K, (b) with an additional exposure of 0.1 L O_2 at 85 K and (c) further additional exposure of 1.0 L CO at 85 K.

surfaces are presented below.

In curve a of Fig. 6.7, the HREEL spectrum of a CO-covered $RuO_2(110)$ surface, which had been prepared by 1.0 L CO exposure to $RuO_2(110)$ at RT, was reproduced. After it was cooled down to LT, 0.1 L oxygen was exposed. The corresponding HREEL spectrum is shown in curve b. The loss peak at 103 meV appears again, indicating the O-cus species on the surface. By further exposing 0.5 L CO to the surface, two new loss peaks appear at 40 and 260 meV, which are typical values of ν_{S-CO} and ν_{C-O} of the CO-cus species. Obviously, this is a coadsorption phase composed by O-cus, CO-cus and CO-bridge. The TD spectra for this coadsorption phase were shown in Fig. 6.8.

In Fig. 6.8, a desorption peak of CO_2 was found around 260 K, which was also accompanied by a CO desorption peak. Here we see again, the CO_2 formation occurs in a parallel channel of thermal activation of the adsorbed CO. Compared to Fig. 6.6, the CO_2 desorption peak shifts to lower temperature. Since the bond of the CO-cus species with $RuO_2(110)$ is weaker than that of CO-bridge, the main part of CO_2 on

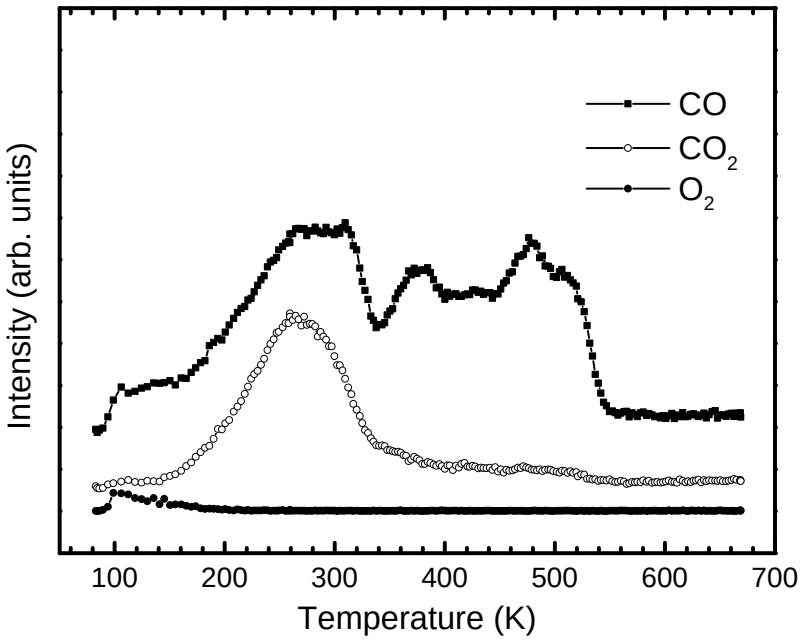

Figure 6.8: TD spectra after first 0.1 L O_2, then 1.0 L CO exposure to CO-covered $RuO_2(110)$ (prepared by 1.0 L CO exposure at RT) at 85 K.

Fig. 6.8 should result of the combination of O-cus with CO-cus, i.e., CO-cus reacts with O-cus first.

Another kind of coadsorption of O-cus and CO-cus, in which all of the Ru-bridge sites are occupied by O-bridge, can be prepared by exposure of CO and oxygen to the bare $RuO_2(110)$ surface at low temperature. In order to distinguish the O-cus and O-bridge, the oxygen isotope, $^{18}O_2$, was exposed. In order to understand the influence of the coverage of O-cus, three different exposure sequences were performed, first 0.2 L CO, then 0.2 L $^{18}O_2$, first 0.2 L $^{18}O_2$, then 0.2 L CO and first 0.1 L $^{18}O_2$, then 0.1 L CO. The corresponding HREEL spectra were taken and shown in curves a, b and c in Fig. 6.9, respectively.

All three curves in Fig. 6.9 show the loss peaks of both CO-cus and O-cus. Due to the use of $^{18}O_2$, the energy loss of the O-cus stretching mode is found at 99 meV, i.e., with an isotopic shift. From curve a to b or c, the CO-induced peaks decrease while that of the oxygen-induced peak increases. The stretching energy of the C–O mode increases from 262 to 265 meV with increasing of oxygen coverage, which shows the decrease of the back donation from the substrate. The TD spectra of three corresponding surfaces are shown in Fig. 6.10.

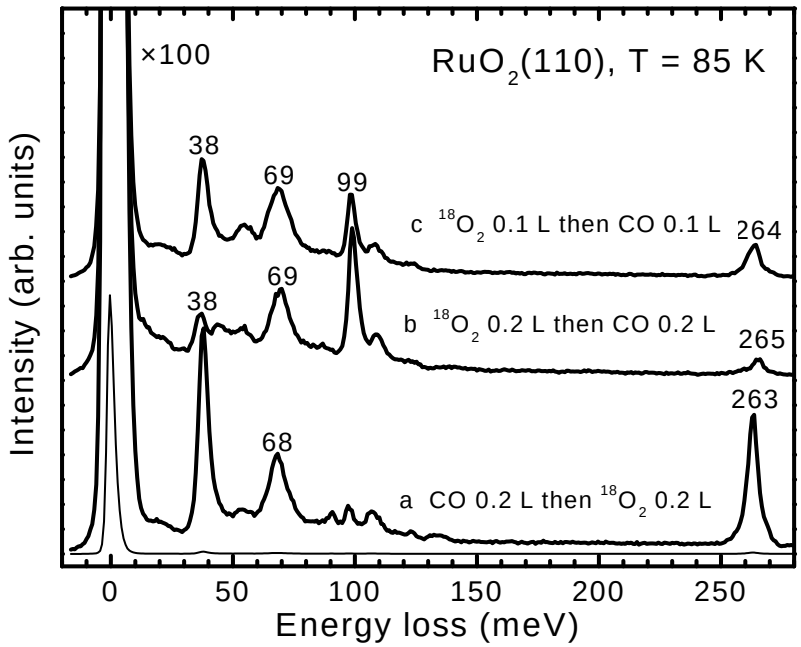

Figure 6.9: HREEL spectra recorded at 85 K: (a) first 0.2 L CO, then 0.2 L $^{18}O_2$,(b) first 0.1 L $^{18}O_2$, then 0.1 L CO and (c) first 0.2 L $^{18}O_2$, then 0.2 L CO.

The desorption temperature of CO in Fig. 6.10 increases from around 300 K to 320 K with increasing oxygen coverage. This indicates that the bond of CO with $RuO_2(110)$ becomes stronger with coadsorption of oxygen, although the higher C–O stretching energy indicates the weaker back donation from the substrate to the CO $2\pi^*$ orbital. Since the coadsorption with oxygen is favorable for the electron donation, but not for the back donation, the main contribution of the stronger CO bond results of the stronger donation from CO to the substrate, instead of the back donation from the substrate to CO.

Due to the exposure of $^{18}O_2$, ^{18}O-cus atoms are prepared besides ^{16}O-bridge atoms. Hence, the production of CO reacting with O-cus is CO_2 with mass 46 ($C^{18}O^{16}O$), whereas CO reacting with O-bridge gives normal CO_2 with mass 44 ($C^{16}O_2$). Thus, the CO_2 product from the reactions of CO with O-cus or with O-bridge can be distinguished. Interestingly, the evolution of CO_2, both of the mass 44 and mass 46, is shown in the same temperature range of CO desorption in all three TD spectra. The temperature of CO_2 (both mass 44 and 46) formation shifts from around 300 K to 320 K with increasing oxygen coverage. This indicates that a higher coverage of O-cus can raise the CO_2 formation barrier for the reaction of

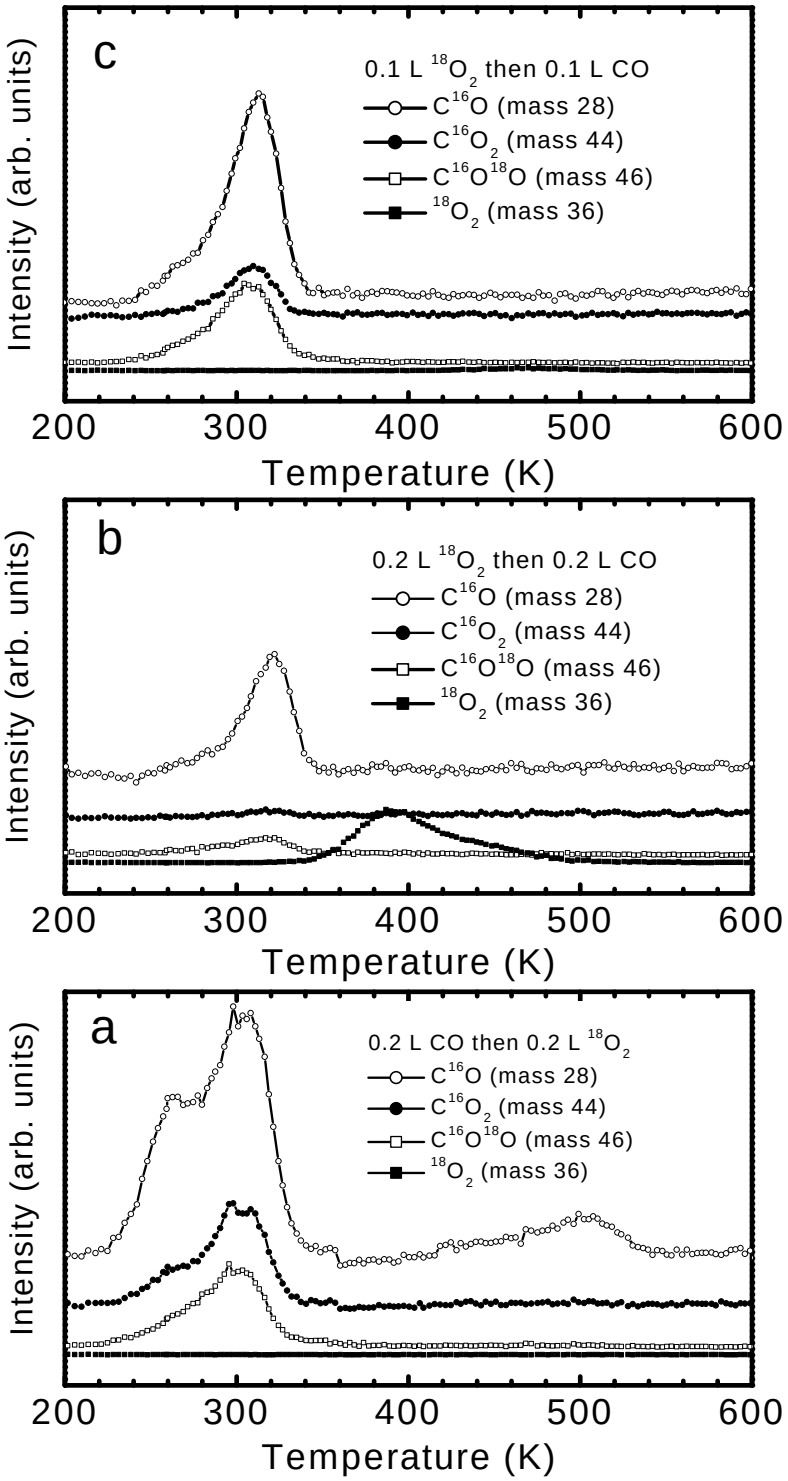

Figure 6.10: TD spectra after exposure of CO and oxygen at 85 K. (a) first 0.2 L CO, then 0.2 L $^{18}O_2$,(b) first 0.2 L $^{18}O_2$, then 0.2 L CO and (c) first 0.1 L $^{18}O_2$, then 0.1 L CO.

CO-cus with both O-cus and O-bridge.

Fig. 6.10 shows that the desorption of both, mass 44 and mass 46, is in the same temperature range, but it does not mean that both CO_2 formation processes, CO with O-cus and CO with O-bridge, have the same reaction barrier. Since CO-cus coexists with O-cus and O-bridge on the same surface, the two oxidation processes, CO with O-cus and CO with O-bridge, will compete with each other. Obviously, the reaction via a lower barrier will correspond to the higher CO_2 formation rate. When exposing first 0.2 L $^{18}O_2$, then 0.2 L CO, the oxygen coverage is very high because the desorption of oxygen can be clearly observed in the TD spectrum. The peak of mass 44 is very weak, indicating that the reaction between O-bridge and CO-cus is nearly inhibited. When exposing first 0.1 L $^{18}O_2$, then 0.1 L CO, the oxygen coverage is not so high because all oxygen atoms are consumed by reaction with CO, and therefore no desorption peak of oxygen appears in the spectrum of Fig. 6.10c. The intensity of mass 44 is obviously smaller than that of mass 46, indicating an obviously lower reaction barrier for O-cus with CO-cus. When exposing first 0.2 L CO, then 0.2 L $^{18}O_2$, the coverage of oxygen is small. Thus, the spectra of CO and CO_2 with mass 44 are similar to that of CO on the bare $RuO_2(110)$ surface. The desorption peak of mass 46 is somewhat smaller than that of mass 44. Since the amount of O-cus is smaller than that of O-bridge, the CO-oxidation barrier for CO with O-cus is still lower than that of CO-cus with O-bridge.

According to the above discussion, we can conclude the following: For the coadsorption of O-cus, CO-cus, and O-bridge, the reaction between O-cus and CO-cus proceeds prior to that between O-bridge and CO-cus. At low coverage of O-cus, the reaction between CO-cus and O-bridge is noticeable. With decreasing coverage of O-cus, the reaction barrier of CO-cus with O-bridge is more and more suppresion. At very high O-cus coverage, the reaction channel of CO-cus with O-bridge is nearly prohibited. This fits very well with the conclusion derived in section 6.2. The suppress of the reaction between O-bridge and CO-cus may be due to the change of the local charge distribution of O-bridge by the adsorbed O-cus.

It is interesting to note that the CO_2 formation occurs in the same temperature range as CO desorption in all kinds of coadsorption of CO with oxygen. This indicates that some factor correlated to CO will determine the barrier of CO oxidation. For the reaction between CO-cus and O-bridge, it was found by Liu and Hu [27]

using DFT methods that the displacement of CO is larger than that of O-bridge in order to reach the transition state of the CO reaction, and the CO–Ru distance is remarkably lengthened in the transition state. Hence, the activation energy for CO to reach the transition state could be close to that for CO desorption. Thus, the CO_2 formation is parallel to the desorption of CO. For other reaction channels, the CO_2 formation is also parallel to the CO desorption. Therefore, the CO displacement in the transition state should be larger than that of the oxygen species also for the other channels in order to reach.

6.5 Summary

It was confirmed that CO can react with the bare and the O-rich $RuO_2(110)$ surface at RT. Two reaction channels are identified as the reactions of CO with atomic oxygen weakly bonded to Ru-cus (O-cus) and with the bridge oxygen (O-bridge). For the exposure values studied, only surface oxygen takes part in the CO oxidation, and the oxygen depleted surface can be restored by O_2 exposure at RT. The system $RuO_2(110) + O_2 + CO$ turned out to be a remarkable surface redox system operating at 300 K. Both the HREELS titration experiments and the TDS measurements for coadsorption confirm that the reaction of CO with O-cus takes place prior to that of CO with O-bridge. At high O-cus coverage, the reaction between CO and O-bridge is suppressed.

7 Steady-state CO oxidation

7.1 Introduction

The CO oxidation under "real" catalysis conditions does not proceed by exposing solely CO onto the bare or O-rich $RuO_2(110)$ surface. Instead, CO and O_2 are simultaneously exposed at an appropriately chosen pressure ratio. The ratio is given by a dynamic balance between the adsorption and desorption of the reactants and the CO_2 formation. In order to elucidate the microscopic mechanisms of this reaction, the investigation of the steady-state kinetics under UHV conditions is necessary. As shown in the last chapter, the exposed CO molecules can be oxidized by the oxygen species of the surface, and the oxygen depleted surface can be restored by O_2 exposure at RT. Hence, the system $RuO_2(110)$ + O_2 + CO is a remarkable surface redox-system at RT. From these results we expected the CO oxidation to work under steady-state conditions.

In view of the fact that the real catalysis operates mostly at a pressure of up to 100 bar, methods based on surface science have access to only a very limited pressure window. If the reactivity is different within the two pressure regimes, one talks about the so-called "pressure gap" in catalysis. With respect to the CO oxidation on $RuO_2(110)$, we should mention a recent report on CO oxidation under atmospheric pressure conditions at RuO_2 particles prepared from aqueous solution [32]. In this chapter it will be shown that the temperature dependence of the rate for an identical p_{CO}/p_{O_2} ratio exhibits a quite remarkable agreement between the data measured under UHV conditions and under atmospheric pressure conditions, despite the fact that the absolute pressure differed by up to ten orders of magnitude. We believe

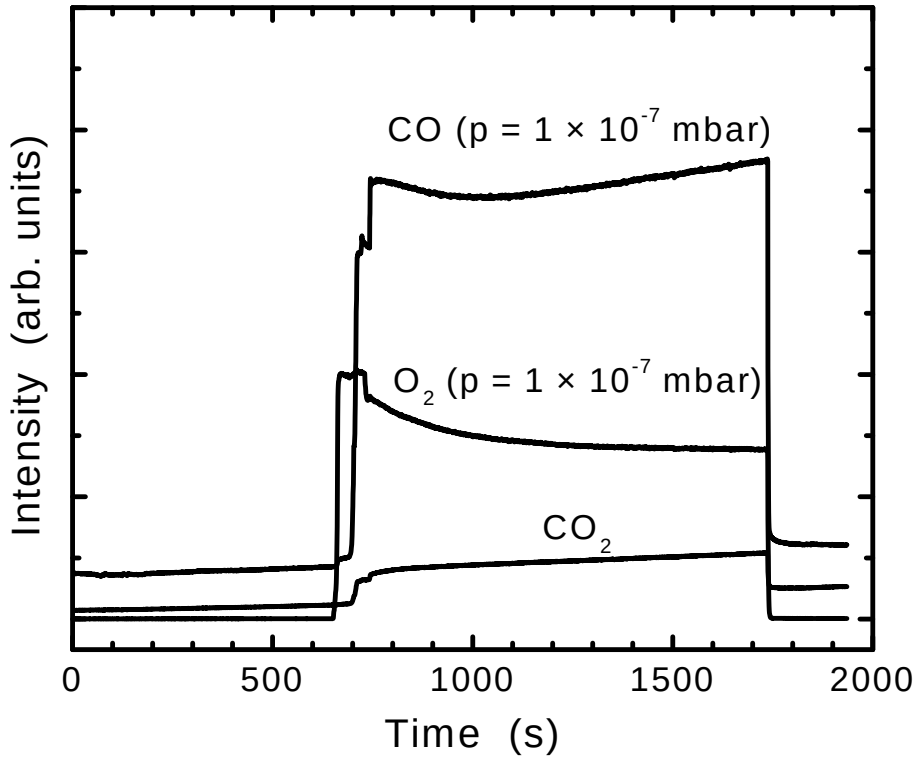

Figure 7.1: The ion current of CO, O_2 and CO_2 as a function of time. The partial pressures of CO and O_2 are maintained at about 2×10^{-7}, and 1×10^{-7} mbar, respectively. The sample temperature is 350 K.

that this represents a distinct example of "bridging the pressure gap".

In this chapter the steady-state kinetics of the CO oxidation on the $RuO_2(110)$ surface under UHV conditions is presented, and the analysis of the data will be based on the knowledge of the adsorptive properties of this surface.

The $RuO_2(110)$ + CO + O_2 system is a remarkable surface redox system operating at RT. Hence, the $RuO_2(110)$ surface is expected to be able to efficiently catalyze the CO oxidation under steady-state conditions. In order to check this hypothesis, the measurements discussed below were carried out. At a constant temperature (350 K), the reactants (CO and oxygen) were introduced to the $RuO_2(110)$ surface and their partial pressures were kept constant. One example for the variation of the CO_2, CO and O_2 partial pressures, as recorded by using the mass spectrometer, are shown in Fig. 7.1. When the oxygen valve was opened, nothing happened. When the CO valve was opened in addition, a CO_2 signal appeared. After keeping the

partial pressure of CO and oxygen constant for a period, the signal of CO_2 reached a nearly constant value, i.e., the reaction reached a steady state. The steady state could last for a long time (longer than 20 minute). After closing the valves of O_2 or CO, the signal of CO_2 went back to the value before opening the O_2 and CO valves. Only the background somewhat increased. This experiment clearly shows that CO oxidation can be performed under steady-state conditions on the $RuO_2(110)$ surface.

The $RuO_2(110)$ surface has been introduced in Chapter 3, and the adsorption of oxygen and CO has also been discussed in the preceding chapters. In contrast to a transition-metal surface, in which there is only one kind of metal atom, the situation on the $RuO_2(110)$ surface is more complicated. The surface exposes two types of Ru atoms, denoted by Ru-cus and Ru-bridge, which can each be occupied by either O (O-cus and O-bridge) or CO (CO-cus and CO-bridge). In order to rationalize the results of the kinetic measurements, the adsorption and desorption properties of these various species are briefly reviewed as follows.

i) O-cus desorbs around 400 K and hinders the formation of CO-cus. However, O-cus occupies up to about 80 % of the cus sites at 300 K. Thus, the formation of CO-cus is not completely suppressed.

ii) O-bridge desorbs around 1000 K and hinders the formation of CO-bridge.

iii) CO-cus desorbs around 300 K, i.e., this species will be pumped off above RT in vacuum. It can be stabilized up to 320 K by the coadsorption with O-cus.

iv) CO-bridge desorbs with two peaks around 400 and 550 K and hinders adsorption of O-bridge, but not so efficiently as in the opposite case because of the marked difference in adsorption energy.

The product, CO_2, will immediately be released from the surface above RT [99].

The kinetic behavior revealed to be rather complex, because the CO_2 formation rate (r_{CO_2}) is determined by the partial pressures of both O_2 and CO (p_{O_2} and p_{CO}) as well as by the reaction temperature (T). The data will be presented as a function of each of these parameters while the other two are kept constant.

7.2 CO_2 formation rate as a function of O_2- and CO-pressure at T = 350 K

For the steady-state measurements, a temperature of 350 K was chosen because this temperature represents an optimum under certain aspects. In order to suppress background and "memory" effects by too heavy gas loads, the partial pressures of the reactants were usually kept below 3×10^{-6} mbar.

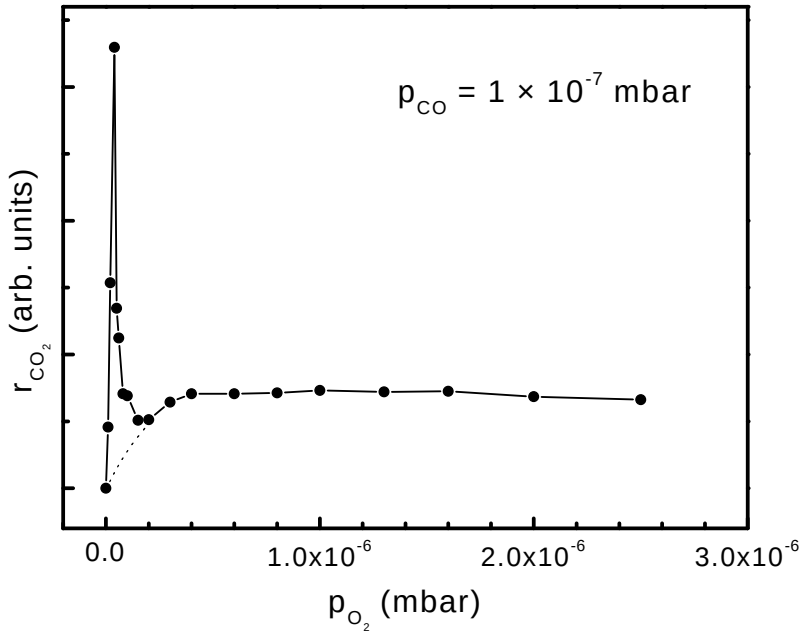

Figure 7.2: The variation of the reaction rate with O_2 partial pressure under steady-state conditions. The partial pressure of CO was kept at 1×10^{-7} mbar. The temperature is at 350 K.

Fig. 7.2 was recorded by fixing the CO partial pressure (p_{CO}) at 1×10^{-7} mbar and varying the oxygen partial pressure (p_{O_2}) from 1×10^{-8} to 2.5×10^{-6} mbar. Clearly, the variation of r_{CO_2} with the p_{O_2} can be divided into three p_{O_2} regions. First, r_{CO_2} increases linearly with p_{O_2} and reaches a maximum near $p_{O_2} = 4 \times 10^{-8}$ mbar, i.e., close to the stoichiometric CO : O_2 composition (2 : 1). Further increase of p_{O_2} causes a decease of r_{CO_2} until a minimum is reached around $p_{O_2} = 2 \times 10^{-7}$ mbar. By further increasing p_{O_2}, the variation of r_{CO_2} is not obvious. As discussed in the last chapter, the oxygen consumption rate (equal to the CO_2 formation rate) is

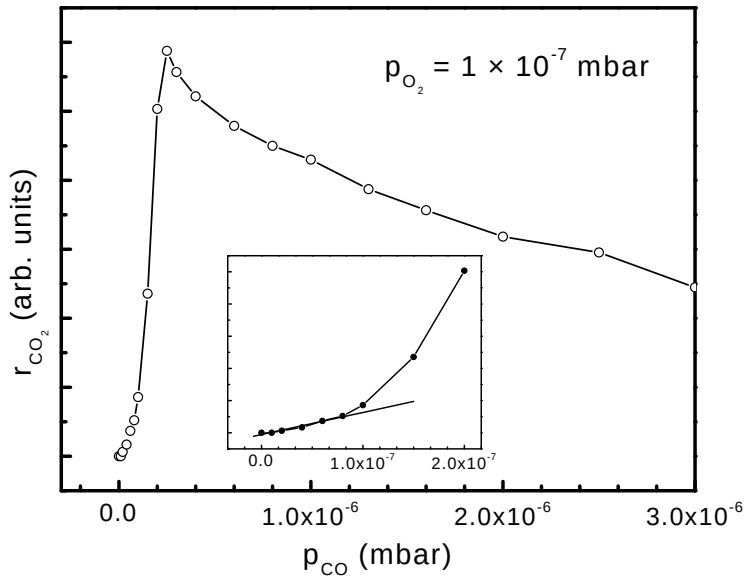

Figure 7.3: The variation of the reaction rate with the CO partial pressures under the steady-state condition. The partial pressure of O_2 was kept at 1×10^{-7} mbar. The temperature was kept at 350 K.

obviously slower if CO impinges onto the oxygen-rich $RuO_2(110)$ surface, in which most of cus sites are occupied by O-cus, than that to the bare $RuO_2(110)$ surface. The relatively low value of r_{CO_2} for $p_{O_2} > 1 \times 10^{-7}$ mbar indicates that the reaction is similar to the former case. Thus, it is now dominated by the interaction between O-cus and CO-cus. Since the saturation coverage of O-cus is near to 80 % at RT, the CO adsorption on the remaining cus sites is still possible, even at a very high ratio of O_2 / CO (such as 25 : 1 at $p_{O_2} = 2.5 \times 10^{-6}$ mbar). The value of r_{CO_2} at $p_{O_2} = 1 \times 10^{-7}$ mbar, i.e., $p_{CO} : p_{O_2} = 1 : 1$, is similar to the value at high p_{O_2}. This indicates that the reaction is mainly dominated by the interaction of O-cus and CO-cus.

Fig. 7.3 shows the variation of the reaction rate with CO partial pressure by fixing p_{O_2} at 1×10^{-7} mbar and keeping the temperature at 350 K. p_{CO} varies from 1×10^{-8} to 3.0×10^{-6} mbar. Similarly to the dependence shown in Fig. 7.2, the variation of r_{CO_2} with p_{CO} can also be divided into three regions. At the beginning, r_{CO_2} increases linearly but slowly here with p_{CO} until $p_{CO} = 1.0 \times 10^{-7}$ mbar. The absolute value of r_{CO_2} in this p_{CO} range is quite low. This indicates that the reaction is dominated by the interaction between O-cus and CO-cus. For $p_{CO} \geq 1 \times 10^{-7}$ mbar, r_{CO_2} increases

steeply until a maximum is reached around $p_{CO} = 2.5 \times 10^{-7}$ mbar, i.e., again near the stoichiometric gas composition ($p_{CO} : p_{O_2} = 2:1$). For $p_{CO} > 2.5 \times 10^{-7}$ mbar, r_{CO_2} decreases with increasing p_{CO}.

Similar to the reaction on transition metal surfaces, the oxidation of CO on RuO_2 proceeds via the Langmuir-Hinshelwood mechanism by interaction between chemisorbed O and CO. Thus, both species are present on the surface during the reaction. For T $\leq$ 350 K, the following reaction steps have to be formulated (where "cus" refers to the Ru-cus site and "bridge" refers to the Ru-bridge site):

$$O_2 + 2\text{cus} \rightleftharpoons 2O - \text{cus} \quad , \tag{7.1}$$

$$O - \text{cus} + \text{bridge} \rightarrow O - \text{bridge} + \text{cus} \quad , \tag{7.2}$$

$$O_2 + 2\text{bridge} \rightarrow 2O - \text{bridge} \quad , \tag{7.3}$$

$$CO + \text{cus} \rightleftharpoons CO - \text{cus} \quad , \tag{7.4}$$

$$CO - \text{cus} + \text{bridge} \rightarrow CO - \text{bridge} + \text{cus} \quad , \tag{7.5}$$

$$O - \text{cus} + CO - \text{cus} \rightarrow CO_2 \uparrow + 2\text{cus} \quad , \tag{7.6}$$

$$O - \text{cus} + CO - \text{bridge} \rightarrow CO_2 \uparrow + \text{cus} + \text{bridge} \quad , \tag{7.7}$$

$$O - \text{bridge} + CO - \text{cus} \rightarrow CO_2 \uparrow + \text{bridge} + \text{cus} \quad , \tag{7.8}$$

$$O - \text{bridge} + CO - \text{bridge} \rightarrow CO_2 \uparrow + 2\text{bridge} \quad . \tag{7.9}$$

These reactions are further commented as follows:

Step (7.1): O_2 may dissociatively adsorb on cus sites, from where it recombinatively desorbs around 400 K [21]. STM images taken at RT indicate that the O-cus species appear almost exclusively as pairs (or multiples of pairs) and exhibit rather limited mobility [25]. As a consequence, the concentration of sites for dissociative oxygen adsorption will essentially be proportional to the concentration of cus sites. For this reason, it is a good approximation to formulate the kinetics of this step as a first-order rate process as done later in the Eqs. (7.14) and (7.18).

Step (7.2): Since bonding of O to a bridge site is stronger than that to a cus site, this transition will take place if a neighboring empty bridge site is available [21].

Step (7.3): Direct occupation of bridge sites through dissociative adsorption of O_2 is unlikely, but cannot be ruled out. It is hard to distinguish from route (7.1) + (7.2). The O-bridge species is rather strongly held and desorbs only around 1000 K [21].

Step (7.4) + (7.5): Similarly, CO adsorbs on cus sites, where it is weakly held and desorbs below 300 K, as well it occupies bridge sites, from where desorption occurs around two desorption peaks at 400 and 500 K, respectively, as shown in Chapter 5.

Step (7.6)–(7.9): In principle, CO_2 formation might take place according to all four routes indicated, which was shown in the measurement for a composite-adsorbate surface in section 6.4 of the last chapter.

For these reasons, the results in the following discussion will be restricted to T < 350 K and will be more of qualitative nature rather than full kinetic modelling will be attempted.

The complex variation of r_{CO_2} with p_{O_2} at fixed $p_{CO} = 1 \times 10^{-7}$ mbar and T = 350 K, as depicted in Fig. 7.2, can be rationalized as follows: At low p_{O_2}, the surface will be largely covered by CO-bridge species, while the concentration of CO-cus will be fairly low due to its weak bonding. Incoming O_2 molecules will dissociatively adsorb on cus sites (step (7.1)), the oxygen atom will then react first with CO-cus (step (7.6)) or either react with CO-bridge (step (7.7)) or jumps to the more strongly held O-bridge sites (step (7.2)), from where the reaction according to step (7.9) takes place. Since under these conditions oxygen adsorption will be rate limiting, r_{CO_2} increases linearly with p_{O_2} until a maximum is reached if the bridge sites are occupied equally by CO and O. This maximum occurs for $p_{O_2} = 4 \times 10^{-8}$ mbar (at $p_{CO} = 1 \times 10^{-7}$ mbar), suggesting about equal sticking coefficients (probably close to unity) for adsorption of both O_2 and CO.

Upon further increase of p_{O_2}, the bridge sites become increasingly occupied by O-bridge, so that the formation of CO-bridge is hindered, and thus reaction step (7.9) becomes continuously inhibited, and r_{CO_2} decreases. Since the temperature is not high enough for oxygen desorption, oxygen can be consumed only by reacting with CO, i.e., the rate of oxygen consumption is equal to r_{CO_2}. Thus, upon the further increase of p_{O_2}, the rate of oxygen consumption decreases together with the decrease of r_{CO_2}, but the impinging rate of oxygen increases. Therefore, the sticking coefficient of oxygen should decrease in the steady state. On the other hand, the sticking coefficient of oxygen on the bare $RuO_2(110)$ surface is fairly high [15, 23], and the concentration of CO-cus is quite low at 350 K. Thus, only after most of the Ru-bridge sites and some Ru-cus sites are occupied by oxygen, the sticking coefficient of

oxygen can obviously decrease. Therefore, there is a critical p_{O_2} which is somewhat higher than that at maximum r_{CO_2}: Below this pressure, the main reaction step is the step (7.9). At higher p_{O_2}, most of the Ru-bridge sites will be occupied by oxygen and the main reactions shift to steps (7.6) and (7.8). The concentration of CO-cus will be very low because of the weak bonding of this species (according to step (7.4)). As a consequence, the value of r_{CO_2} is relatively low. Further increase of p_{O_2} will now continuously lead to an increasing population of O-cus. As discussed in the last chapter, the high coverage of O-cus can inhibit the reaction step (7.8) (between O-bridge and CO-cus). When the reaction step (7.8) is prohibited, the reaction takes place only via the reaction step (7.6) (between O-cus and CO-cus) and r_{CO_2} becomes quite low.

When p_{O_2} is higher than 1×10^{-7} mbar, the value of r_{CO_2} varies only slightly. Since the oxygen concentration is close to the saturation value in this p_{O_2} range, the concentrations of CO and oxygen vary slightly. Since the saturation coverage of O-cus is close to 80 % [15], the CO adsorption cannot be completely blocked, and hence the rate drops only slowly (presumably to zero), even if p_{O_2} is as high as 2.5×10^{-6} mbar. For further discussion it is important to note that for $p_{O_2} = 1 \times 10^{-7}$ mbar, the rate has already decreased to a value typical for reaction step (7.6) (between O-cus and CO-cus), so that it is concluded that the reaction has changed from step (7.9) to step (7.6) already at this pressure.

Next we discuss the data of Fig. 7.3 which show the variation of r_{CO_2} with p_{CO} for fixed $p_{O_2} = 1 \times 10^{-7}$ mbar and T = 350 K. At very low p_{CO}, the surface is largely covered by both O-bridge and O-cus. Under these conditions, essentially only CO-cus and O-cus are expected to be involved in the CO_2 formation, i.e., step (7.6) is in operation. r_{CO_2} will increase proportionally to the concentration of CO-cus. Because of the weak binding of CO-cus, r_{CO_2} will be quite low, and hence in turn, proportional to p_{CO}. This explains the initially linear and slow increase of r_{CO_2} with p_{CO} (inset of Fig. 7.3). For the temperature dependence of r_{CO_2} discussed below, it is important to note the situation for $p_{CO} = 1.0 \times 10^{-7}$ mbar: This is just the pressure where the reaction step (7.8) between O-bridge and CO-cus sets in, but the overwhelming part of the reaction takes place still along reaction step (7.6) between O-cus and CO-cus.

With increasing p_{CO}, O-cus will be increasingly consumed, and the reaction chan-

nel of reaction (7.8) between O-bridge and CO-cus begins to open. Since both channels (7.6) and (7.8) for CO oxidation are now opened, the r_{CO_2} increases more strongly than before. By further increasing p_{CO}, more and more bridge sites will also become oxygen-free and thus accessible for the formation of CO-bridge. After a critical p_{CO}, which is near to that at maximal r_{CO_2}, most cus sites are empty due to the stronger bond of oxygen and CO species with bridge sites. The reaction step thus transfers mainly to the step (7.9) (between O-bridge and CO-bridge) again. When a maximum is reached, about equal concentrations of O-bridge and CO-bridge species are again expected.

Further increase of p_{CO} then causes increasing concentration of CO-bridge and thereby hinders the formation of O-bridge. Parallel to the suppression of reaction (7.9), there will, however, still be parallel occurrence of steps (7.6) and (7.7). The weak bonding of CO-cus ascertains that even at higher p_{CO} the cus sites will not become completely blocked by CO, and hence the rate decreases only relatively weakly with increasing CO pressure.

7.3 r_{CO_2} as a function of temperature

The dependence of the reaction rate on temperature for given gas compositions is reproduced in Fig. 7.4 in the form of Arrhenius-plots. Four typical ratios of p_{O_2}/p_{CO}, 6 : 1, 2.5 : 1, 1 : 1 and 1 : 8, were selected. 6 : 1 and 1 : 8 represent the O-rich and CO-rich phases. 2.5 : 1 corresponds to the ratio for the maximum r_{CO_2}. The ratio of 1 : 1 was also measured because the dependence of r_{CO_2} on the temperature at this ratio and under atmospheric pressure conditions was recently reported [32]. The temperature range for these measurements are from 320 to 450 K. This temperature range is, admittedly, rather narrow for the following reasons: Below RT the reaction becomes very sluggish. Above 450 K the reaction channel of CO with oxygen diffusion from the bulk begins to open [15], therefore the reaction will be more complex.

For the temperature range from 320 K to 350 K, the value of $\ln(r_{CO_2})$ decreases linearly with 1/T in the Arrhenius-plot of the four kinds of ratios. The reaction rate is given by

$$r_{CO_2} = k_r \cdot [CO] \cdot [O] \quad , \tag{7.10}$$

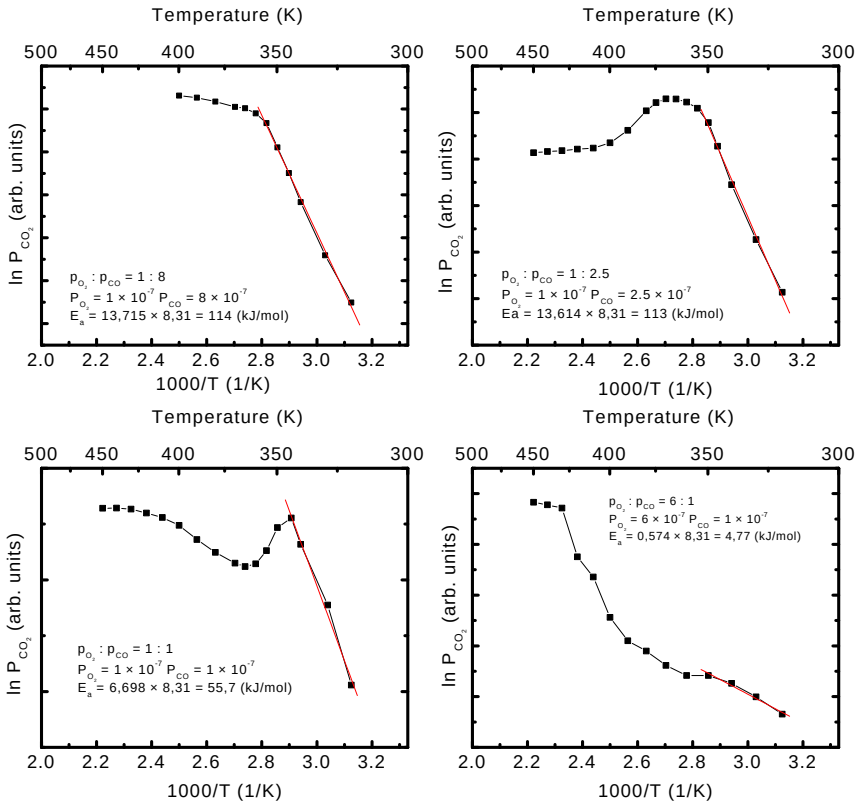

Figure 7.4: The temperature dependence of $r_{\mathrm{CO_2}}$ on temperature for the four ratios of CO and oxygen.

in which k_{r}, [CO] and [O] denote the reaction coefficient, CO coverage and oxygen coverage, respectively. If the [CO] and [O] vary only little with the temperature, i.e., if they are nearly constant, then in which C = ln([CO][O]) ≈ constant. Since $k_{\mathrm{r}} \propto \exp(-\mathrm{E}/\mathrm{kT})$, $\ln(r_{\mathrm{CO_2}})$ decreases linearly with 1/T. According to the Eq. (7.11), the activation energy E of the reaction can be derived. The activation energy is 4.8, 55.7, 113 and 114 kJ/mol, corresponding to the $p_{\mathrm{O_2}}$ /p_{CO} ratio 6 : 1, 2.5 : 1, 1 : 1 and 1 : 8, respectively. The value at ratio 1 : 8 is nearly the same as that at ratio 1 : 2.5. This indicates that the reaction processes for these two ratios are nearly the same. This is consistent with our above discussion, in which the main reaction step at these ratios is between O-bridge and CO-bridge.

$$\ln(r_{\mathrm{CO_2}}) = \ln(k_{\mathrm{r}}) + \mathrm{C} \quad , \tag{7.11}$$

As discussed above, the dominant reaction step at both ratios of 1 : 1 and 6 : 1 is

the reaction step (7.6), i.e., the reaction between O-cus and CO-cus. But the derived active energies are quite different, 60 kJ/mol for the ratio 1 : 1 and 4.8 kJ/mol for ratio 6 : 1. The activation energy for ratio 6 : 1 is fairly small. These unusual results can be understood as follows: In fact, the desorption of CO-cus is noticeable in this temperature range, i.e., the variation of [CO] is noticeable. Thus, the derived activation energy also includes the contribution of CO desorption. At the ratio of 6 : 1, p_{O_2} is much higher than p_{CO}, and thus the coverage of O-cus is near to the saturation value. During the increase of temperature, the change of the O-cus coverage is quite small, but the CO coverage obviously decreases. This trend of [CO] is against the increase of the reaction coefficient with temperature. Thus, the derived activation energy for this ratio is very small. For the 1 : 1 ratio, the situation is different. Since p_{O_2} is not so high, the coverage of O-cus is not near to the saturation value. During the increase of temperature, the CO-cus coverage decreases, and hence the O-cus coverage will somewhat increase. In addition, a higher coverage of O-cus can somewhat increase the desorption temperate of CO-cus, as discussed in the last chapter. Due to these effects, the coverage of CO-cus does not decrease as fast as at the ratio of 6 : 1. Together with these factors, the activation energy derived from the Arrhenius-plot for a ratio of 1 : 1 is obviously higher than that for the ratio of 6 : 1, although the dominating reaction step between O-cus and CO-cus is the same for both ratios.

Further increase of the temperature, the relation between $\ln(r_{CO_2})$ and 1/T deviates from a linear dependence, indicating a noticeable desorption of CO and O. For ratios of 6 : 1 and 1 : 8, the increase of r_{CO_2} becomes slow with temperature. For the ratio of 1 : 1, r_{CO_2} begins to decrease at T > 350 K. For the ratio of 1 : 2.5, r_{CO_2} begins to decrease at T > 370 K . At these temperatures, the desorption of CO-bridge becomes noticeable and O-cus also begins to desorb. This is in good agreement with the deviation from a linear dependence because CO-bridge is the reactant in the CO-rich condition (ratios of 1 : 8 and 1 : 2.5) and O-cus is the reactant in the O-rich condition (ratios of 6 : 1 and 1 : 1). Since p_{CO} for the ratio of 1 : 8 is obviously higher than that for ratio 1 : 2.5, the decrease of [CO] is not so significant for this ratio. Thus, r_{CO_2} still increases slowly for the ratio of 1 : 8, while r_{CO_2} begins to decrease at T > 370 K for the ratio of 1 : 2.5. Due to similar reasons, r_{CO_2} still increases slowly for the ratio of 6 : 1 at T > 350 K but begins to decrease for the ratio of 1 : 1.

By further increasing the temperature, r_{CO_2} at ratio 1 : 2.5 becomes nearly constant at temperatures above 420 K, opposite to its decrease at the temperature range from 370 to 420 K. This means that another reaction channel opens. Due to the obvious desorption of CO-bridge, the bridge sites will be more and more occupied by O-bridge with increasing temperature. This can hinder the transfer of CO-cus to CO-bridge and therefore, the reaction step (7.8) (between the O-bridge and CO-cus) can no longer be neglected. The new reaction channel can compensate the decrease of r_{CO_2} via step (7.9), resulting in the near independence on the temperature at T > 420 K.

r_{CO_2} increases more steeply at the ratio of either 1 : 1 or 6 : 1 at T > 400 K. This indicates that new reaction channels are opened for the two ratios. As discussed in chapter 4, the desorption of O-cus becomes significant at T > 400 K. Hence, the O-cus coverage could become very low. As discussed in the last chapter, the reaction channel between O-bridge and CO-cus could be opened. Therefore, r_{CO_2} increases more steeply, although the surface concentrations of O-cus, and CO-cus decrease obviously. This variation for the ratios 1 : 1 and 6 : 1 supports the conclusion in the last section, that the dominating reaction step for both ratios is the reaction step (7.6), i.e., the reaction between O-cus and CO-cus.

The temperature dependence of r_{CO_2} in the four ratios supports the suggestions in the last section: The dominating reaction in the CO-rich region up to the ratio at the maximum reaction rate is between O-bridge and CO-bridge, and the dominating section for $p_{O_2}/p_{CO} > 1$ is between O-cus and CO-cus.

7.4 Does there exist a "pressure gap"?

In a recent study on the oxidation of CO by a catalyst based on RuO_2 particles, prepared from an aqueous solution of $RuCl_3$ and supported on TiO_2 and SiO_2, Zang and Kisch [32] reported the remarkable activities even down to RT. The rate data determined for different temperatures for a gas mixture with $p_{CO} = p_{O_2} = 500$ mbar are included in the Arrhenius-plot of Fig. 7.5. Although the authors derived from their four data points (open squares) an activation energy of only about 0.4 eV, these data points are fully consistent with the results of this work obtained for

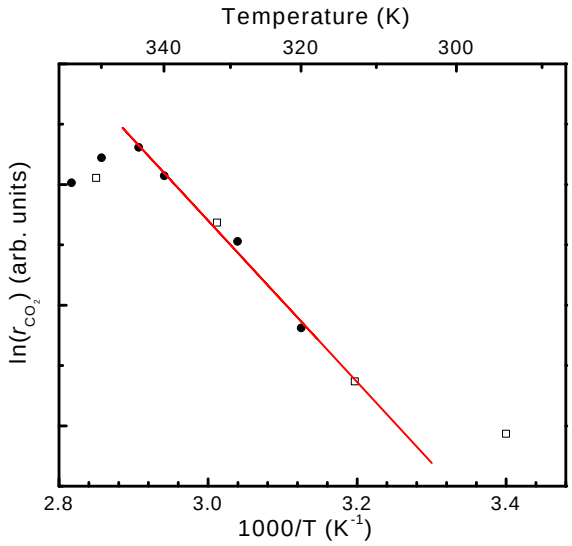

Figure 7.5: Arrhenius plot, $\ln(r_{CO_2})$ vs. 1/T. Solid circle: UHV data for $RuO_2(110)$ at $p_{CO} = p_{O_2} = 10^{-7}$ mbar, Open square: Data from Zang and Kisch [32] for small RuO_2 at $p_{CO} = p_{O_2} = 500$ mbar.

$p_{CO} = p_{O_2} = 10^{-7}$ mbar. It has to be admitted, however, that this agreement so far only holds for the slope (≡ activation energy), but not for the absolute scale which should be related to the active surface area. Instead the y-axis in Fig. 7.5 is given in arbitrary units on which both sets of data were arbitrarily displaced vertically until best agreement was reached. However, an attempt can be made to reach at least an order of magnitude estimate for the absolute reaction rate as follows:

The rate data for the single-crystal work was quantified according to the equation:

$$r_{CO_2} = \frac{p_{CO_2} v}{RT} \cdot N_0 \quad \text{(molecules/s)} \quad , \tag{7.12}$$

where p_{CO_2} is the partial pressure of CO_2, v is the pumping speed in the UHV chamber, $N_0 = 6.022 \times 10^{23}$ is Avogadro's number, and T the gas temperature (300 K). Inspection of Figs. 7.2 and 7.3 reveals that, around the stoichiometric $CO : O_2$ composition, r_{CO_2} was of the order of 10^{12} molecules·cm^{-2}·s^{-1} at 350 K. Inspection of Fig. 7.5 leads to the conclusion that at room temperature this number will be reduced by about half an order of magnitude so that a value of the order 10^{12} molecules·cm^{-2}·s^{-1} is reached. A rough estimate can, on the other hand, be made for the 'real' catalyst. For ≈ 0.5 g RuO_2 powder deposited onto SiO_2 with a specific surface area of 340 m^2/g, an initial rate of CO consumption of 71 ml/min at

300 K was reported [32]. If we assume the same surface area of the catalyst as that of the SiO_2 support (i.e. 170 m_2 for 0.5 g), simple arithmetic transforms this number into a rate of CO_2 formation of 7×10^{12} molecules·cm^{-2}·s^{-1}. The agreement of the (roughly) estimated activities for the two quite different conditions is considered to be rather remarkable.

How can we rationalize that the reaction rate appears to be obviously largely independent of the total pressure over ten orders of magnitude, as long as the same ratio of partial pressures ($p_{CO} : p_{O_2} = 1:1$) is established? The measurements on the variation of r_{CO_2} with temperature underlying Fig. 7.5 were performed for $p_{CO} = p_{O_2} = 1 \times 10^{-7}$ mbar, T up to 350 K. Under these conditions, the reaction mainly takes place between O-cus and CO-cus with only a minor part occurring between O-bridge and CO-cus, and the thermal desorption of O-cus is fairly slow. Under these conditions the mechanism of the reaction may be approximated as:

$$\mathrm{CO + cus} \underset{k_{-1}}{\overset{k_1}{\rightleftharpoons}} \mathrm{CO{-}cus} \quad , \tag{7.13}$$

$$\mathrm{1/2O_2 + cus} \overset{k_2}{\rightarrow} \mathrm{O{-}cus} \quad , \tag{7.14}$$

$$\mathrm{CO{-}cus + O{-}cus} \overset{k_2}{\rightarrow} \mathrm{CO_2 \uparrow + 2cus} \quad , \tag{7.15}$$

where cus represents a Ru-cus site and CO-cus and O-cus represent the surface species of CO and O on the cus site, respectively. The rate will be given by

$$r_{CO_2} = k_3 \cdot [\mathrm{CO - cus}] \cdot [\mathrm{O - cus}] \quad . \tag{7.16}$$

At steady state:

$$\frac{\mathrm{d[CO - cus]}}{\mathrm{dt}} = k_1 \cdot p_{CO} \cdot [\mathrm{cus}] - k_{-1} \cdot [\mathrm{CO - cus}] - k_3 \cdot [\mathrm{CO - cus}] \cdot [\mathrm{O - cus}] = 0 \quad , \tag{7.17}$$

and within a mean field approximation for the site of O_2 dissociation:

$$\frac{\mathrm{d[O - cus]}}{\mathrm{dt}} = k_2 \cdot p_{O_2} \cdot [\mathrm{cus}] - k_3 \cdot [\mathrm{CO - cus}] \cdot [\mathrm{O - cus}] = 0 \quad , \tag{7.18}$$

where [cus], [CO-cus] and [O-cus] are concentrations of surface species. The formation of O-cus is taken to be proportional to [cus] and not to [cus]^2, as assumed for normal dissociation kinetics. This is justified since O_2 dissociates mostly in creating a pair of O-cus and not statistically distributed O-cus [25]. Also:

$$[\mathrm{cus}] + [\mathrm{CO - cus}] + [\mathrm{O - cus}] = 1 \quad . \tag{7.19}$$

Since at 350 K the desorption rate of CO is much higher than the production rate of CO_2, we can omit the term $k_3 \cdot$ [CO-cus] $\cdot$ [O-cus] in Eq. (7.17). Then Eq. (7.17) can be written as:

$$\frac{\mathrm{d}[\mathrm{CO}-\mathrm{cus}]}{\mathrm{dt}} = k_1 \cdot p_{\mathrm{CO}} \cdot [\mathrm{cus}] - k_{-1} \cdot [\mathrm{CO}-\mathrm{cus}] = 0 \quad , \tag{7.20}$$

Solving the Eqs. (7.18) to (7.20), we get:

$$[\mathrm{O}-\mathrm{cus}] = \frac{k_2 k_{-1}}{k_3 k_1} \cdot \frac{p_{\mathrm{O_2}}}{p_{\mathrm{CO}}} \quad , \tag{7.21}$$

$$[\mathrm{CO}-\mathrm{cus}] = \frac{1 - \frac{k_2 k_{-1}}{k_3 k_1} \cdot \frac{p_{\mathrm{O_2}}}{p_{\mathrm{CO}}}}{1 + \frac{k_{-1}}{k_1 p_{\mathrm{CO}}}} \quad . \tag{7.22}$$

For $p_{\mathrm{CO}} = 500$ mbar, $\frac{k_{-1}}{k_1 p_{\mathrm{CO}}}$ is much smaller than 1, and Eq. (7.22) can be simplified to:

$$[\mathrm{CO}-\mathrm{cus}] = 1 - \frac{k_2 k_{-1}}{k_3 k_1} \cdot \frac{p_{\mathrm{O_2}}}{p_{\mathrm{CO}}} \quad . \tag{7.23}$$

For $p_{\mathrm{CO}} = 10^{-7}$ mbar, we estimate the two terms, k_{-1} and $k_1 \cdot p_{\mathrm{CO}}$, to be of the same order of magnitude. According to Eq. (7.22), the CO concentration decreases by less than one order of magnitude. Thus, the approximation (7.23) still holds except for the quoted factor. Furthermore, since k_1, k_{-1}, k_2 and k_3 are rate constants for elementary steps, it follows in turn that the surface concentrations of O and CO are only given by the pressure ratio of oxygen and CO, but not by the absolute pressure of each reactant. Since the overall reaction rate (7.16) is proportional to [CO-cus] and [O-cus], we can conclude that the reaction rate on this surface will be independent of the total pressure! This conclusion is in full accordance with our suggestion given above that the estimated absolute numbers of CO_2 production in real catalysis and in our UHV steady-state experiments are identical within an order of magnitude, although the pressures during the reactions differ by more than ten orders of magnitude. We therefore conclude that a pressure gap does not exist for the CO oxidation at the RuO_2 surface under the discussed conditions (i.e., equal partial pressures and T $\leq$ 350 K).

Finally, although we have derived a rather simple expression for the $r_{\mathrm{CO_2}}$ (see Eq. (7.16) together with (7.21) and (7.22)), the activation energy derived from the experimental data of Fig. 7.5 cannot simply be identified with a specific single process, since both k_{-1} and k_3 enter Eq. (7.16) and are expected to be temperature dependent.

7.5 Summary

Since the bonding among the surface atoms of a catalyst is usually of comparable strength to that of the coupling to the adsorbates involved, a catalytic reaction will in general affect the configuration of these surface atoms, i.e., the reaction "digs its own bed". The reason for the apparent "pressure gap" in CO oxidation on Ru lies in the fact that rather high oxygen exposures are required (which will not be attained in regular UHV studies) to establish the catalytically active RuO_2 phase. With the latter the $RuO_2(110)$ surface grown epitaxially on a Ru(0001) substrate as well as a bulk RuO_2 sample exposing its (110) plane was found to be of comparable reactivity [21].

In the present study, the absence of a "pressure gap" and the remarkable agreement of the kinetic data were found between the $RuO_2(110)$ single crystal surface, typically operated at 10^{-7} mbar pressure and small supported RuO_2 particles working at atmospheric pressure. This could be traced back to the fact that, under the conditions discussed above, the surface is in both cases essentially saturated with about similar fractions of O- and CO- species adsorbed at Ru-cus sites, so that a variation of the total pressure (at a fixed $CO : O_2$ ratio) has only little effect. The situation will, however, change if this $CO : O_2$ ratio is varied, since now the participation of the bridge sites may become more relevant, e.g., at temperatures above 350 K, where the surface structure may undergo more profound alterations. The results again demonstrate that the comparison of catalytic activities is only reasonable in connection with a careful analysis of the state of the catalyst's surface; the absolute total pressure may then become irrelevant.

Finally, it should be noted that the pressure gap described above actually turns out to be a material gap. This conclusion can be drawn mainly also from the results of this thesis.

8 Hydrogen adsorption on Ru(11$\bar{2}$1)

8.1 Introduction

Recently, it was found that Ru-based catalysts can be used for NH_3 synthesis [33, 34]. As an important step for ammonia synthesis, the investigation of hydrogen adsorption on Ru surfaces is necessary. In order to better understand the details of the reactions involved, a number of experiments on Ru single-crystal surfaces were set up [37]. One parameter to be changed is the crystallographic orientation of the Ru surface. Up to now, the adsorption of H on Ru(0001) and H on Ru(10$\bar{1}$0) was investigated by LEED, TDS and HREELS [47–53, 59, 100], but no investigation of hydrogen adsorption on Ru(11$\bar{2}$1) was reported. Compared to Ru(0001) and Ru(10$\bar{1}$0), Ru(11$\bar{2}$1) exhibits a higher activity for the dissociation of ammonia [56, 57]. Hence, the investigation of hydrogen adsorption on Ru(11$\bar{2}$1) is also important. In this chapter, studies of hydrogen adsorption on the Ru(11$\bar{2}$1) surface are presented.

The structure of H adsorbed at transition metal surfaces is also an interesting topic. It is well known that H preferentially adsorbs at the highest-coordinated site available on the surface [101]. For example, it adsorbs at the fourfold sites of fcc(100) surfaces and at the threefold sites of fcc(111) or hcp(0001) surfaces. These surfaces contain only one kind of high-coordinated sites, whereas some open surfaces offer both threefold and fourfold sites. Then the question arises at which site the adsorption occurs. In earlier contributions it was found that hydrogen adsorbs at a threefold site on Rh(311) [102], at a threefold site at the beginning and at a fourfold site for higher doses on Ni(311) [103], or at a fourfold site at the beginning and at a threefold site at higher doses Pd(311) [104]. The Ru(11$\bar{2}$1) surface (see

Fig. 8.1) offers both threefold and fourfold coordinated sites, but the symmetry is different from that of fcc(311) surfaces. In this chapter, the vibrational structure of H adsorbed at Ru(11$\bar{2}$1) is presented and a model for the adsorption sites is derived.

The early work of hydrogen adsorption on metal surfaces has been reviewed by Christmann [101, 105]. The H/Ru(0001) system was studied by LEED [47–49], TDS [50] and HREELS [51–53]. Above 75 K the chemisorbed H is disordered, and the maximum coverage of 1 ML can be reached at very large doses. Below 75 K several ordered structures were observed. H occupies the fcc threefold-hollow sites [47]. Two desorption peaks around 380 and 320 K appear in the TD spectra at high coverages [50, 53]. The HREEL results show that: Only one Ru–H stretching mode at 85 meV was observed at low coverage, while three loss peaks were observed at 85, 95 and 140 meV at high coverage. The H/Ru(10$\bar{1}$0) system was studied by LEED, TDS and HREELS [59, 100]. The TD spectra exhibit two strong peaks and two weaker features at intermediate temperatures of the two strong peaks. The four peaks correspond to four ordered LEED patterns. The maximum coverage can reach 2 ML. Two kinds of threefold coordinated sites are occupied by hydrogen.

In this chapter it will be shown that hydrogen is adsorbed on Ru(11$\bar{2}$1) in three different states which we tentatively identify with adsorption sites of different symmetry. From the vibrational energy we argue that the threefold sites are filled prior to the fourfold site.

8.2 Results

As shown in Fig. 8.1, the Ru(11$\bar{2}$1) surface is a very open surface. Four topmost layers can be observed in the "top view" of Fig. 8.1. The vectors of the Ru(11$\bar{2}$1) lattice are 4.69 Å along [1$\bar{1}$00] and 5.07 Å along [0$\bar{1}$11], respectively. The angle between the two vectors is 116.89°. For a clean Ru(11$\bar{2}$1) surface a (1 × 1) LEED pattern was observed, indicating that this surface is not reconstructed. No other LEED pattern was found during the whole adsorption process. Thus, the absolute coverage of hydrogen cannot be derived with the help of a LEED pattern here.

Fig. 8.2 shows a series of rather unusual TD spectra. Three desorption states can be observed in the spectra, which are denoted as α-, β-, γ-states. It is interesting

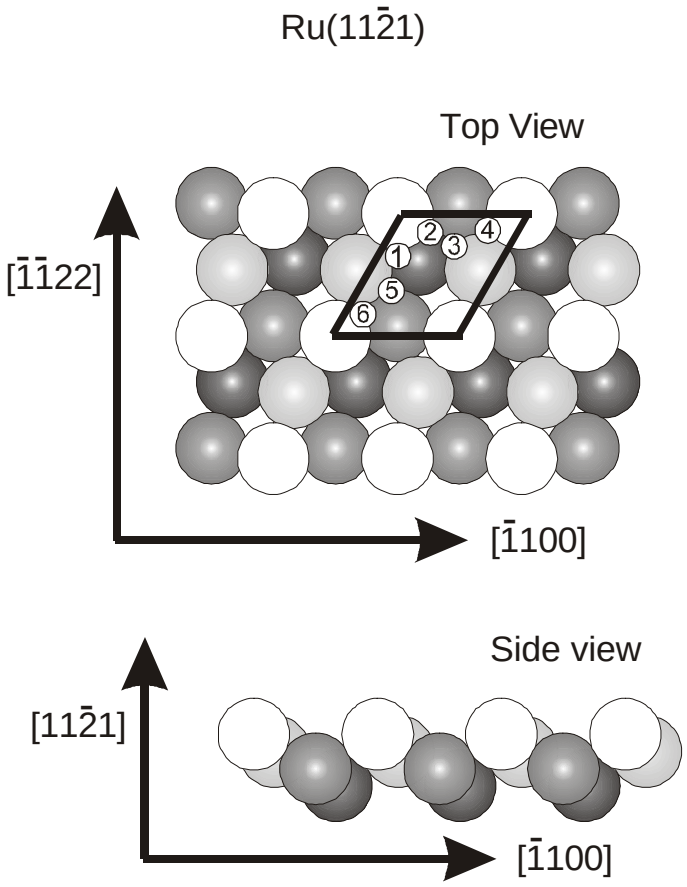

Figure 8.1: Top view and side view of the bulk-truncated Ru(11$\bar{2}$1) surface. The top layer is light, the layers below are indicated darker with increasing depth. The four topmost layers are shown.

to note that the width of the TD spectra for the γ- and β-state is very wide. This means that the interaction among the hydrogen atoms is strongly repulsive. The desorption temperature of the γ-state is around 345 K. A very wide desorption state, which is labelled β-state and whose temperature is in the range between 280 and 175 K, appears at higher doses. The α-state is observed at even higher doses, and the desorption temperature is at about 115 K. The shape of the α-state exhibits a very narrow half width in temperature. Besides it, the desorption temperature of the α-state is very low. In a first view, one might think that these findings indicate that the α-state evolves from the bulk. On the other hand, the amount of the α-state does not increase very much in intensity for exposures higher than 1.2 L H_2; even after dosing of 2400 L its intensity increases only little. This observation is

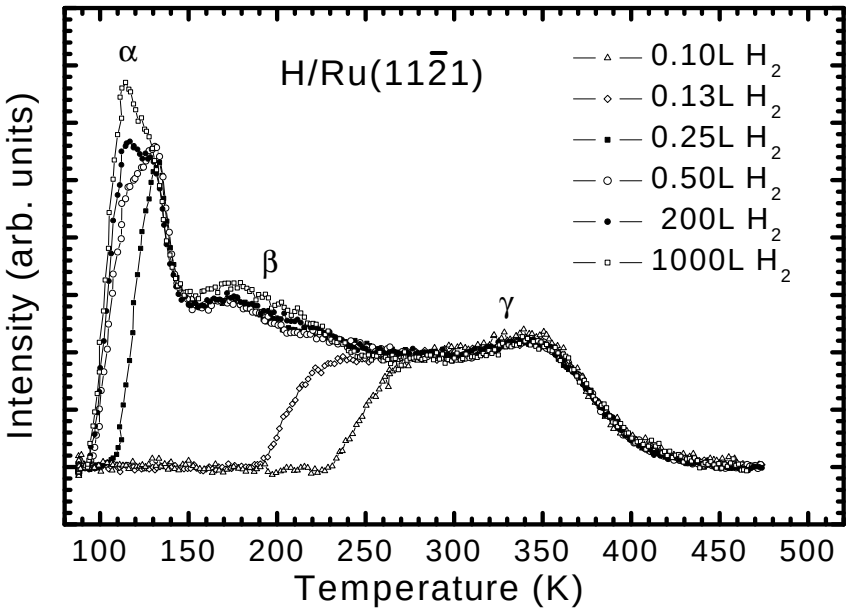

Figure 8.2: TD spectra (m/e = 2) for a sequence of H_2 exposures on Ru(11$\bar{2}$1) at 90 K.

against the idea of the α-state originating from the bulk. TDS measurements were also performed by exposing H_2, following sample cooling with liquid He, in order to check whether the desorption temperature of the α-state was below 90 K. This was found not to be the case. Therefore, it is concluded that the α-state does not evolve from the bulk, but from the surface.

Fig. 8.3 shows the HREEL spectra recorded directly after dosing at 90 K. As a main result, three different states can be observed also in HREELS, which can be easily identified as the corresponding α-, β- and γ-H states in TDS. At the beginning, for 0.12 L H_2, three loss peaks of γ-H appear at 62, 92 and 145 meV (see Table 8.1). With increasing exposure three new peaks appear, whose energies are 64, 115 and 160 meV, respectively. The three new peaks belong to β-H. At 0.24 L, the γ-H nearly disappears. At 0.36 L, two new peaks appear at 42 and 92 meV, obviously belonging to α-H. Compared with the spectrum at 0.24 L, the relative intensity of β-H has been changed. This shows that the dipole moment had been changed with increasing exposure. This goes along with a strong repulsive interaction among the hydrogen atoms indicated in the TD spectra. At 0.60 L, the α-H has increased and a new loss peak at 193 meV is observed. We interpret it as an overtone of the mode at 92 meV. At 2.4 L, the α-H has fully developed. A summary of the observed vibrations

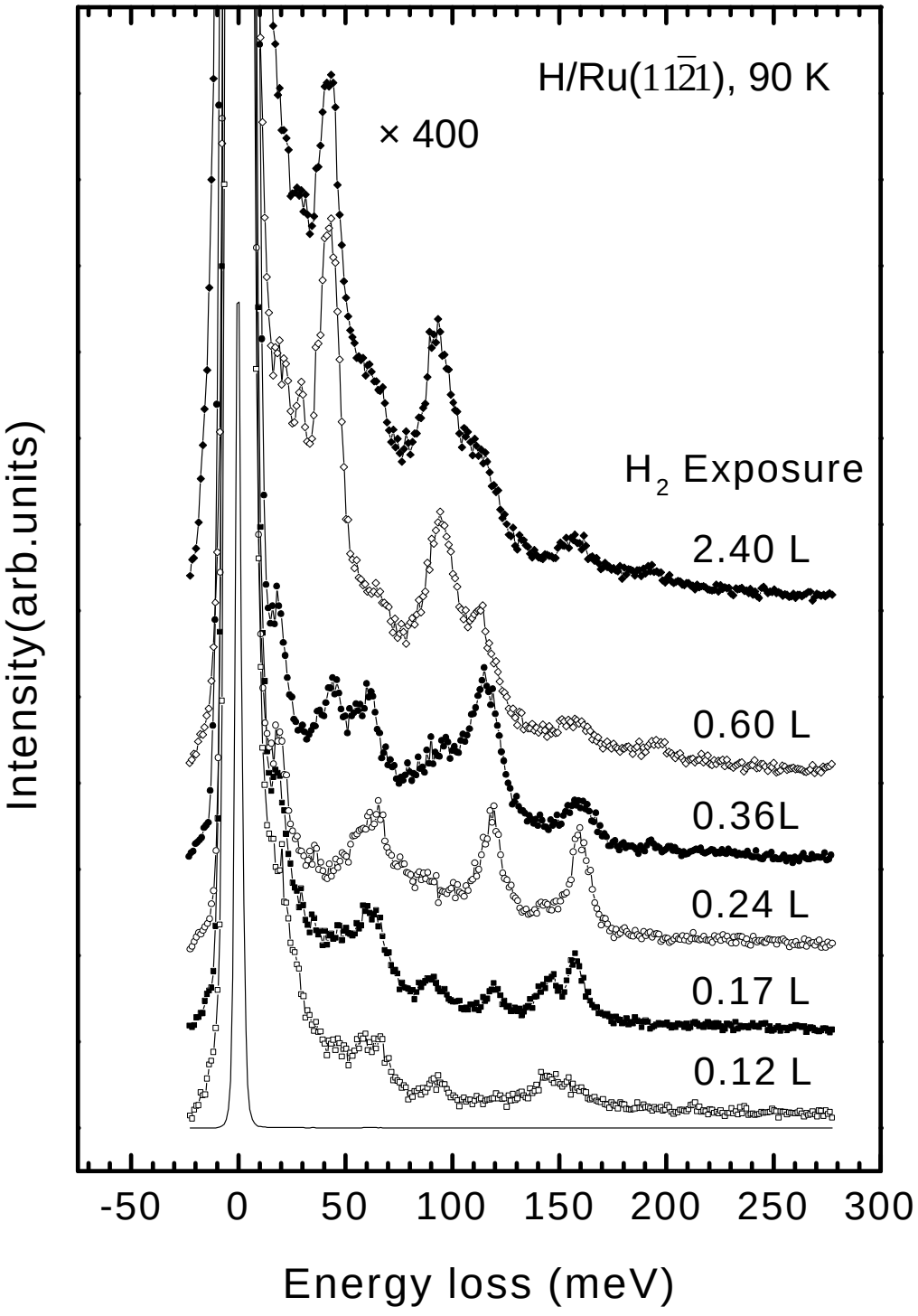

Figure 8.3: HREEL spectra of H chemisorbed on the Ru(11$\bar{2}$1) surface for a sequence of H_2 exposures at 90 K.

Table 8.1: Summary of the vibrational energies (meV) of the different hydrogen species for increasing hydrogen exposures on Ru(11$\bar{2}$1)

states	γ	β	α
desorption temperature (K)	345	175—280	115
exposure (L)	energy loss (meV)		
0.12	62, 92, 145		
0.17	62, 90, 145	64, 120, 158	
0.24		65, 119, 160	
0.36		61, 115, 160	45, 97
2.40		64, 114, 157	43, 93, 193

and TDS results is given in Table 8.1. All vibrational modes are dipole active, as proven by off-specular measurements because their intensity decreases quickly with increasing off-specular angle. As the symmetry of the Ru(11$\bar{2}$1) surface is C_s, we do not expect any forbidden peaks according to the selection rules for dipole scattering.

In order to confirm the relation between the desorption states in TDS and the species in HREELS, temperature-dependent experiments were performed. Fig. 8.4 shows a series of spectra taken after annealing at increasing temperatures starting from 2.4 L H_2 adsorption at 90 K. Comparing the spectra with the TDS results, one notices the following: After heating to 165 K, the α-state has disappeared completely. The same is true for the β-state after heating to 320 K. Thus, it can be concluded that the three states found in TDS give rise to characteristically different HREEL spectra, as summarized in Table 8.1.

8.3 Discussion

It is very difficult to deduce adsorption sites of hydrogen from HREELS data. In general, comparisons between specular and off-specular measurements offer symmetry information about the adsorption site. However, as the symmetry of Ru(11$\bar{2}$1) is only C_s, the off-specular measurements are of no help. Therefore, we try to reach some conclusions from an analysis of the vibrational energies. A calculation us-

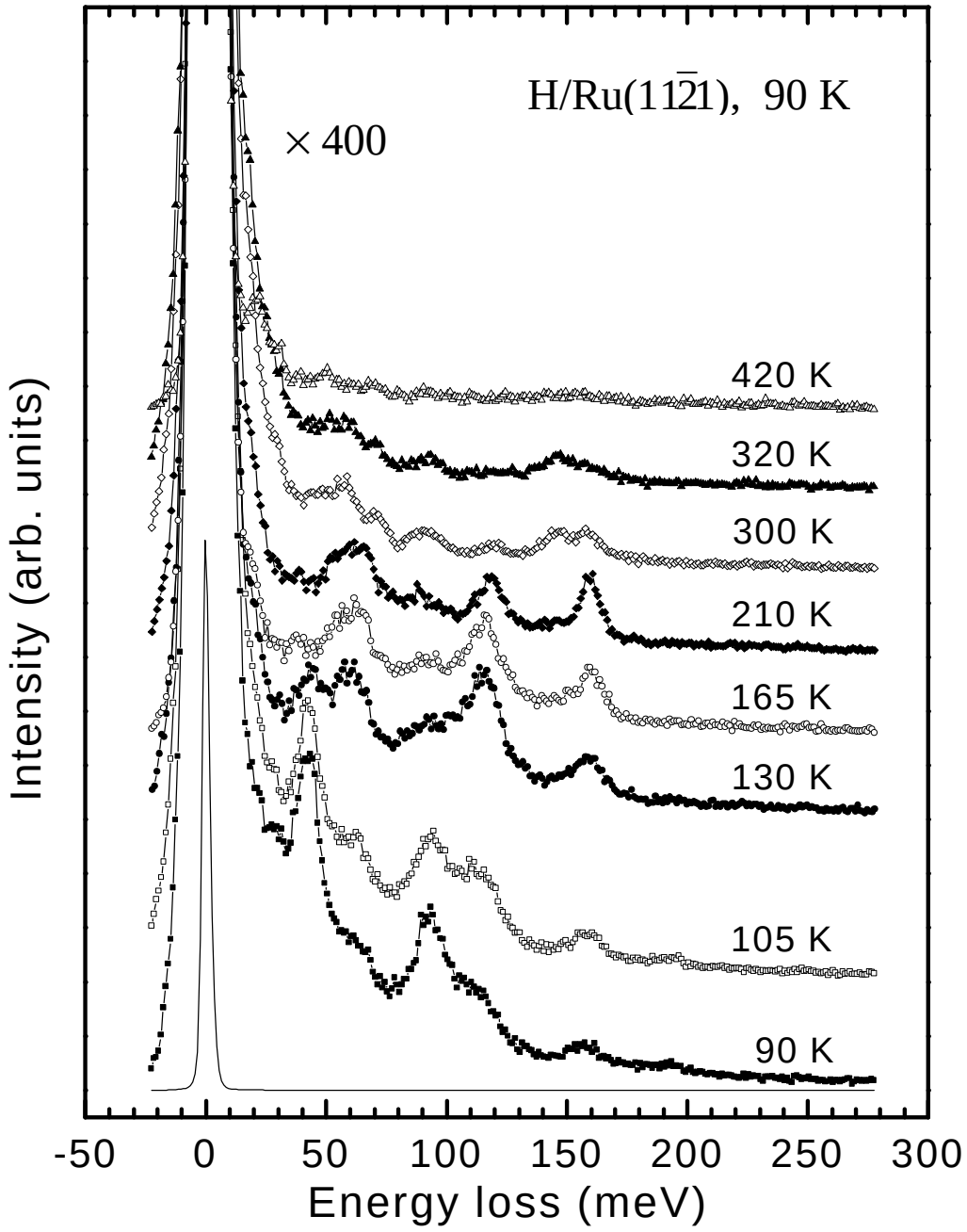

Figure 8.4: HREEL spectra of Ru(11$\bar{2}$1) exposed to 2.4 L H_2 at 90 K. The sample was subsequently annealed to the indicated temperatures. The spectra were recorded with the sample at 90 K.

ing the effective medium theory showed that a simple relation exists between the perpendicular vibration frequency, the bond length and the coordination [106]: The perpendicular mode decreases in energy for an increase in coordination. This means, it may be useful to compare our results with those from other metal surfaces, especially from the other low-index faces of Ru (see Table 8.2).

Table 8.2: Vibrational energies for atomic hydrogen on the Ru(0001) and Ru(10$\bar{1}$0) surfaces

Surface	$\nu_\perp$ (meV)	$\nu_\parallel$ (meV)	Reference
Ru(0001) (< 0.36 L)	85	—	[53]
Ru(0001) (41 L)	141	90, 102	[53]
Ru(10$\bar{1}$0) ($\theta_H = 1.0$)	150	27, 40	[59]
Ru(10$\bar{1}$0) ($\theta_H = 2.0$)	165	27, 45	[59]
	128	78, 100	

The number of energy loss peaks for one adsorption state can also supply some information on the site symmetry. When H adsorbs at a threefold-symmetric hollow site (C_{3v} symmetry), e.g., at hcp(001) or fcc(111), the two parallel modes are degenerate. If H is shifted off the center position or if the surrounding is not symmetric, this degeneracy is lifted. In these cases, the energy difference between the two parallel modes is larger when the surrounding of the site is more asymmetric. For a twofold-symmetric (bridge) site (C_{2v} symmetry) the difference is large. There is another configuration, in which the hydrogen atoms sit on a three-fold hollow site but also with a C_{2v} symmetry due to the interaction of two neighbor hydrogen atoms. This situation was observed on the H/Ni(110) system [107]. The situation is complex for the Ru(11$\bar{2}$1) surface. Within the unit cell there is a larger number of what we want to call pseudo-threefold sites: The local coordination is threefold, but the plane through the three neighboring atoms is tilted against the Ru(11$\bar{2}$1) surface. In this case, all three (one $\perp$ and two $\parallel$) motions of H are expected to be observable. The six pseudo-threefold sites are numbered in Fig. 8.1. One also recognizes a fourfold site near to the lower right hand corner and four bridge sites.

From the comparison with the Ru(0001) and the Ru(10$\bar{1}$0) surfaces we assign the modes of the highest energy to the $\perp$ vibration. Using these principles, the three states were associated with different adsorption sites. This approach is certainly

rather qualitative. It is also difficult since the real structure of the Ru(11$\bar{2}$1) surface is not known yet. It is known from LEED that there is no reconstruction, but any kind of relaxation cannot be excluded so far. Therefore, our discussion is based on the bulk-truncated structure as depicted in Fig. 8.1.

First, we discuss the γ-H. The number and energies of the observed vibrations compare favorably with those found for high-coverage phases on Ru(0001) and Ru(10$\bar{1}$0) (see Table 8.2). The energy difference between two parallel modes for Ru(11$\bar{2}$1) is somewhat larger than that for Ru(0001) and Ru(10$\bar{1}$0). Since the surrounding of the pseudo-threefold site is more asymmetric for the Ru(11$\bar{2}$1) surface, it is reasonable for us to assign the γ-H to adsorb at one of the pseudo-threefold hollow sites (No. 1–6 in Fig. 8.1).

Second, we turn to the β-H. As seen from Table 8.1, it is distinctly different from the γ-H. Although the number of the observed modes is appropriate for a pseudo-threefold site, we were first tempted to assign it to a bridge site since the energy for one of the two parallel modes is much larger than for the γ-H. Besides the six pseudo-threefold hollow sites, as indicated in Fig. 8.1, there are at least four bridge sites in the 1×1 unit cell. On the other hand, an alternative interpretation is more likely. From the HREELS spectra it is observed that the γ-H vanishes while the β-H fully develops. Thus, it seems that γ-H is transferred into β-H at higher coverage. This observation is in good agreement with the TDS results. It is well known that in TDS two states may be simulated due to repulsive interaction among the adsorbed atoms although the adsorption occurs always at the same site. In addition, hydrogen preferentially adsorbs at the highest-coordinated site available on the surface [101]. Therefore, the β-H is assigned to adsorb at the neighbor site of γ-H. Thus, only β-H was observed with a similar symmetry of C_{2v} because the potential-energy surface for H adsorption is changed by the arrival of the second H atom, so that the HREEL spectrum changes appreciably. Since the Ru(11$\bar{2}$1) unit cell is rather large, it is reasonable to assume that for the β-state a second H atom is adsorbed per unit cell.

Third, we turn to the α-state for which the vibrational energies are relatively small. This compares favorably with the data from hydrogen adsorbed on fourfold sites of other metal surfaces, which is shown in Table 8.3. The comparison with the H data from the other Ru surfaces also support this idea. As on Ru(0001) and

Table 8.3: Vibrational energies for hydrogen at a fourfold hollow site

Surface	Vibrational energy	Reference
Rh(100)	70 (⊥), 50 (∥) 82 (⊥), 65 (∥)	[109]
Ni(100)	72—74	[110]
Ni(100)	66 (⊥) (low coverage) 78 (⊥) (high coverage)	[111]
Ni(510)	73 (⊥), 48 (∥) (low coverage) 80 (⊥), 58 (∥) (high coverage)	[112]
Ni(311)	43, 90	[103]
Pd(100)	63 (⊥), 76 (∥)	[113]
Pd(311)	56, 85	[104]

Ru(10$\bar{1}$0), there are no fourfold sites, and the vibrational energies are higher than for the α-state on Ru(11$\bar{2}$1). Therefore, it is tentatively concluded that the α-state is due to a third hydrogen atom in the unit cell adsorbed at the fourfold-symmetric site. In addition, the line width of the α-H loss peaks are smaller than those for the other two species. This supports our assignment, because effective-medium calculations produced smaller line widths for the fourfold site compared to the threefold site [108]. The saturation coverage of H is near to 1.0 ML on Ru(0001) [53] and 2.0 ML on Ru(11$\bar{2}$1) [59], respectively. In both cases, the concentration of hydrogen is about 1.5×10^{15} atoms/cm^2. Thus, it is reasonable to assume three hydrogen atoms in one unit cell on the Ru(11$\bar{2}$1) surface. Fig. 8.5 gives a possible model for hydrogen to adsorb on Ru(11$\bar{2}$1) according to the above discussion. For this model it was assumed that the hydrogen atoms are distributed as evenly as possible.

8.4 Summary

The hydrogen adsorption at the very open Ru(11$\bar{2}$1) surface was studied by using TDS and HREELS. Both methods made it possible to differentiate three different adsorption states which are filled sequentially. The first two states very likely occupy two of the six pseudo-threefold sites available in the bulk-truncated (1×1) unit cell.

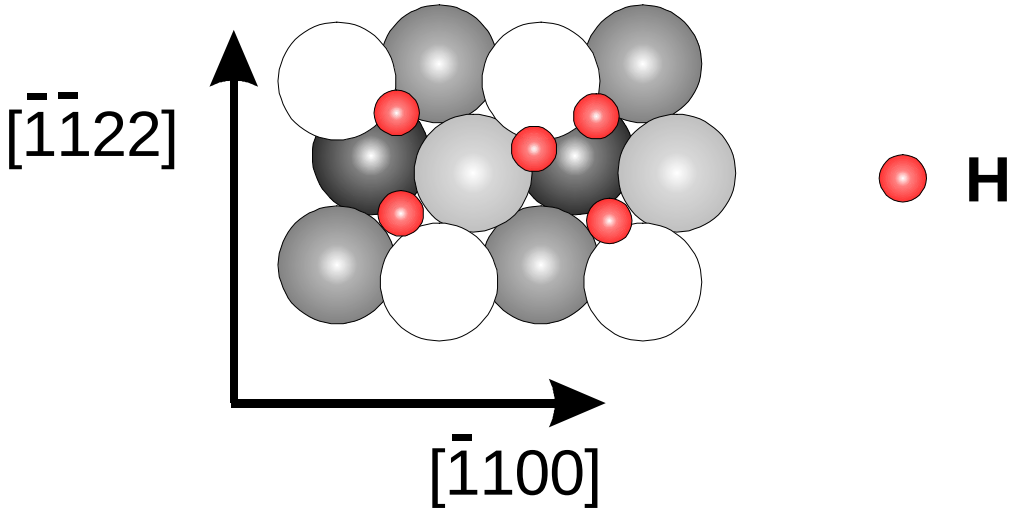

Figure 8.5: The model of hydrogen absorbed at the Ru(11$\bar{2}$1) surface.

The arrival of the second hydrogen atom changes the potential-energy surface of H adsorption, so that both H atoms per unit cell appear as the β-H in HREELS. In the α-state, a third H atom is squeezed into the unit cell for high exposures. It may be adsorbed at the fourfold symmetric site.

9 CO adsorption and dissociation on Ru(11$\bar{2}$1)

9.1 Introduction

The adsorption of CO on metal surfaces serves as a prototype system for understanding chemical reactions of molecules on surfaces and has been widely investigated in the past [114, 115]. The adsorption and dissociation of CO are important steps in many catalytic reactions such as CO oxidation, CO methanation or Fischer-Tropsch synthesis [38, 39]. The dissociation of CO on transition-metal surfaces has been widely studied. It is generally found that, going from the left- to the right-hand side and from 3d- to 5d-metals in the periodic table, the activity for dissociation decreases [116]. There is a boundary line in the periodic table for CO dissociation on metal surfaces at RT: CO dissociates on the left-hand side of Fe, Tc and W (including them) but adsorbs as a molecule on the right-hand side of Co, Ru and Re (including them). This behavior is due to the so-called electronic factor. Besides the electronic factor, the geometrical factor is important for the dissociation of CO. A more open surface is usually more efficient in CO dissociation. In general, the metal in the boundary line shows high catalytic activity for many reactions. On the metal of the left-hand side the bonding of dissociated products with the substrate is too strong to be available for further reaction steps, although the dissociation is favorable, while on the metal of the right hand side the adsorbate does not easily dissociate. As a metal in the boundary line of the periodic table, Ru shows very good catalytic activity in CO methanation and Fischer-Tropsch synthesis.

As far as Ruthenium is concerned, most studies deal with the basal Ru(0001) surface [40–46, 96]. Only a few reports exist for the more open surfaces, such as Ru(10$\bar{1}$0) [117, 118] and Ru(11$\bar{2}$0) [119–121] as well as a stepped Ru(0001) surface, namely Ru(1 1 10). There are not many studies on Ru(11$\bar{2}$1). Only the decomposition of nitrogen or of ammonia was reported [56, 57], and the hydrogen adsorption was discussed in the last chapter. In order to rationalize the results of CO adsorption on the Ru(11$\bar{2}$1) surface, the adsorption and dissociation of CO on other Ru surfaces are recalled as follows: On the Ru(0001) surface CO adsorbs at an on-top site for coverages below 0.33 ML with a $\sqrt{3} \times \sqrt{3}$ structure. For coverages above 0.33 ML, some CO shifts off the on-top site but still bonds linearly with the surface (CO molecular axis perpendicular to the surface bonding by only one bond). The maximum coverage at low temperature can reach about 0.67 ML [41]. On the Ru(10$\bar{1}$0) surface, five different ordered structures were found. CO molecules bond linearly to the surface for coverages below 1.0 ML, and the part of CO above 1.0 ML adsorbs on the bridge sites [117]. The maximum coverage of CO on the Ru(10$\bar{1}$0) surface is about 1.22 ML. On the Ru(11$\bar{2}$0) surface, a (1 × 2) LEED pattern was observed with the (0,1/2) and (0,-1/2) spots missing at saturation, indicating a mirror glide plane [119], which was recently explained as a p(1 × 2)p2mg phase [120]. Besides this, another p(1 × 2) phase is found for smaller coverage. The maximum coverage is about 0.5 ML, and CO adsorbs always at an on-top site.

Dissociation of adsorbed CO was not observed for Ru(0001) and Ru(10$\bar{1}$0) surfaces at RT and during heating, which is consistent with its position in the periodic table. On the other hand, dissociation of CO was observed in TD spectra of the stepped Ru(1 1 10) surface, and a kind of inclined CO, which is favorable to dissociate, was also confirmed by UPS [122]. Recently, the dissociation of adsorbed CO was also observed on the Ru(11$\bar{2}$0) surface even at RT [121]. It is interesting to note that the dissociation of adsorbed ammonia exhibits similar properties. The dissociation of ammonia on Ru(0001) and on Ru(10$\bar{1}$0) is not achieved at a temperature below RT [56, 57] but the adsorbed ammonia can dissociate on Ru(1 1 10) [122] and Ru(11$\bar{2}$0) [123] during heating. The adsorbed ammonia was found to dissociate on Ru(11$\bar{2}$1) [56, 57]. Thus, we expected that the CO can also dissociate on the Ru(11$\bar{2}$1) surface.

In this chapter the TDS and HREELS results of CO adsorption on the Ru(11$\bar{2}$1)

surface are presented. CO dissociation is found even at RT. The factors affecting the CO dissociation will be discussed.

9.2 TDS of CO on Ru(11$\bar{2}$1)

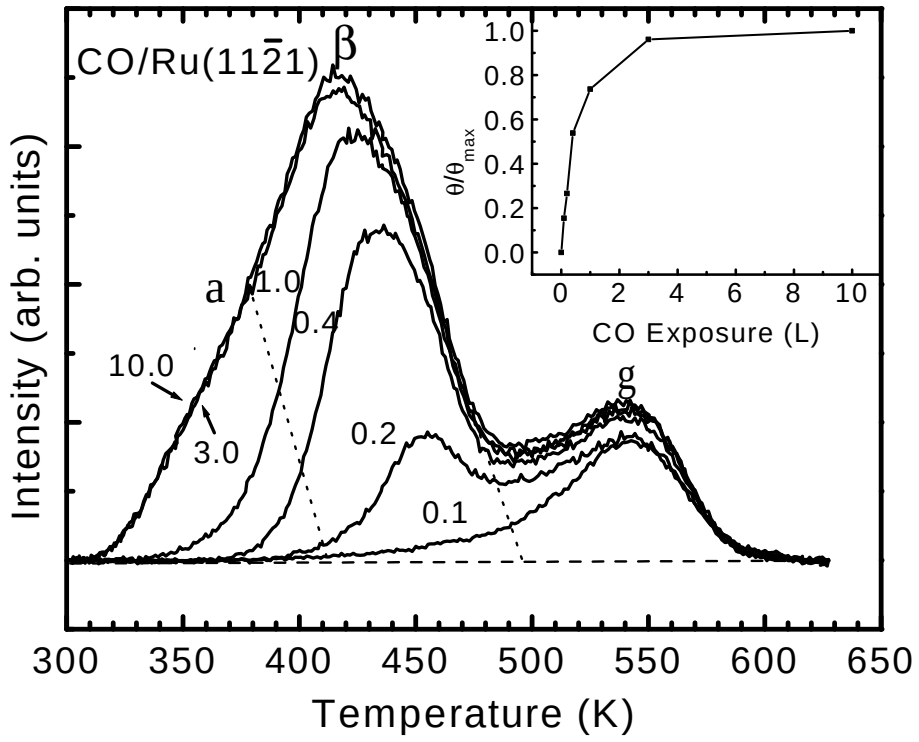

Figure 9.1: TD spectra following a series of CO adsorption on the Ru(11$\bar{2}$1) surface.

TD spectra of CO adsorbed on Ru(11$\bar{2}$1) at RT are shown in Fig. 9.1. For exposures below 0.1 L, only one peak around 540 K is observed, which is denoted as γ-state. With increasing CO exposure, a new peak around 450 K appears and gradually shifts to 420 K. This desorption state is denoted as β-state. For a CO exposure of 3.0 L, the adsorption of CO is nearly saturated since the TD spectrum for 10.0 L does not change anymore. At this exposure, a shoulder around 360 K appears, which is denoted as α-state. In order to estimate the amount of CO in different desorption states, we divide the TD spectrum for 3.0 L CO exposure into three regions with dashed lines, as shown in Fig. 9.1. The area on the right-hand region represents the γ-state. Its area can be estimated by integrating the TD spectrum for 3.0 L CO exposure from 490 to 600 K. The area on the left-hand region

approximately represents the α-state. Its area is nearly equal to the area difference between the spectra for 3.0 and 1.0 L CO exposure. The area of the α-, β- and γ-states are approximately 27 %, 54 % and 19 %, respectively, of the total area of the TD spectrum for saturation coverage. The relative coverage of CO as a function of CO exposure is also shown in the inset of Fig. 9.1. The CO coverage increases linearly up to 0.4 L exposure. This indicates that CO adsorbs via a precursor state in this CO exposure range, so that the sticking coefficient is nearly constant.

Differently from the TD spectra of CO on Ru(0001) and Ru(10$\bar{1}$0), for which the high-temperature state is the main desorption state, the area of the γ-state is quite small. CO desorbs around 410 and 475 K on the Ru(0001) surface [44] and around 380, 400 and 500 K on the Ru(10$\bar{1}$0) surface [117], but for Ru(11$\bar{2}$1) the desorption maximum of the γ-state is around 540 K which is higher than the value on Ru(0001) or Ru(10$\bar{1}$0). The relatively higher desorption temperature and the relatively small amount for the γ-state indicate that the γ-state results from the recombination of dissociated CO. Adsorbed CO does not dissociate on the Ru(0001) and Ru(10$\bar{1}$0) surfaces during heating. A desorption state with a desorption maximum around 580 K was observed in the TD spectra of the CO covered Ru(1 1 10) surface and was assigned to recombination of dissociated CO [122]. Recently, the dissociation of CO was also found on the Ru(11$\bar{2}$0) surface [121]. The desorption maxima of two dissociated states are around 500 and 540 K, respectively. Comparing the desorption temperatures of CO from molecular adsorption and from dissociated CO, the γ-state of Ru(11$\bar{2}$1) can be suggested to result from the recombination of dissociated CO, while the other two desorption peaks around 360 and 420 K result from the molecular adsorption.

9.3 HREELS of CO adsorbed on the Ru(11$\bar{2}$1) surface

Fig. 9.2 shows a series of HREEL spectra for various CO exposures on the Ru(11$\bar{2}$1) surface at RT. For 0.1 L CO, the C–O stretching vibration appears at 240 meV and the Ru–CO one at 55 meV. With increasing CO exposure, a continuous shift of the C–O stretching mode is observed to higher energy, up to 254 meV for 3.0 L. This

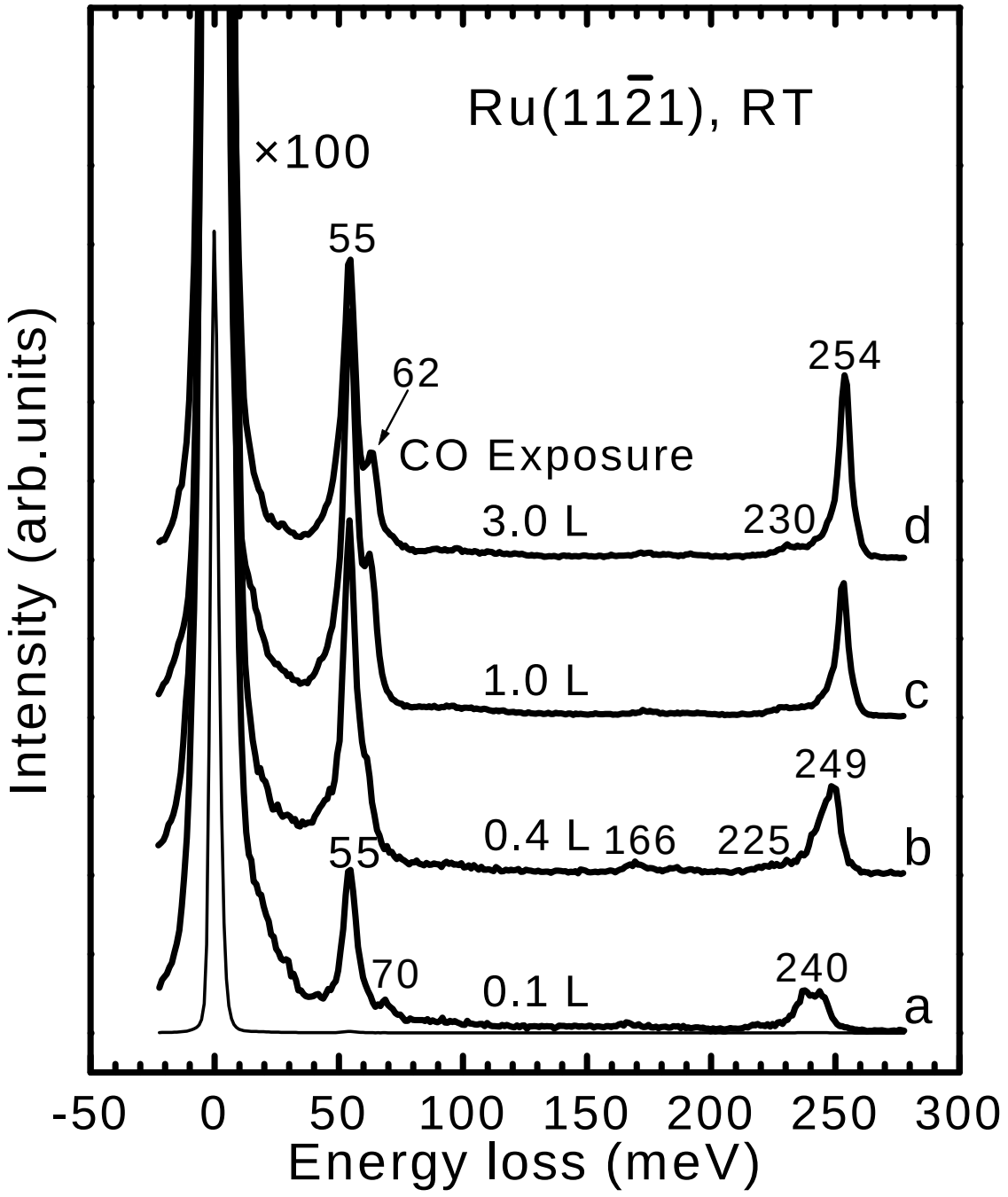

Figure 9.2: HREEL spectra for CO on the Ru(11$\bar{2}$1) surface with increasing CO exposures at RT.

indicates a terminally bonded CO molecule, as it is found for CO adsorption on other Ru surfaces for low or medium coverage. Normally, CO fills-in the high-temperature state first. This CO species should correspond to the γ- and β-state in TD spectra. Obviously, for low CO exposure (e.g. <0.1 L), the CO species dissociates first and then recombines and desorbs as γ-state during increasing the temperature; for higher CO coverage, it partially desorbs as β-state in TDS, and also partially dissociates first and then recombines and desorbs as γ-state. The CO species is denoted as β-CO.

In addition to the CO related losses, a loss peak around 70 meV is observed. This peak can be assigned to the Ru–O stretching mode of oxygen, which results from the dissociation of CO and will be discussed in detail later. This observation supports the suggestion that γ-CO results from the recombination of dissociated CO. For CO exposure above 0.4 L, another C–O stretching mode appears as a small peak around 225 meV and shifts to 230 meV at higher coverage. At the same time, a peak around 62 meV appears as a shoulder of the peak at 55 meV. The peak grows also in intensity with increasing CO exposure. Obviously, the loss peak at 61 meV can be assigned to a Ru–CO stretching mode of another CO species whose energy of the C–O stretching mode is at 230 meV. According to the "frequency rule" it belongs to CO on a kind of bridge site. This CO species can be attributed to α-CO, which corresponds to the α-state in the TD spectra. A CO adsorbed at a bridge site was also reported for the Ru(10$\bar{1}$0) surface at a coverage above 1.0 ML [117]. Another peak around 169 meV appears in the spectrum for 0.4 L CO exposure and disappears again for 1.0 L. It is assigned to a precursor state for CO dissociation and will be discussed later.

In order to avoid the CO dissociation, CO was also exposed at 85 K. The corresponding HREEL spectra are shown in Fig. 9.3. The missing of a loss peak at 70 meV in all spectra shows that CO does not dissociate at 85 K. The spectra of CO, exposed at 85 K, are somewhat different from those at RT. At low coverage more peaks appear in the spectra, and at high coverage the intensity of the α-CO stretching mode is obviously stronger than that at RT. This can be explained by the following consideration. The mobility of the CO molecules is insufficient to reach real equilibrium at LT, so that the relative distribution of different CO species on the surface depends also on the temperature. Hence, more loss peaks can appear on

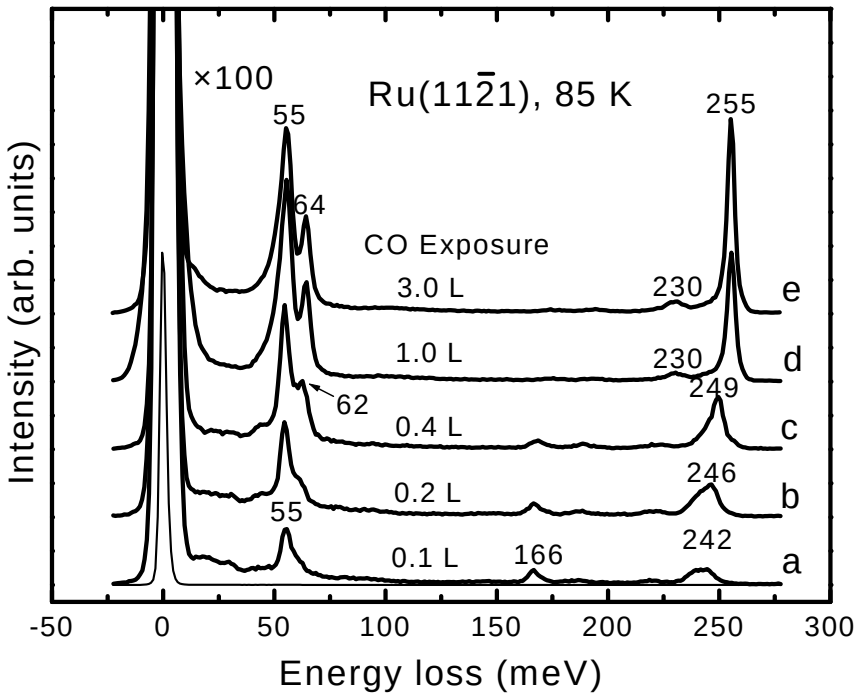

Figure 9.3: HREEL spectra for CO on the Ru(11$\bar{2}$1) surface with different CO exposures at 85 K.

the HREEL spectra for CO exposure at LT. In addition, the saturation coverage for CO exposure at LT is usually somewhat higher than that at RT. For example, the coverage of CO on Ru(0001) is 0.54 ML for RT, but 0.67 ML for LT [41, 45]. Thus, the intensity of the loss peaks of α-CO for high CO exposure at 85 K is relatively stronger than that at RT, which was shown in Fig. 9.2.

The spectrum for low CO exposure on Ru(11$\bar{2}$1) at LT is obviously different from that at RT. Four loss peaks in the regime of the C–O stretching mode can be distinguished in the spectra. The peak at 240 meV, which grows in intensity and shifts to 254 meV at high CO coverage, is from the C–O stretching mode of the β-CO. The very weak peak at 220 meV, which shifts to 230 meV at high CO coverage, is from α-CO. The peak at 185 meV is also very weak in intensity and disappears at high coverage. Thus, it can be attributed to the C–O stretching mode for CO at defect sites, e.g., steps. The peak at 166 meV is also attributed to a C–O stretching mode, although its energy is unexpectedly small. One may consider therefore that it is not due to CO. On the other hand, the main residual gases are H_2 and CO. As known from the last chapter, the energy of vibrational modes, which are induced by

hydrogen on Ru(11$\bar{2}$1), is lower than 160 meV. Also the loss peaks of hydrogen do not appear as one peak alone, so that the possibility that the peak around 166 meV originates from hydrogen can be excluded. Therefore the loss peak at 166 meV is attributed to a CO-induced vibration. That four CO species appear in the same spectrum may be correlated with the large number of possible adsorption sites on the Ru(11$\bar{2}$1) surface, as indicated in Fig. 8.1 of the last chapter, and the insufficient mobility of the CO molecules at LT. This explanation is supported by the nitrogen adsorption on the same surface. After ammonia dehydrogenation, six different N–Ru stretching modes were observed in the HREEL spectrum [57].

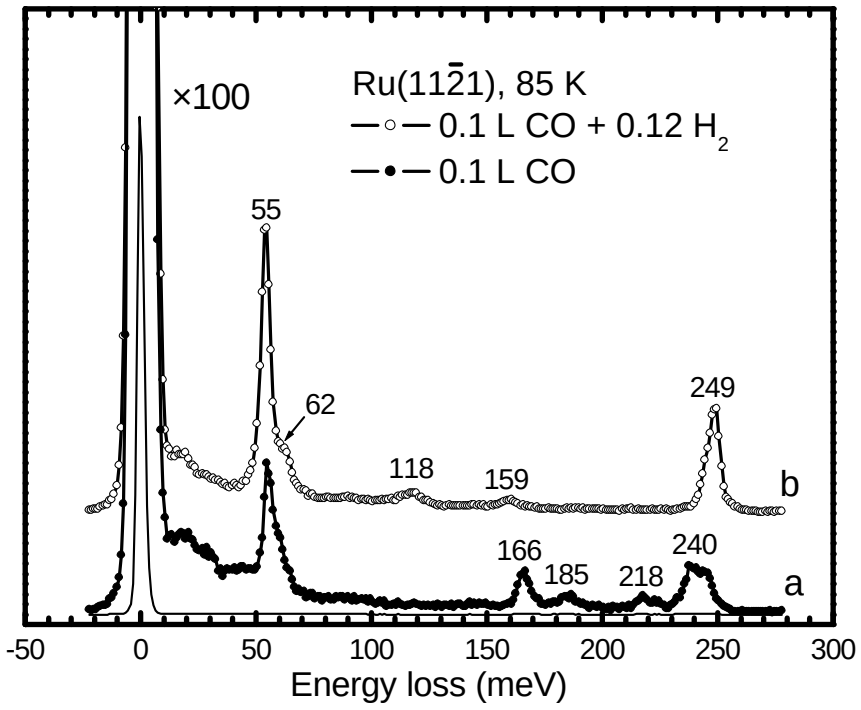

Figure 9.4: HREEL spectra of coadsorption of CO and hydrogen on the Ru(11$\bar{2}$1) surface

In order to investigate the effect of coadsorption on the CO species with the low C–O stretching energy, coadsorption experiments of H_2 and CO were performed for which the HREEL spectra are shown in Fig. 9.4. Curve (a) is the spectrum of 0.1 L CO exposure at LT and shows the four different groups of the C–O stretching mode described above. After an additional 0.24 L H_2 exposure, loss peaks of the C–O stretching modes shift to 249 meV or disappear. This indicates that all CO molecules are shifted to on-top sites. Except for the Ru–CO stretching mode at

55 meV and C–O stretching mode at 249 meV, three loss peaks appear at 62, 118 and 159 meV in curve (b), which belongs to β-H on the Ru(11$\bar{2}$1) surface, as shown in the last chapter. Obviously, the energy of a loss peak, induced by coadsorbed hydrogen, is not at 166 meV. This furthermore supports our conclusion that the loss peak at 166 meV is not due to hydrogen, instead, it results from CO molecules.

9.4 Thermal dissociation of CO on Ru(11$\bar{2}$1) surface

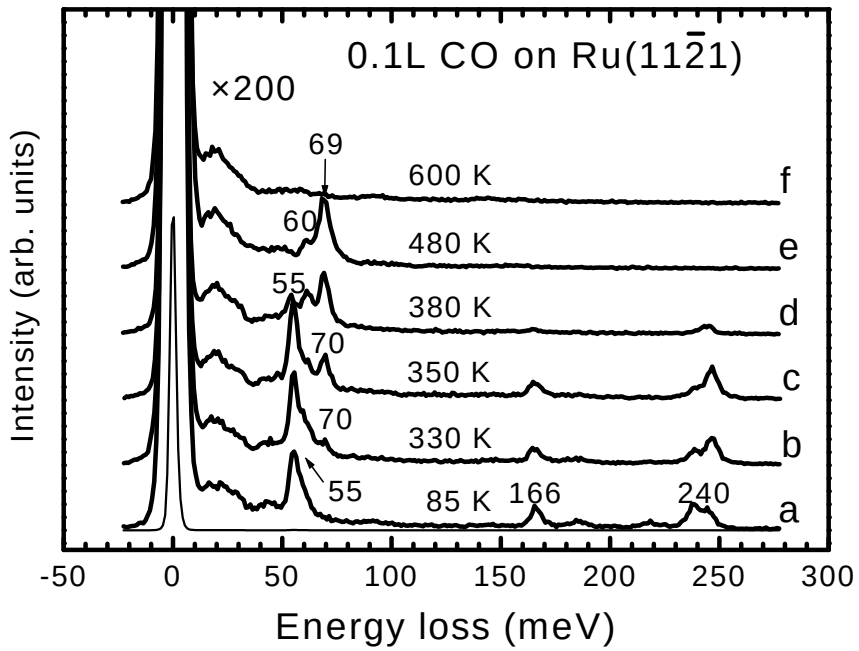

Figure 9.5: HREEL spectra of CO on the Ru(11$\bar{2}$1) surface after an exposure of 0.1 L CO at 85 K. The spectra were obtained at 85 K after annealing at noted temperatures for 1 minute.

In the TD spectra, only the γ-state was observed for 0.1 L CO exposure. The γ-state is suggested to be due to associatively desorbed CO. In order to verify this suggestion, a series of HREEL spectra was recorded (Fig. 9.5) after 0.1 L exposure at 85 K and subsequent annealing to various temperatures for one minute. After annealing the sample to 330 K, a loss peak at 70 meV appears in the spectrum, which was assigned to the Ru–O stretching mode as described above, indicating the dissociation of CO. At the same time, the loss peak at 166 meV decreases in intensity.

Most CO molecules dissociate after heating to 380 K. The loss peak at 166 meV nearly disappears. All the CO dissociates after heating to 480 K, and only two peaks around 50 and 70 meV are left in the spectrum, which is similar to the spectrum after CO dissociation on Ru(11$\bar{2}$0) [121]. The two peaks are attributed to the stretching modes of carbon and oxygen against the Ru surface atom. After flashing to 600 K, the spectrum of the clean Ru(11$\bar{2}$1) surface is recovered. This sequence of experiments indicates that the adsorbed CO can dissociate during heating, inducing loss peaks at 60 and 70 meV due to the dissociation products. Obviously, the loss peak at 70 meV is a key feature for CO dissociation on the Ru(11$\bar{2}$1) surface. The existence of the 70 meV peak in curve (a) of Fig. 9.2 indicates that CO can dissociate on the Ru(11$\bar{2}$1) surface at low coverage even at RT. This suggests that the γ-state in the TD spectrum results from the associative desorption of CO on Ru(11$\bar{2}$1) because CO is dissociated after annealing to 480 K.

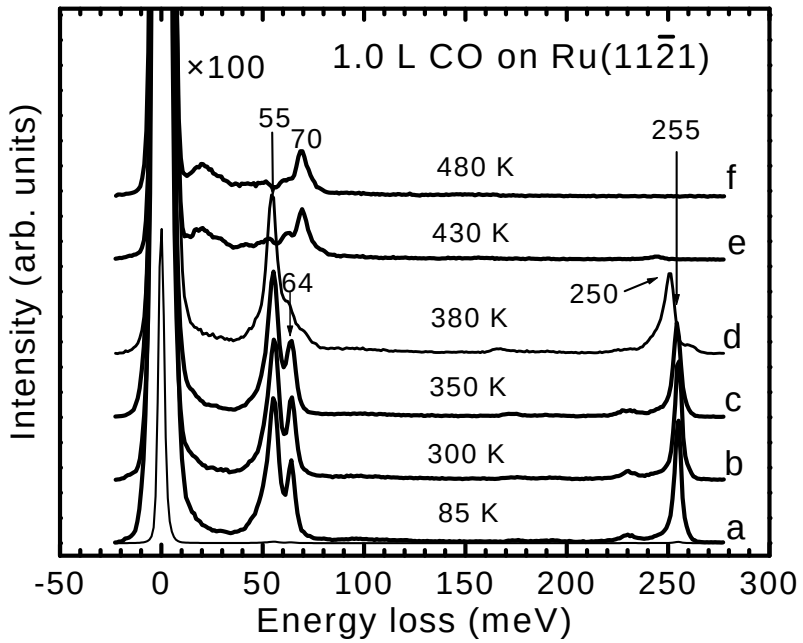

Figure 9.6: HREEL spectra of CO on the Ru(11$\bar{2}$1) surface after an exposure of 1.0 L CO at 85 K. The spectra were obtained at 85 K after the sample was annealed at noted temperatures for 1 minute.

The question arises whether the CO coverage can influence the dissociation. Fig. 9.6 shows a series of HREEL spectra recorded after 1.0 L CO exposure at 85 K, followed by sequently annealing to various temperature for one minute. Curve

(a) shows the α- and β-CO again. After heating the sample to 300 K, the loss peaks of 62 and 230 meV are somewhat reduced in intensity, indicating partial desorption of α-CO. After heating to 380 K, the loss peaks of α-CO nearly disappear, which is consistent with the desorption temperature of α-CO. Different from the spectrum for 0.1 L CO exposure, most β-CO molecules still remain on the surface. Only a small amount of CO dissociates, which is indicated by the weakness of the loss peak at 70 meV. A loss peak at 167 meV appears with small intensity at the same time. After heating to 430 K, the intensity of the loss peaks at 55 and 250 meV becomes very small. The loss peak around 170 meV disappears again. After heating to 480 K, only the products of CO dissociation remain on curve (e), which is similar to the spectrum after annealing the sample with 0.1 L CO exposure to 480 K. After annealing to 600 K (not shown), the carbon and oxygen species on the Ru(11$\bar{2}$1) surface have been recombined and desorbed.

9.5 Discussion

9.5.1 The adsorption structure of CO on Ru(11$\bar{2}$1)

During the whole CO exposure process no ordered LEED pattern was observed. Thus, the absolute coverage cannot be determined here. The coverage can only be estimated by combining the TD and HREEL spectra and comparing them with the results of CO adsorption on other Ru surfaces. When CO is exposed to Ru(0001), CO adsorbs on an on-top site for a coverage below 0.33 ML, and a $\sqrt{3} \times \sqrt{3}$ structure is formed at 0.5 ML. Since the distance of adjacent Ru on-top sites is too close for CO (2.7 Å), the interaction between CO molecules adsorbed on two adjacent on-top sites will be strongly repulsive. At a coverage above 0.33 ML, a compression phase of CO is formed, in which part of CO is shifted off its on-top position but still remains linearly bonded to the surface. The saturation coverage of the CO compression phase at low temperature is about 0.67 ML, i.e., about 1.04×10^{15} molecules/cm^2. When CO is exposed to Ru(10$\bar{1}$0), CO adsorbs on an on-top site for coverages below 0.5 ML, and a 2×1 structure is formed at 0.5 ML. Up to 1.0 ML, the CO molecules also shift off the standard on-top sites but still remain linearly bonded to the surface, which is similar to the behavior on Ru(0001). At 1.0 ML, CO occupies

all on-top sites and forms zig-zag rows [117], similar to that found for CO adsorbed on Ni(110) [124] and Pb(110) [125, 126]. By further increasing the CO coverage, the additional CO molecules adsorb on bridge sites, and the coverage of CO is about 1.22 ML at saturation, i.e., 1.05×10^{15} molecules/cm^2 [117]. The density of unit cells on Ru(11$\bar{2}$1) is about $4.72 \times 10^{14} \cdot \mathrm{cm}^{-2}$, which is somewhat smaller than the density of $\sqrt{3} \times \sqrt{3}$ single cells on Ru(0001). Therefore, for a coverage below 1.0 ML, it is reasonable to assume that all CO molecules adsorb on the on-top sites. If one assumes that each unit cell carries one CO molecule at the "on-top" site with its molecular axis perpendicular to the surface, too little space would be left for any further adsorption. For saturation it is therefore likely that CO shifts somewhat off the standard on-top site, so that an additional CO molecule can be placed in a bridge site in the middle of a unit cell. This leads to a total coverage near 1.5 ML. The behavior of CO which shifts off its on-top site at saturation is also observed for Ru(0001) and Ru(10$\bar{1}$0). According to our estimate, the area of the α-state in the TD spectrum at saturation is near to 1/3 of the total area, i.e., β-CO takes 2/3 and α-CO 1/3 of the total coverage of 1.5 ML.

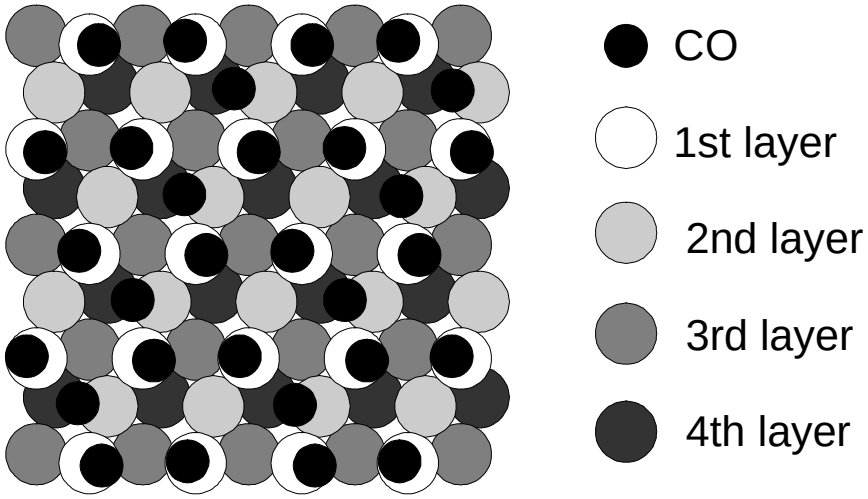

Figure 9.7: One possible adsorption mode of CO on the Ru(11$\bar{2}$1) surface at the saturated coverage.

Fig. 9.7 shows a possible model for CO at saturation on Ru(11$\bar{2}$1). Interestingly, the intensity of the Ru–CO stretching mode of α-CO is about half of that of β-CO. In our model the second kind of CO adsorbs on a bridge site, similar to the finding for CO adsorption on Ru(10$\bar{1}$0). It also fits well to the loss peak at 230 meV in the

HREEL spectra, which indicates bridge-CO. The intensity of the C–O stretching mode of α-CO is very small. This is somewhat unusual, but the intensity of bridge-CO on Ru(10$\bar{1}$0) is also very small. The explanation for the small intensity may be as follows: The α-CO could be somewhat tilted in order to reduce the repulsive interaction with the neighbor CO molecules, so that the dipole moment perpendicular to the surface is reduced and the cross section for its vibrational excitation is decreased. In addition, the position of the α-CO is somewhat lower than that of β-CO. Hence, it could be somewhat screened by β-CO, so that its intensity is furthermore decreased.

9.5.2 The dissociation precursor

Normally, a CO species with very low C–O stretching vibrational energy is a precursor state for CO dissociation. For low CO exposure at LT, the loss peak around 166 meV is relatively strong and the CO species is easily dissociated. The loss peak is suppressed for high coverage. When heating the surface, some CO desorbs first and the loss peak at 166 meV appears again, accompanying the CO dissociation at this temperature. This indicates that this CO species correlates with the CO dissociation. Thus, the peak at 166 meV can be attributed to a precursor for CO dissociation.

Table 9.1: The CO species with very low C–O stretching energy on different transition-metal surfaces

surface	Cr(110)	Mo(110)	W(110)
energy (meV)	143–161	140–168	169
reference	[127], [128]	[129]	[130]
surface	Mo(001)	Fe(001)	Fe(111)
energy (meV)	132–153	150	164
reference	[131]	[132], [133]	[134]
surface	Ru(11$\bar{2}$1)	Ru(11$\bar{2}$0)	Ni[5(111) $\times$ (1$\bar{1}$0)]
energy (meV)	166	195	190
reference	this thesis	[121]	[135]

The chemisorption bond between CO and a transition-metal surface is a combi-

nation of an electron donation from CO 5σ into the metal valence bands and a back donation of an electron from the valence into CO $2\pi^*$ orbital. The back-donation can weaken the intra molecular CO bond, thus reducing the C–O stretching energy. If a CO molecule adsorbs strongly inclined and at a highly-coordinated hollow site, the back donation is very strong and the intra-molecular CO bond is strongly weakened, inducing a very low C–O stretching energy. This is the so-called precursor state for dissociation. Although the back donation from the substrate to the $2\pi^*$ orbital for this kind of CO is very strong, obviously stronger than that for an upright species, CO usually prefers to adsorb upright and to take the on-top site (but sometimes also the bridge site) for the metal on the right-hand side of boundary line. So, the existence of the precursor is determined by the ability for back-donation of the substrate into the CO $2\pi^*$ orbital. It has been suggested [116] that the transition metals on the left-hand side of the boundary line are more available for CO back donation because the atomic electron-negativity for transition metals is generally lower at the left-hand side. For the Cr, Mo and W surface, the back donation is strong enough, so that the energy of the adsorption state is more favorable for the CO precursor than that for linearly bonded CO. Thus, the precursor exists even for close-packed surfaces such as Cr(110) [127], Mo(110) [129] and W(110) [130] and is filled first. The ability of back donation for the metals, which lie at the boundary line, is not so strong, and the precursor does not exist on the close-packed surfaces of these metals, e.g., on Fe(110) and Ru(001). Obviously, on these surfaces the linearly bonded CO is more favorable in energy. On the other hand, the configuration of Fe atoms on the Fe(001) surface is very suitable for electron back donation, so that a strong precursor with vibrational energy as low as 150 meV was observed and the species exists up to 0.5 ML [132, 133]. The stronger ability of back donation on bcc(001) was also observed for Mo. The CO dissociation precursor on the Mo(001) surface shows lower C–O vibrational energy than that on the Mo(110) surface [129, 131]. For Fe(111) the precursor is very weak, which indicates that the adsorption energy of CO on this surface is more in favor of linearly bonded CO because the geometrical structure on the surface is not suitable enough for electron back donation. For the metals on the right-hand side of the boundary line, the low C–O stretching mode was observed only for open or stepped surfaces, e.g.: for Ni[$5(111) \times (1\bar{1}0)$] [135], Ru($11\bar{2}0$) [121] and in this work also for the Ru($11\bar{2}1$) surface. The C–O stretching energy for these examples is presented in Table 9.1. Obviously, it can be concluded

that the existence of the molecule precursor of CO dissociation is mainly given by the ability of electron back donation from the surface.

By coadsorption with alkali-metal atoms the property of the surface becomes like that of the metal on its left-hand side in the periodic table since the alkali-metal can transfer the electron to the substrate. A largely tilted or "side-on" CO species with low C–O stretching energy was observed for K/Fe(110) [137], Cs/Ru(0001) [138] and Cs/Ru(10$\bar{1}$0) [139] coadsorption systems. On the other hand, by coadsorption with highly electron-negative elements, the electron of the substrate can be consumed, resulting in a reduction of the back donation into the CO $2\pi^*$ orbital. Thus, the electronic property of the surface is like that of a metal on the right-hand side in the periodic table, inducing the suppression of the CO species with very low C–O stretching energy. The coadsorption with oxygen atoms was found to push the precursor to on-top sites on Cr(110) and Mo(110) [127, 129]. This general influence was nicely confirmed in this work by coadsorption with 0.24 L hydrogen, which inhibits the dissociation precursor. The electron is strongly back-donated into the CO $2\pi^*$ orbital for the inclined CO. This precursor can easily be suppressed by any coadsorbed species, by dissociation products or even by CO itself. The effect is more significant for the metals in the right-hand side of the boundary line than for those on the left-hand side. At high CO coverage, the CO dissociation precursor disappears on Ru(11$\bar{2}$0) [121], Ru(11$\bar{2}$1) and Ni[5(111) $\times$ (1$\bar{1}$0)] [135], but there is still a small amount of it on Fe(001) [132], Mo(001) [131] and Cr(110) [127]. On W(110) [130] the low C–O stretching state disappears only at saturation.

9.5.3 The partial dissociation of CO: the bonding-competition effect

During heating of Ru(11$\bar{2}$1), dissociation occurs together with desorption. The maximum amount of dissociation CO is about 20 % at saturation at RT, as described from the TD spectra. As discussed in the last two sections, the saturated CO coverage on the Ru(11$\bar{2}$1) surface at RT is estimated to be near to 1.5 ML. So, the maximum amount of dissociated CO can be estimated to be near to 0.3 ML, i.e., to be somewhat smaller than one CO molecule in every three unit cells. It is interesting to note that the maximum amount of ammonia dissociation on the Ru(11$\bar{2}$1) surface

is also near to 0.3 ML in the TD spectra after adsorption of NH_3 on the Ru(11$\bar{2}$1) surface at T < 180 K [57].

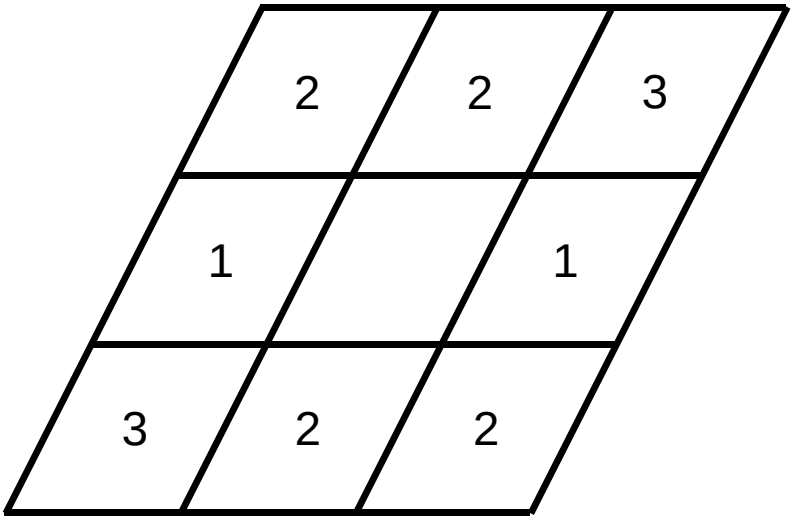

Figure 9.8: The distribution of neighboring sites.

Considering identical sites on the Ru(11$\bar{2}$1) surface, there are two nearest sites (in unit cell (1)) with a distance of 4.69 Å, four second-nearest sites (in unit cell (2)) with a distance of 5.01 Å, and two third-nearest sites (in unit cell (3)) with a distance of 8.32 Å for a site, as shown in Fig. 9.8. These eight identical sites are in the eight unit cells around the center site. The two third-nearest sites are obviously farther away than the other six sites. If another CO molecules is adsorbed on one of the two third-nearest neighboring sites, the interaction between the two adsorbates is obviously weaker than that on the other six unit cells. So, we do not include the two third-nearest neighboring unit cells, i.e., we consider only six neighboring unit cells. This situation, six empty unit cells around a filled one, corresponds to a coverage of 1/3 ML. If the adsorbates distribute not so evenly, the maximum amount of adsorbate in this state is somewhat smaller than 1/3 ML, in order to reach the condition that there is no adsorbate on one of the six neighboring unit cells. So, from the fact that only an amount of CO, somewhat smaller than 1/3 ML, can dissociate in the TD spectra, the following conclusion can be drawn: If CO does not occupy any neighboring unit cell, it will dissociate during heating. Otherwise, some CO will first desorb until no CO is adsorbed at neighbor unit cells.

This kind of relation between the CO dissociation and occupation of neighboring

unit cells has been also observed on other surfaces. On the Ru(11$\bar{2}$0) surface, the maximum amount of dissociated CO on the Ru(11$\bar{2}$0) surface is about 20 % of a saturated CO layer at RT [121]. The saturation coverage of CO adsorption on the Ru(11$\bar{2}$0) surface at RT is about 0.5 ML. So, the amount of dissociated CO is somewhat smaller than one CO molecule in four unit cells (because there are two Ru atoms in one unit cell). The lattice of the Ru(11$\bar{2}$0) surface has a rectangular structure. There are two nearest, two second-nearest and four third-nearest sites for each site at the unit cell, which are at distances of 4.34, 4.74 and 6.45 Å, respectively. Obviously, the distance to the third-nearest sites on Ru(11$\bar{2}$0) surface is not so far away as that on the Ru(11$\bar{2}$1) surface. Here, all of the eight surrounding unit cells should be included as neighboring cells. Hence, CO does not adsorb on a neighboring unit cell of another CO when 1/4 ML CO distributes evenly on the Ru(11$\bar{2}$0) surface. Therefore, a similar conclusion can be drawn, according to the fact that only an amount somewhat smaller than 1/4 ML CO can dissociate, when an adsorbed CO layer on the Ru(11$\bar{2}$0) surface is heated. If CO does not occupy neighboring unit cells, it will dissociate. Otherwise, some CO molecules will desorb until no CO is adsorbed in a neighboring unit cell. The similar relation between CO dissociation and occupation of neighboring unit cell exists also on the Fe surfaces. The maximum amount of dissociated CO is about 1/4 ML in the TD spectra of CO on the Fe(001) surface [140, 141]. The lattice of Fe(001) surface is a square lattice, thus, all of the eight surrounding unit cells should be included as neighboring unit cells, which fits well with the relation described above. The maximum amount of dissociated CO on Fe(111) during heating is about 0.22 of the saturated coverage which was estimated to be about 1.5 ML [136]. So, about 1/3 ML of adsorbed CO can dissociate on the Fe(111) surface during heating of a saturated adlayer. The lattice of Fe(111) is a lattice with hexagonal symmetry, so that two identical sites in the eight surrounding unit cells are obviously farther away than the other six sites. So, only six unit cells should be included as neighboring unit cells. Thus, the dissociation of CO on the Fe(111) surface also fits the relation.

The general tendency for CO dissociation on an open Ru or Fe surface indicates that the interaction with an adsorbate on a neighboring unit cell can significantly hinder the CO dissociation. The influence of occupation of neighboring unit cells on the adsorption energy has been investigated by using DFT calculations [142]. Liu

and Hu have calculated the adsorption energies of carbon and oxygen, which is in an optimized site (hcp hollow site) in a separate p(2×2) unit cell, respectively, and the total adsorption energy of a carbon and oxygen coadsorption, in which the carbon is at a hcp hollow site and the oxygen at the neighboring hcp site, and both are fixed in structure of the carbon and oxygen adsorbed separately. It was found that the total adsorption energy of carbon and oxygen without another atom on neighboring unit cells is obviously higher than that in the coadsorption case. This kind of effect was nominated a bonding-competition effect towards the top-layer metal atoms.

The bonding competition can also be used to explain the relation between CO dissociation and occupation of neighboring unit cells for the open Ru or Fe surfaces. When CO adsorbs in a neighboring unit cell, some metal atoms of the substrate will take part in the bonding with both CO molecules. The bonding-competition effect between the two CO molecules can significantly weaken the back donation of the charge into the CO $2\pi^*$ orbital and can therefore increase the dissociation barrier significantly, thus hindering the dissociation of CO. The influence of the metal position in the periodic table on the bonding competition has also been investigated by the same authors [142]. The effect becomes more significant for the element going from the left- to the right-hand side in the periodic table [142]. This indicates: If the transition metal is more unfavorable for electron back donation, the bonding-competition effect is stronger. Similarly, the conclusion can be drawn that the bonding-competition effect is stronger when more electron back donation is needed during forming an adsorption bond. This can explain that CO shifts from the state with very low C–O stretching energy (the dissociation precursor) to the state with linearly bonded (the normal chemisorbed CO) for high CO coverage as described in this work. Since the back donation for the state with the low C–O stretching energy is significantly stronger than that for the linearly bonded state, the bonding competition for this state is more significant at high coverage, and therefore the energy of this state becomes unfavorable. This results in the suppression of the CO dissociation precursor at high CO coverage.

The series of HREEL spectra for 0.1 and 1.0 L CO exposure at 85 K and heating to higher temperature shows that the dissociation temperature of CO for 1.0 L is obviously higher than that for 0.1 L, which indicates the higher dissociation barrier for 1.0 L. This barrier increase is due to the stronger bonding-competition effect for high

coverage. The increase of the dissociation barrier for high coverage is also observed on other metal surfaces, e.g., the Cr(110) [127] and the W(110) [130] surfaces. However, the maximum dissociated amount of adsorbed CO during heating is different between the metals on the left-hand side and on the boundary line in the periodic table. The dissociated amount of adsorbed CO for the W(110) surface is about 0.5 ML [130], obviously higher than the amount for Fe or Ru. As discussed above, the effect of bonding competition is not so strong for the metals on the left-hand side in the periodic table as for Fe or Ru; thus, the increase of the dissociation barrier is not so significant. Besides this, the difference of the barriers between dissociation and desorption are also very important, as will be discussed in the following.

Actually, there are two parallel processes for the adsorbed CO during heating, the dissociation and the desorption. The amount of dissociated CO is determined by the competition of the two processes. If another CO adsorbs in a neighboring cell of a CO dissociation precursor, the bonding competition can strongly reduce the back donation and thus significantly increase the dissociation barrier. On the surface of a metal, which lies in the left-hand side of boundary line, e.g., on Cr(110) [127] or W(110) [130], the dissociation barrier of CO is very low (the dissociation temperature is obviously lower than RT). On the other hand, the bonding competition is not so strong as for Fe or Ru and thus the increase of dissociation barrier is not so strong. For a not too high coverage, the dissociation barrier is still lower than the desorption barrier. So, the dissociated amount of adsorbed CO is very high, e.g., about 0.5 ML for CO on W(110) [130]. For the metal, which lies in the boundary line such as Ru or Fe, the situation is different. On the Ru(11$\bar{2}$1) and Ru(11$\bar{2}$0) surfaces, CO was found to dissociate at low coverage even at RT, due to the favorable geometrical structure on the two surfaces, but the amount at RT is very small (only a very weak loss peak of 70 meV in the HREEL spectrum). Similarly, the amount of CO dissociation on Fe surfaces at RT is also small. This indicates that the difference between the dissociation and the desorption barriers is not so big on these surfaces. When another CO adsorbs on a neighboring unit cell, the bonding-competition effect can increase the dissociation barrier and decrease the desorption barrier, so that the dissociation barrier becomes higher than the desorption barrier and the CO molecules prefer to desorb until no CO is adsorbed in a neighboring unit cell. So, on these surfaces the dissociation of adsorbed CO during heating correlates to the occupation

of the neighboring unit cells. Since the distance of a CO with two third-nearest neighbors among eight neighboring unit cells is 8.32 Å, the distance is far enough, so that the effect of bonding competition of Ru atoms is not so strong. This is the reason for us to consider only six neighboring unit cells, and the maximum amount of dissociated CO on Ru(11$\bar{2}$1) is near to 0.3 ML. For the similar reason, the maximum dissociated amount of chemisorbed ammonia is also about 0.3 ML. Since there is no ordered structure of CO on the Ru(11$\bar{2}$1) surface, the CO molecules on Ru(11$\bar{2}$1) surface distribute not so evenly. In addition, some dissociated products can also share bonding metal atoms with CO. Therefore, the maximum amount of dissociation of CO on Ru(11$\bar{2}$1) is somewhat smaller than 1/3 ML. Obviously, the bonding competition significantly affects the CO dissociation on the metal surface, which lies in the boundary line in the periodic table.

9.6 Summary

The chemisorption and the dissociation of CO on Ru(11$\bar{2}$1) were investigated by using HREELS and TDS. By comparing with the results of CO adsorption on Ru(0001) and Ru(10$\bar{1}$0), the saturated coverage of CO on the Ru(11$\bar{2}$1) surface is estimated to be about 1.5 ML. For low coverage, CO is adsorbed at an on-top site. For high coverage, CO forms a compression phase, in which 1.0 ML CO shifts somewhat off the on-top site but remains linearly bonded with the substrate, and additional CO adsorbs on a bridge site, similarly to that on Ru(10$\bar{1}$0). CO was found to be dissociated on the Ru(11$\bar{2}$1) surface at low coverage even at RT, similarly to Ru(11$\bar{2}$0). The dissociation of CO during heating is significantly affected by the CO occupation at a neighboring unit cell. This was explained by the bonding competition between CO in two neighboring unit cells. Several examples from the earlier works are presented which support our interpretation.

10 Conclusion

In this thesis, several adsorption systems, relevant for catalysis, were studied by means of HREELS and TDS. The systems comprise the Ru(11$\bar{2}$1) substrate, which is important in NH_3 synthesis and Fischer-Tropsch synthesis, and RuO_2(110), which turned out to be the reactive part in CO oxidation on Ru recently. The latter conclusion is reached based in part on the research of this thesis.

The bare RuO_2(110) surface is terminated by coordinatively unsaturated O (O-bridge) and Ru (Ru-cus) atoms. By exposure of oxygen at RT, a weakly held atomic oxygen can be adsorbed at Ru-cus, which is called O-cus. This surface is more oxygen rich than the bare one and is called O-rich RuO_2(110) for this reason. The Ru–O stretching mode of O-bridge and O-cus are observed at 69 and 103 meV, respectively. By oxygen exposure at 85 K, also a molecular oxygen species is adsorbed together with O-cus, both bonded to Ru-cus. The O–O stretching mode is found at 142 meV, indicating that it is a superoxo-like species (O_2^-).

Due to the high reactivity of RuO_2(110), the adsorption of CO at RT is totally different from that at LT (85 K). At LT the CO molecule adsorbs at Ru-cus, but as soon as the temperature reaches values around 250 K, CO either desorbs or reacts with neighboring O-bridge atoms, decapping the underlying Ru-bridge atoms. Thus, contrary to a previous suggestion [19], Ru-cus is not able to stabilize CO at RT. Instead, CO reacts with O-bridge immediately. When O-bridge has been removed, CO adsorbs at Ru-bridge, which forms stronger bonds with CO than Ru-cus. It is concluded that, for temperatures above 250 K, Ru-cus only acts as transient adsorption site, from which CO and presumably other adsorbate species may be supplied for further reactions, thus enabling the rather remarkable catalytic activity of this system.

HREELS titration experiments were performed, showing that CO can react with the bare and the O-rich $RuO_2(110)$ surface at RT. Two reaction channels are identified as the reactions of CO with O-cus and with O-bridge. At high O-cus coverage, the main reaction channel is the reaction of CO with O-cus while the reaction with O-bridge is suppressed. After most of O-cus has been consumed, the reaction of CO with O-bridge becomes dominant. For the exposure values applied, only surface oxygen takes part in the CO oxidation, and the oxygen depleted surface can be restored by O_2 exposure at RT. $RuO_2(110)$ + O_2 + CO turned out to be a remarkable surface redox system operating at 300 K. The TDS measurements for coadsorption also confirm that the reaction of CO with O-cus is prior to that of CO with O-bridge at high O-cus coverage. After reduction, e.g., by CO interaction, the $RuO_2(110)$ surface may expose temporarily the Ru-atom underneath O-bridge which is caled Ru-bridge. So, during reaction $RuO_2(110)$ may expose two types of Ru atoms which can each be occupied by either O (O-cus and O-bridge) or CO (CO-cus and CO-bridge). Thus, there might be four routes of CO_2 formation, O-cus with CO-cus, O-cus with CO-bridge, O-bridge with CO-cus and O-bridge with CO-bridge. The TDS measurements for coadsorption show that all of the four routes of CO_2 formation can take place.

The remarkable surface redox system, $RuO_2(110)$ + O_2 + CO, is able to work under steady-state conditions. The CO_2 formation rate reaches a maximum at the near stoichiometric gas phase composition (p_{CO}/p_{O_2} = 2:1). A remarkable agreement of the kinetic data was found between the $RuO_2(110)$ single crystal surface, typically operated at 10^{-7} mbar pressure, and small supported RuO_2 particles working at atmospheric pressure. This could be traced back to the fact that, under the conditions discussed above, the surface is essentially saturated with about similar fractions of O- and CO- species adsorbed at Ru-cus sites, so that variation of the total pressure (at a fixed CO : O_2 ratio) has only little effect. This indicates that there is no "pressure gap" for the reaction on $RuO_2(110)$. Actually, the different behavior of CO oxidation on Ru surfaces under UHV and under high pressure conditions is due to a "material gap": The catalytic part of Ru surfaces is composed of low reactivity Ru(0001)-(1×1)O under UHV conditions and high reactivity $RuO_2(110)$ under high pressure and oxidizing conditions. The situation will, however, change if the CO : O_2 ratio is varied, since now participation of the bridge-sites may become

more relevant, e.g., at temperatures above ≈ 350 K, where the surface structure may undergo more profound alterations. The results again demonstrate that the comparison of catalytic activities is only reasonable in connection with careful analysis of the state of the catalyst's surface; the absolute total pressure may then become irrelevant.

Three different adsorption states were observed when exposing hydrogen to the very open Ru(11$\bar{2}$1) surface at 90 K. Using both TDS and HREELS methods made it possible to differentiate the three states which are filled sequentially. The first two states are very likely due to occupation of two out of the six pseudo-threefold sites available in the bulk-truncated (1×1) unit cell. The arrival of the second hydrogen atom obviously changes the potential-energy surface of H adsorption, so that both H atoms per unit cell appear as belonging to the same β-H state in HREELS. In the α-state, a third H atom is squeezed into the unit cell at high exposures. It may be adsorbed at the fourfold symmetric site.

Three desorption states of CO were observed for the CO adsorption on Ru(11$\bar{2}$1). Two states result from the molecularly adsorbed CO, and the other one results from the recombination of dissociated CO. By exposure of CO at LT, CO adsorbs molecularly. By comparison with the results of CO adsorption on Ru(0001) and Ru(10$\bar{1}$0), the saturated coverage of CO on the Ru(11$\bar{2}$1) surface is estimated to be about 1.5 ML. At low coverage, CO is adsorbed at on-top sites. At high coverage, CO forms a compression phase, in which some CO molecules are shifted somewhat off the on-top sites but remain linearly bonded to the substrate, and additional CO adsorbs on bridge sites, similarly to the behavior on Ru(10$\bar{1}$0). CO was found to be dissociated on the Ru(11$\bar{2}$1) surface at low coverage even at RT. During heating the adsorbed CO partially dissociates. The dissociation of CO is mainly determined by the CO occupation at the neighboring unit cells. This was explained by the so-called "bonding competition" between CO in neighboring unit cells.

Bibliography

[1] P. Stoltze and J.K. Nøskov, J. Catal. 110, 1 (1988).

[2] G. Ertl, in Catalytic ammonia synthesis (J.R. Jennings, ed.), Plenum Press 1991, p109.

[3] S. Dahl, J. Senested, C.J.H. Jacobsen, E. Törnqvist, and I. Chorkendorff, J. Catal. 192, 391 (2000).

[4] O. Hinrichsen, F. Rosowski, M. Muhler and G. Ertl, 51, 1683 (1996).

[5] S.H. Oh, G.B. Fischer, J.E. Carpenter and D.W. Goodman, J. Catal. 100, 360 (1986).

[6] T. Engel and G. Ertl, Adv. Catal. 28, 1 (1979).

[7] C.H.F. Peden, in Surface Science of Catalysis: In Situ Probes and Reaction Kinetics, edited by D.J. Dwyer and F.M. Hoffman (American Chemical Society, Wanshington DC, 1992).

[8] J. Wintterlin, S. Völkening, T.V.W. Janssens, T. Zambelli and G. Ertl, Science 278, 1931 (1997).

[9] M. Valden, X. Lai and D.W. Goodman, Science 281, 1647 (1998).

[10] H.-I. Lee and J. M. White, J.Catal. 63, 261 (1980); V. I. Savchenko, G. K. Boreskov, A. V. Kalinkin, A. N. Salanow, Kinet. Catal. 24, 983 (1984).

[11] N. W. Cant, P. C. Hicks, B. S. Lennon, J. Catal. 54, 372 (1978); C. H. F. Peden in Surface Science of Catalysis, D. J. Dwyer and F. M. Hoffmann, Eds.

(ACS Symposium Series 483, American Chemical Society, Washington, DC, 1992), p. 143.

[12] C. H. F. Peden and D. W. Goodman, J. Phys. Chem. 90, 1360 (1986).

[13] A. Böttcher, H. Niehus, S. Schwegmann, H. Over and G. Ertl, J. Phys. Chem. B 101, 11185 (1997).

[14] A. Böttcher, M. Rogozia, H. Niehus, H. Over and G. Ertl, J. Phys. Chem. B 103, 6267 (1999).

[15] A. Böttcher and H. Niehus, Phys. Rev. B 60, 14396 (1999).

[16] A. Böttcher and H. Niehus, J. Chem. Phys. 110, 3186 (1999).

[17] A. Böttcher, H. Conrad and H. Niehus, J.Chem. Phys. 112, 4779 (2000).

[18] A. Böttcher, H. Conrad and H. Niehus, Surf. Sci. 452, 125 (2000).

[19] H. Over, Y. D. Kim, A. P. Seitsonen, S. Wendt, E. Lundgren, M. Schmid, P. Varga, A. Morgante, and G. Ertl, Science 287, 1474 (2000).

[20] Y.D. Kim, A.P. Seitsonen and H. Over, Surf. Sci. 465, 1 (2000).

[21] Y.D. Kim, H. Over, G. Krabbes and G. Ertl Topics in Catalysis 14, 95 (2001).

[22] Y.D. Kim, A.P. Seitsonen and H. Over, Phys. Rev. B 63, 115419 (2001).

[23] Y.D. Kim, A.P. Seitsonen, S. Wendt, J. Wang, C. Fan, K. Jacobi, H. Over, and G. Ertl, J. Phys. Chem. B 105, 3752 (2001).

[24] H. Over, A.P. Seitsonen, E. Lundgren, M. Wiklind and J.N. Andersen, Chem. Phys. Lett. 342, 467 (2001).

[25] H. Over, A.P. Seitsonen, E. Lundgren, M. Schmid and P. Varga, J. Am. Chem. Soc. 123, 11807 (2001).

[26] A.P. Seitsonen, Y.D. Kim, M. Knapp, S. Wendt and H. Over, Phys. Rev. B 65, 035413 (2002).

[27] Z.P. Liu and P. Hu, J. Chem. Phys. 114, 8244 (2001).

[28] K. Reuter and M. Scheffler, Surf. Sci. 490, 20 (2001).

[29] K. Reuter, C. Stampfl, M.V. Ganduglia-Pirovano and M. Scheffler, Chem. Phys. Lett. 352, 311 (2002).

[30] K. Reuter, M.V. Ganduglia-Pirovano, C. Stampfl, and M. Scheffler, Phys. Rev. B, in press.

[31] K. Reuter and M. Scheffler, Phys. Rev. B 65, 035406 (2002).

[32] L. Zang, and H. Kisch, Angew. Chem. Int. Edit. 39, 3921 (2000).

[33] S.R. Tennison, in; Catalytic Ammonia Synthesis, ed. J.R. Jennings (Plenum, New York,1991) p. 303.

[34] K. Aika, Angew. Chem. Int. Ed. Engl. 25, 558 (1986).

[35] T.A. Czuppon, S.A. Knez, R.V. Schneider and G. Worobets, Chem. Engineering 100, No.3, 19 (1993).

[36] K. Jacobi, H. Dietrich and G. Ertl, Appl. Surf. Sci. 121/122, 558 (1997).

[37] K. Jacobi, Phys. Stat. Sol. A 37, 177 (2000) and references therein.

[38] G.A. Somorjai, Introduction to surface Chemistry and Catalysis, Wiley, New York, 442 (1994).

[39] R.D. Kelley, D.W. Goodman, The Chemical Physics of Solid Surface and Heterogeneous Catalysis, vol. 4, Elsevier, Amsterdam, 427, (1982).

[40] G.E. Thomas and W.H. Weinberg, Phys. Rev. Lett. 41, 1181 (1978).

[41] G.E. Thomas and W.H. Weinberg, J. Chem. Phys. 70, 1437 (1979).

[42] H. Pfnür, D. Menzel, F.M. Hoffmann, A. Ortega and M.A. Brashaw, Surf. Sci. 93, 431 (1980).

[43] G. Michalk, W. Moritz, H. Pfnür and D. Mezel, Surf. Sci. 129, 92 (1983).

[44] H. Pfnür, P. Feulner and D. Menzel, J. Chem. Phys. 79, 4613 (1983).

[45] P. He, H. Dietrich and K. Jacobi, Surf. Sci. 345, 241 (1996).

[46] P. Jakob, Phys. Rev. Lett. 77, 4229 (1996).

[47] M. Sokolowski, T. Koch and H. Pfnür, Surf. Sci. 243, 261 (1991).

[48] G. Held, H. Pfnür and D. Menzel, Surf. Sci. 271, 21 (1992).

[49] M. Lindroos, H. Pfnür, P. Feulner and D. Menzel, Surf. Sci. 180, 237 (1987).

[50] P. Feulner and D. Menzel, Surf. Sci. 154, 465 (1985).

[51] M.A. Barteau, J.Q. Broughton and D. Menzel, Surf. Sci. 133, 443 (1983).

[52] H. Conrad, R. Scala, W. Stenzel and R. Unwin, J. Chem. Phys. 81, 6371 (1984).

[53] H. Shi and K. Jacobi, Surf. Sci. 313, 289 (1994).

[54] F. Boszo, G. Ertl, M. Grunze and M. Weiss, J. Catal. 49, 18 (1977).

[55] F. Boszo, G. Ertl and M. Weiss, J. Catal. 50, 519 (1977). Zambelli, and G. Ertl, Science 278, 1931 (1997).

[56] H. Dietrich, K. Jacobi and G. Ertl, 352-354, 138 (1996).

[57] K. Jacobi, Y. Wang, C.Y. Fan and H. Dietrich, J. Chem. Phys. 115, 4306 (2001).

[58] P. He and K. Jacobi, Phys. Rev. B 55 (1997) 4751

[59] M. Gruyters, K. Jacobi, J. Electron. Spectr. & Relat. Phenom. 64/65, 591 (1993).

[60] M. Gruyters, Dissertation TU-Berlin (1993).

[61] N.V. Richardson, Curr. Opinion Solid State Material Sci. 517, 2 (1997).

[62] J.B. Miller, H.R. Siddiqui, S.M. Gates, J.N. Russel, J.T. Yates, J.C. Tully and M.J. Cardillo, J. Chem. Phys. 87, 6725 (1987).

[63] D. King, Surf. Sci. 47, 384 (1975).

[64] E. Bauer, F. Bonzeek, H. Poppa and G. Todd, Surf. Sci., 53, 87 (1975).

[65] C. Chan, R. Aris and H. Weinberg., Appl. Surf. Sci. 1, 360 (1978).

[66] C.H.F. Peden and D.W. Goodman, J. Vac. Sci. Technol. A3, 1558 (1985).

[67] T.E. Madey, H. A. Engelhardt, and D. Menzel, Surf. Sci. 48, 304 (1975).

[68] T.S. Rahman, A.B. Anton, N. R. Avery, and W.H. Weinberg, Phys. Rev. Lett. 51, 1979 (1983).

[69] W.J. Mitchell, Y. Wang, M. Schick, and W.H. Weinberg, J. Chem. Phys. 102, 8185 (1995).

[70] F. M. Hoffmann, M. D. Weisel, and C. H. F. Peden, Surf. Sci. 253, 59 (1991).

[71] C. Stampfl and M. Scheffler, Phys. Rev. B54, 2868 (1996).

[72] J. Segner, W. Vielhaber and G. Ertl, Israel J. Chem. 22, 375 (1982).

[73] B.A. Banse and B.E. Koel, Surf. Sci. 232, 275 (1990).

[74] I.J. Malik and J. Hrbek, J. Vac. Sci. Technol. A10, 2565 (1992).

[75] W.J. Mitchell and W.H. Weinberg, J. Chem. Phys. 104, 9127 (1996).

[76] C. Stampfl, S. Schwegmann, H. Over, M. Scheffler, and G. Ertl, Phys. Rev. Lett. 77, 3371 (1996).

[77] K.L. Kostov, M.Gsell, P. Jakob, T. Moritz, W. Widdra and D. Menzel, Surf. Sci. Lett. 394, L138 (1997).

[78] T. Moritz, D. Menzel, and W. Widdra, Surf. Sci. 427-428, 64 (1999).

[79] K.L. Kostov, H. Rauscher and D. Menzel, Surf. Sci. 278, 62 (1992).

[80] C.H.F. Peden, D.W. Goodman, M.D. Weisel and F.M. Hoffmann, Surf. Sci. 253, 44 (1991).

[81] F.M. Hoffmann, M.D. Weisel, and C.H.F. Peden, J. Electron Spectrosc. Relat. Phenom. 54/55, 779 (1990).

[82] C.J. Zhang, P. Hu and A. Alavi, J. Am. Chem. Soc. 121, 7931 (1999)

[83] C.J. Zhang and P. Hu, J. Am. Chem. Soc. 122, 2134 (2000)

[84] C.J. Zhang and P. Hu, J. Chem. Phys. 112, 10564 (2000).

[85] C. Stampfl and M. Scheffler, Phys. Rev. Lett. 78, 1500 (1997).

[86] C. Stampfl and M. Scheffler, Surf. Sci. 377–309,808 (1997).

[87] C.Stampfl and M. Scheffler, J. Vac. Sci. Technol. A 15, 1635 (1997).

[88] C. Stampfl and M. Scheffler, Surf. Sci. 433–435, 119 (1999).

[89] L.F. Mattheis, Phys. Rev. B 13, 2433 (1976).

[90] R.R. Daniels, G. Margaritondo, C.A. Goerg and F. Levy, Phys. Rev. B 29, 1813 (1984).

[91] L. Atanasoska, W.E. O'Grady, R.T. Atanasoski and F.H. Pollak, Surf. Sci. 202, 142 (1988).

[92] V.E. Henrich and P.A. Cox, The Surface science of Metal Oxides, Cambridge Univ. Press, Cambridge, 1996.

[93] J.G. Kay, D.W. Green, K. Duca and G.L. Zimmerman, J. Mol. Spectrosc. 138, 49 (1989)

[94] Richard I. Masel, in Principles of adsorption and reaction on solid surfaces (John Wiley & Sons. Inc., 1996), P396.

[95] G. Blyholder, J. Phys. Chem. 68, 2772 (1964).

[96] P. Jakob, B.N.J. Persson, Phys. Rev. B 56, 10644 (1997).

[97] U. Diebold, J. Lehman, T. Mahmoud, M. Kuhn, G. Leonardelli, W. Hebenstreit, M. Schmid and P. Varga, Surf. Sci. 411, 137 (1998).

[98] J. Wintterlin, J. Trost, S. Renisch, R. Schuster, T. Zambelli and G. Ertl, Surf. Sci. 394, 159 (1997).

[99] Y. Wang, A. Lafosse and K. Jacobi, submited to J. Phys. Chem..

[100] G. Lauth, E. Schwarz and K. Christmann, J. Chem. Phys. 91, 3729 (1989).

[101] K. Christmann, Surf. Sci. Rep. 9, 1 (1988).

[102] D. Farias et.al., J. Chem. Phys. 106, 8254 (1997).

[103] P. Schilbe et.al. Surf. Sci. 360, 157 (1996).

[104] P. Schilbe, D. Farias, K. H. Rieder, Surf. Rev. Lett. 5, 473 (1998).

[105] K. Christmman, Prog. in Surf. Sci., 48, 15 (1995).

[106] P. Nordlander, S. Holloway, J. K. Norskov, Surf. Sci. 136, 59 (1984).

[107] B. Voigtländer, S. Lehwald and H. Ibach, Surf.Sci., 208, 113 (1989).

[108] M. J. Puska, R.M. Nieminen, M. Manninen et. al., Phys. Rev. Lett. 51, 1081 (1983).

[109] L.J. Richter, T.A. Germer, J.P. Sethna et. al., Phys. Rev. B 38, 10403 (1998).

[110] S. Andersson, Chem. Phys. Lett. 55, 185 (1978).

[111] P.-A. Karlsson, A.-S. Martensson, S. Andersson et. al. Surf. Sci. Lett. 175, L759 (1986).

[112] A.-S. Martensson, C. Nyberg, S. Andersson, surf. Sci. 205, 12 (1988).

[113] H. Conrad, M.E. Kordesch, W. Stenzel et. al., J. Electron. Spectr. Rel. Phenom. 38(1986)289

[114] S.-I. Ishi, Y. Ohno and B. Viswanathan, Surf. Sci. 161, 349 (1985).

[115] H. Ueba, Surf. Sci. 188, 421 (1987).

[116] G. Broden, T.H. Rhodin, C. Brucker, R. Benbow and Z. Hurych, Surf. Sci. 59, 593 (1976).

[117] G. Lauth, T. Solomun, W. Hirschwald and K. Christmann, Sruf. Sci. 210, 201 (1989).

[118] G. Rotaris, A. Baraldi, G. Comelli, M. Kiskinova, and R. Rosei, Surf. Sci. 359, 1 (1996).

[119] J.J. Carroll, T.E. Madey, A.J. Melmed and D.R. Sandstrom, Surf. Sci. 96, 508 (1980).

[120] J. Wang, Y. Wang and K. Jacobi, Surf. Sci. 482-485, 153 (2001).

[121] J. Wang, Y. Wang and K. Jacobi, Surf. Sci. 488, 83 (2001).

[122] Eriko Shincho, Chikashi Egawa, Shuichi Naito and Kenzi Tamaru, Surf. Sci. 149, 1 (1985).

[123] Y. Wang, A. Lafosse and K. Jacobi, Surf. Sci. in press.

[124] M.A. Chesters, B.J. Bandy, P. Hollins, J. Pritchard and N. Sheppard, J. Mol. Struct. 80, 203 (1982).

[125] M.A. Chesters, G.S. Mcdoucall, M.E. Pemble, N. Sheppard, Surf. Sci. 164, 425 (1985).

[126] H. Kato, H. Okuyama, S. Ichihara, M. Kawai and J. Yoshinobu, J. Chem. Phys. 112, 1925 (2000).

[127] N.D. Shinn and T.E. Madey, Phys. Rev. Lett. 53, 2481 (1984).

[128] N.D. Shinn and T.E. Madey, J. Chem. Phys. 83, 5928 (1985).

[129] J.G. Chen, M.L. Colaianni, W.H. Weinberg and J.T. Yates Jr., Chem. Phys. Lett., 177, 113 (1991).

[130] J.E. Houston, Sruf. Sci. 255, 303 (1991).

[131] F. Zaera, E. Kollin and J.L. Gland, Chem. Phys. Lett. 121, 464 (1985).

[132] Carsten Benndorf, Bernd Krüger and Fritz Thieme, Surf. Sci. 163, L675 (1985).

[133] D.W. Moon, S.L. Bernasek, D.J. Dwyer and J.L. Gland, J. Am. Chem. Soc. 107, 4363 (1985).

[134] C.E. Bartosch, L.J. Whitman, and W. Ho, J. Chem. Phys. 85, 1052 (1986).

[135] W. Erley, H. Ibach, S. Lehwald and H. Wagner, Surf. Sci. 83, 585 (1979).

[136] U. Seip, M.-C. Tsai, K. Christmann, J. Küppers and G. Ertl, Surf. Sci. 139, 29 (1984).

[137] L. Zhu, S. Bao, C.Y. Xu et al., SURF. SCI. 260, 267 (1992).

[138] P. He and K. Jacobi, J. Chem. Phys. 106, 3417 (1997).

[139] H.Y. Li, S. Bao, X.S. Zhang et al., J. Phys. Condens Mat. 9, 7291 (1997).

[140] S.D. Cameron and D.J. Dwyer, Langmuir 4, 282 (1988).

[141] M. Nassir, D.J. Dwyer and P. Kleban, Surf. Sci. Lett. 356, L429 (1996).

[142] Z.P. Liu, P. Hu and A. Alavi, J. Chem. Phys., 114, 8244 (2001).

Publications

- **C.Y. Fan**, J. Wang, K. Jacobi and G. Ertl, The oxidation of CO on $RuO_2(110)$ at room temperature, J. Chem. Phys. 114, 10058–10062 (2001).
- **C.Y. Fan** and K. Jacobi, The adsorption of hydrogen on $Ru(11\bar{2}1)$, Surf. Sci. 482–485, 21 (2001).
- J. Wang, **C.Y. Fan**, K. Jacobi and G. Ertl, The kinetics of CO oxidation on $RuO_2(110)$: Bridging the pressure gap, J. Phys. Chem. 106,3422–3427 (2002).
- J. Wang, **C.Y. Fan**, K. Jacobi and G. Ertl, Adsorption and reaction of CO on $RuO_2(110)$ surface, Surf. Sci. 481, 113–118 (2001).
- K. Jacobi, Y. Wang, **C.Y. Fan** and H. Dietrich, Adsorption and thermal dehydrogenation of ammonia on $Ru(11\bar{2}1)$, J. Chem. Phys. 115, 4306–4313 (2001).
- Y.D. Kim, A.P. Seitsonen, S. Wendt, J. Wang, **C. Fan**, K. Jacobi, H. Over, and G. Ertl, Characterization of various oxygen species on an oxide surface: $RuO_2(110)$, J. Phys. Chem. B 105, 3752–3758 (2001).

- **C.Y. Fan**, K. Jacobi, H.-P. Bonzel and G. Ertl, Bonding competition in CO dissociation on the $Ru(11\bar{2}1)$ surface, to be submitted to J. Chem. Phys.
- J. Wang, **C.Y. Fan**, Q. Sun, K. Reuter, K. Jacobi, M. Scheffler and G. Ertl, Surface coordination chemistry: Dihydride versus dihydrogen complexes on $RuO_2(110)$, to be submitted to Phys. Rev. Lett.

Curriculum Vitae

26. 03. 1969	born in Jianou, Fujian province, P.R. China
9/1980–7/1986	first high-school of Jianou (Jianou Yi Zhong), Jianou
9/1986–7/1990	undergraduate in the Department of Physics, Zhejiang University, Hangzhou
9/1990–3/1993	Master student in the Department of Physics, Zhejiang University, Hangzhou
4/1993–1/1998	teacher and researcher in the Department of Physics, Zhejiang University, Hangzhou
2/1998–5/2002	Ph.D. student at the Fritz-Haber-institute of Max-Planck-Society, Berlin